

STELLAR DIAMETERS AND TEMPERATURES. III. MAIN-SEQUENCE A, F, G, AND K STARS: ADDITIONAL HIGH-PRECISION MEASUREMENTS AND EMPIRICAL RELATIONS

TABETHA S. BOYAJIAN^{1,2}, KASPAR VON BRAUN^{3,4}, GERARD VAN BELLE⁵, CHRIS FARRINGTON⁶, GAIL SCHAEFER⁶, JEREMY JONES¹,
RUSSEL WHITE¹, HAROLD A. MCALISTER¹, THEO A. TEN BRUMMELAAR⁶, STEPHEN RIDGWAY⁷, DOUGLAS GIES¹,
LASZLO STURMANN⁶, JUDIT STURMANN⁶, NILS H. TURNER⁶, P. J. GOLDFINGER⁶, AND NORM VARGAS⁶

¹ Center for High Angular Resolution Astronomy and Department of Physics and Astronomy,

Georgia State University, P.O. Box 4106, Atlanta, GA 30302-4106, USA

² Department of Astronomy, Yale University, New Haven, CT 06511, USA

³ NASA Exoplanet Science Institute, California Institute of Technology, MC 100-22, Pasadena, CA 91125, USA

⁴ Max Planck Institute for Astronomy, Königstuhl 17, D-69117 Heidelberg, Germany

⁵ Lowell Observatory, Flagstaff, AZ 86001, USA

⁶ The CHARA Array, Mount Wilson Observatory, Mount Wilson, CA 91023, USA

⁷ National Optical Astronomy Observatory, P.O. Box 26732, Tucson, AZ 85726-6732, USA

Received 2013 February 14; accepted 2013 May 10; published 2013 June 13

ABSTRACT

Based on CHARA Array measurements, we present the angular diameters of 23 nearby, main-sequence stars, ranging from spectral types A7 to K0, 5 of which are exoplanet host stars. We derive linear radii, effective temperatures, and absolute luminosities of the stars using *Hipparcos* parallaxes and measured bolometric fluxes. The new data are combined with previously published values to create an *Angular Diameter Anthology* of measured angular diameters to main-sequence stars (luminosity classes V and IV). This compilation consists of 125 stars with diameter uncertainties of less than 5%, ranging in spectral types from A to M. The large quantity of empirical data is used to derive color–temperature relations to an assortment of color indices in the Johnson (*BVR_IJHK*), Cousins (*R_CI_C*), Kron (*R_KI_K*), Sloan (*griz*), and *WISE* (*W₃W₄*) photometric systems. These relations have an average standard deviation of $\sim 3\%$ and are valid for stars with spectral types A0–M4. To derive even more accurate relations for Sun-like stars, we also determined these temperature relations omitting early-type stars ($T_{\text{eff}} > 6750$ K) that may have biased luminosity estimates because of rapid rotation; for this subset the dispersion is only $\sim 2.5\%$. We find effective temperatures in agreement within a couple of percent for the interferometrically characterized sample of main-sequence stars compared to those derived via the infrared flux method and spectroscopic analysis.

Key words: Hertzsprung–Russell and C–M diagrams – infrared: stars – planetary systems – stars: atmospheres – stars: fundamental parameters – stars: general – stars: solar-type – techniques: high angular resolution – techniques: interferometric

Online-only material: color figures, machine-readable table

1. INTRODUCTION

Aside from our Sun, stars are often considered unresolved point sources, with no readily measurable two-dimensional structure obtainable. However, current technology enables measurements of angular diameters of stars with somewhat large angular sizes ($\theta > \text{a few} \times \sim 0.1$ mas, where θ is the angular diameter) to be spatially resolved via long-baseline optical/infrared interferometry (LBOI; see references in Table 3 for examples). The two general flavors of observable stellar diameters include evolved stars (giants/supergiants), whose extended linear diameter compensates for their relatively large distance from the observer, and main-sequence stars, whose linear size remains non-inflated from stellar evolution and therefore must reside in the observer’s close vicinity. It is these nearby stars with known parallaxes and interferometrically measured angular sizes that enable us to empirically determine the absolute properties of the star, namely, the linear radius and effective temperature (e.g., Boyajian et al. 2012a).

Stellar properties can also be indirectly estimated from comparisons of spectral lines and predictions from atmospheric models. Strengths in such stellar atmosphere and evolutionary models as well as less-direct methods of characterizing stellar properties do not just rely upon the input physics; very often it is necessary to calibrate the zero points from direct measurements.

The ability to characterize empirically the fundamental properties of stars through interferometry provides us with the critical information needed to constrain and allow improvements for stellar atmosphere and evolutionary models (Andersen 1991; Torres et al. 2010).

General characterization of stars using spectroscopic analysis in combination with evolutionary models (e.g., Valenti & Fischer 2005; Takeda 2007) is dependent on the accuracies of models and uniqueness of solutions obtainable. Such model atmosphere codes used to analyze the stellar spectrum are dependent on many variables such as metallicity, temperature, gravity, and microturbulent velocity, and existing degeneracies between parameters make for difficult analysis given such a large and correlated parameter space. Spectroscopic solutions for effective temperature, surface gravity, and atmospheric abundances are the leading constraints to subsequent analysis using evolutionary models, where the stellar mass and radius may be determined.

The work in Boyajian et al. (2012a) compares interferometrically determined properties to those using model-dependent methods. They find that the use of spectroscopically or photometrically defined properties tends to overestimate the effective temperatures compared to directly measured values. This discrepancy in temperature is strongly correlated to an offset in spectroscopically measured surface gravities—consequently

yielding higher masses and younger ages for the stars studied (see their Figures 22 and 23). Offsets in spectroscopic surface gravities have also been noted to be present through spectroscopic analysis alone, as discussed in Section 7.4 of Valenti & Fischer (2005). However, as they note, the lack of data available to calibrate these properties limits the accuracies of their solutions. Iterative techniques using interferometrically constrained parameters in combination with spectroscopic analysis have proven to yield robust results, such as the one used in Crepp et al. (2012). Unfortunately, however, such targets are scarce, given the observability requirements (brightness and proximity) of LBOI.

Stellar temperatures from the infrared flux method (IRFM), a technique first developed by Blackwell & Shallis (1977), is a popular substitute for defining stellar properties, and the least model-dependent behind interferometric measurements. The photometrically based IRFM is advantageous in approach because it may be applied to a large number of stars, spanning a large range in metallicities. Tremendous work has blossomed in the field over the past few decades, however its true validity is somewhat plagued by systematic differences between the temperature scales used in the literature, which can be as large as ~ 100 K (see González Hernández & Bonifacio 2009; Casagrande et al. 2010, and references therein). As many argue, the zero-point calibration of the IRFM lacks the empirical data as a good foundation—always referring to the paucity of interferometric measurements available.

A few years later, we embarked on an interferometric survey of main-sequence stars, as previously reported in the works of Boyajian et al. (2012a, 2012b, these are papers entitled Stellar Diameters and Temperatures I and II we hereafter abbreviate as DT1 and DT2, respectively). This work is the third installment of stellar diameters pertaining to this survey (abbreviated DT3), where we continue to populate the literature with accurate stellar parameters of these nearby stars measured with interferometry. In this paper, we report new angular diameters of 18 stars and improved precision on 5 additional stars, with average uncertainty in the angular diameter of 2% (Section 2.1). In Section 2.2, we present an overview of angular diameters, listing all main-sequence stars that have interferometrically measured angular diameters with better than 5% precision. Sections 2.3 and 2.4 describe the radii, temperatures, bolometric fluxes, luminosities, masses, and ages for the entirely interferometrically characterized sample. Finally, in Section 3 we present the results of color–temperature relations calibrated using our empirical data set, and we present our conclusions in Section 4.

2. TARGETS AND ANGULAR DIAMETERS

A census of angular diameter measurements of lower-mass K and M dwarfs recently enumerated in the DT2 yield a total of 33 stars. In this work, we expand on the DT2 sample to describe fully the current state of measured angular diameters including all A-, F-, and G-type main-sequence stars. We follow the same method and criteria as in DT2, admitting only stars where the angular diameter was measured to better than 5%.

In addition to the collection of literature measurements, in this work we present new angular diameters for 23 stars (Section 2.1). Stars with multiple measurements are also examined in Section 2.2, where we determine mean values for use in the determination of their fundamental properties (Section 2.3) and the analysis of the data (Section 3).

2.1. Observations with the CHARA Array

Akin to the observing outlined in DT1 and DT2, observations for this project were made with the CHARA Array, a long-baseline optical/infrared interferometer located on Mount Wilson Observatory in southern California (see ten Brummelaar et al. 2005 for details). The target stars were selected based on their approximate angular size (a function of their intrinsic linear size and distance to the observer). We limit the selection to stars with angular sizes > 0.45 mas, in order to adequately resolve their sizes to a few percent precision with the selected instrument setup. Note that all stars that meet this requirement are brighter than the instrumental limits of our detector by several magnitudes. The stars also have no known stellar companion within 3 arcsec to avoid contamination of incoherent light in the interferometers' field of view. From 2008 to 2012, we used the CHARA Classic beam combiner operating in the H band ($\lambda_H = 1.67 \mu\text{m}$) and the K' band ($\lambda_{K'} = 2.14 \mu\text{m}$) to collect observations of 23 stars using CHARA's longest baseline combinations. A log of the observations can be found in Table 1.

As is customary, all science targets were observed in bracketed sequences along with calibrator stars. To choose an appropriate calibrator star in the vicinity of the science target, we used the SearchCal tool developed by the JMMC Working Group (Bonneau et al. 2006, 2011). These calibrator stars are listed in Table 1, and the value of the estimated angular diameters θ_{EST} is taken from the SearchCal catalog value for the estimated limb-darkened angular diameter. In order to ensure carefully calibrated observations and to minimize systematics, we employ the same observing directive we initiated and followed in DT1 and DT2: each star must be observed (1) on more than one night, (2) using more than one baseline, and (3) with more than one calibrator. Of the 23 stars in Table 1, only HD 136202 did not meet the second requirement of revisiting it on another baseline, but the data give us no reason to reject it only based on this shortcoming, since a sufficient number of observations were collected over time on the nights we did observe this star. All other directive requirements were met by all stars.

In addition to the observing directives mentioned above, we also follow the guidelines described in van Belle & van Belle (2005) for choosing unresolved calibrators in order to alleviate any bias in the measurements introduced with the assumed calibrator diameter. At the CHARA Array, this limit on the calibrator's estimated angular diameter is $\theta_{\text{EST}} < 0.45$ mas, and this criterion is met for 30 of the observed calibrators in this paper. In practice, however, we find that some science stars do not have more than one suitably unresolved calibrator available nearby to observe. As such, we must extend this calibrator size limit to slightly larger, $\theta_{\text{EST}} < 0.5$ mas sizes, adding an additional 14 calibrator stars to our program.⁸ While this is less than ideal, it is important to note that any star observed with a slightly larger calibrator star is also observed with a more unresolved calibrator, and calibration tests show no variance in the calibrated visibilities from these objects compared to each other.⁹ As a whole, the calibrators observed have average magnitudes of $V = 6.0$, $H = 5.0$, $K = 4.9$, and an average angular diameter of 0.41 ± 0.03 mas.

⁸ We mark stars with $\theta_{\text{EST}} > 0.45$ in Table 1.

⁹ These calibrator size limits are also maintained when pertaining to the calibrators observed in DT1 and DT2, as described within the observations section of each respective paper.

Table 1
Observation Log

Object	UT Date	Baseline	Filter	No. of Brackets	Calibrator HD
HD 166	2010 Sep 17	E1/W1	<i>H</i>	4	HD 1404
	2010 Sep 19	S1/E1	<i>H</i>	6	HD 2628 [†]
	2011 Aug 16	S1/E1	<i>H</i>	7	HD 112 [†] , HD 2628 [†]
	2011 Aug 20	E1/W1	<i>H</i>	3	HD 2628 [†]
HD 6210	2010 Sep 20	S1/E1	<i>H</i>	12	HD 3283, HD 9407
	2012 Nov 12	E1/W1	<i>H</i>	3	HD 3283
	2012 Nov 14	E1/W1	<i>K'</i>	5	HD 3283
HD 10476	2012 Sep 13	E1/W1	<i>H</i>	5	HD 8941, HD 9780
	2012 Sep 14	E1/W1	<i>H</i>	2	HD 8941, HD 9780
	2012 Nov 2	S1/E1	<i>H</i>	5	HD 8941, HD 9780
HD 10697	2012 Nov 2	S1/E1	<i>H</i>	5	HD 8941, HD 9780
	2012 Nov 3	S1/E1	<i>H</i>	3	HD 8941, HD 9780
	2012 Nov 14	E1/W1	<i>H</i>	2	HD 8941, HD 9780
HD 11964	2012 Nov 3	S1/E1	<i>H</i>	5	HD 11131, HD 13456
	2012 Nov 4	S1/E1	<i>H</i>	5	HD 11131, HD 13456
	2012 Nov 12	E1/W1	<i>H</i>	2	HD 11131, HD 13456
HD 16765	2011 Oct 2	S1/E1	<i>H</i>	6	HD 14690 [†] , HD 18331
	2011 Oct 3	S1/E1	<i>H</i>	10	HD 14690 [†] , HD 18331
	2012 Nov 12	E1/W1	<i>H</i>	3	HD 14690 [†] , HD 18331
HD 21019	2012 Sep 13	E1/W1	<i>H</i>	3	HD 19107, HD 20395
	2012 Sep 14	E1/W1	<i>H</i>	5	HD 19107, HD 20395
	2012 Sep 26	S1/E1	<i>H</i>	5	HD 19107, HD 20395
HD 38858	2011 Oct 2	S1/E1	<i>H</i>	8	HD 37594, HD 37788
	2011 Oct 3	S1/E1	<i>H</i>	11	HD 37594, HD 37788
	2012 Nov 14	E1/W1	<i>H</i>	4	HD 37594, HD 37788
HD 69897	2010 Apr 8	S1/E1	<i>H</i>	5	HD 74198
	2010 Apr 9	S1/E1	<i>H</i>	5	HD 74198
	2010 Apr 10	S1/E1	<i>K'</i>	4	HD 74198
	2012 Nov 12	E1/W1	<i>H</i>	2	HD 74198, HD 74669 [†]
HD 130948	2010 Apr 8	S1/E1	<i>H</i>	6	HD 135502, HD 137510 [†]
	2010 Apr 9	S1/E1	<i>H</i>	6	HD 137510 [†]
	2011 Apr 11	E1/W1	<i>H</i>	4	HD 137510 [†]
HD 136202	2012 Apr 9	S1/E1	<i>H</i>	5	HD 135599 [†] , HD 137898
	2012 Apr 10	S1/E1	<i>H</i>	5	HD 135599 [†] , HD 137898
HD 140538	2010 Apr 10	S1/E1	<i>H</i>	2	HD 135204
	2011 Apr 13	E1/W1	<i>H</i>	7	HD 135204, HD 147449 [†]
	2012 Apr 10	S1/E1	<i>H</i>	5	HD 135204, HD 147449 [†]
HD 157214	2012 Sep 13	E1/W1	<i>H</i>	4	HD 155524 [†] , HD 159222
	2012 Sep 14	E1/W1	<i>H</i>	5	HD 154029, HD 155524 [†]
	2012 Sep 26	S1/E1	<i>H</i>	5	HD 154029, HD 155524 [†]
HD 158633	2010 Sep 20	S1/E1	<i>H</i>	8	HD 182564
	2011 Aug 1	E1/W1	<i>H</i>	6	HD 156295, HD 160933 [†]
HD 168151	2008 Jul 21	S1/W1	<i>K'</i>	3	HD 159633
	2010 Sep 20	S1/E1	<i>H</i>	8	HD 182564
HD 186408	2011 Aug 16	S1/E1	<i>H</i>	8	HD 185414, HD 191195 [†]
	2011 Aug 19	E1/W1	<i>H</i>	3	HD 191096, HD 191195 [†]
	2011 Aug 20	E1/W1	<i>H</i>	7	HD 185414, HD 191195 [†]
	2011 Aug 21	W1/S1	<i>H</i>	5	HD 185414, HD 191096
HD 186427	2011 Aug 16	S1/E1	<i>H</i>	8	HD 185414, HD 191195
	2011 Aug 19	E1/W1	<i>H</i>	4	HD 191096, HD 191195
	2011 Aug 20	E1/W1	<i>H</i>	7	HD 185414, HD 191195
	2011 Aug 21	W1/S1	<i>H</i>	5	HD 185414, HD 191096
HD 195564	2008 Jun 20	W1/S1	<i>K'</i>	3	HD 195838 [†]
	2008 Jun 27	S1/E1	<i>K'</i>	11	HD 193555, HD 195838 [†]
	2012 Sep 14	E1/W1	<i>H</i>	4	HD 195838 [†] , HD 196692
HD 206860	2011 Aug 17	S1/E1	<i>H</i>	10	HD 206043, HD 209166 [†]
	2012 Nov 12	E1/W1	<i>H</i>	2	HD 206043
HD 217014	2012 Nov 2	S1/E1	<i>H</i>	5	HD 215361 [†] , HD 218235
	2012 Nov 3	S1/E1	<i>H</i>	4	HD 215361 [†] , HD 218235
	2012 Nov 12	E1/W1	<i>H</i>	3	HD 215361 [†] , HD 218235

Table 1
(Continued)

Object	UT Date	Baseline	Filter	No. of Brackets	Calibrator HD
HD 217107	2012 Sep 13	E1/W1	<i>H</i>	6	HD 217131, HD 217877
	2012 Sep 14	E1/W1	<i>H</i>	3	HD 217131, HD 217877
	2012 Nov 4	S1/E1	<i>H</i>	5	HD 217131, HD 217877
HD 219623	2010 Sep 16	E1/W1	<i>H</i>	5	HD 221354
	2010 Sep 18	E1/W1	<i>H</i>	3	HD 221354
	2011 Aug 16	S1/E1	<i>H</i>	9	HD 218470 [†] , HD 221354
HD 222603	2011 Oct 2	S1/E1	<i>H</i>	8	HD 220825, HD 223438
	2012 Sep 13	W1/E1	<i>H</i>	3	HD 220825, HD 223438
	2012 Sep 14	W1/E1	<i>H</i>	2	HD 220825, HD 223438

Notes. Stars marked with a dagger [†] have estimated angular sizes >0.45 mas. See Section 2.1 for details.

The calibrated visibilities for each object are fit to the uniform disk θ_{UD} and limb-darkened θ_{LD} angular diameter functions, as defined in Hanbury Brown et al. (1974). We use a nonlinear least-squares fitting routine written in IDL to solve for each value of θ_{UD} and θ_{LD} as well as the errors, assuming a reduced $\chi^2 = 1$. In order to correct for limb-darkening, we use the linear limb-darkening coefficients from Claret (2000), calculated from ATLAS models. We employ an iterative procedure to identify the correct limb-darkening coefficients to use since those coefficients are dependent on the assumed atmospheric properties of the source. For main-sequence stars in the range of this sample, we find that only the assumed temperature contributes to a marked change in the limb-darkened value, whereas both surface gravity and metallicity do not provide additional constraints. As such, initial guesses of the object's temperature are used for the preliminary fit to determine θ_{LD} . This value for θ_{LD} is used with the measured bolometric flux to derive a temperature, as described in Section 2.3. This new temperature, often not so different from the initial guess, is then used to search for a tweaked limb-darkening coefficient, if needed. This procedure is typically repeated only once, for changes within the grid increments are 250 K, and the average correction needed is on the order of only a few percent.¹⁰

A list of the new angular diameters of the target stars can be found in Table 2. In Figures 1–4 we show the data and limb-darkened diameter fit for each star.

Of the 23 angular diameters we present in this paper, we measured the diameters of 5 stars known to host exoplanets: HD 10697, HD 11964, HD 186427, HD 217014, and HD 217107. Each of these stars has directly measured diameters in the literature from previous works, although with the exception of HD 217014, the previously published values have large errors (see Baines et al. 2008, 2009; van Belle & von Braun 2009). Numerous values for indirectly derived angular diameters are cited for these stars as well, spawning from the application of the IRFM, spectral energy distribution

¹⁰ Although the implementation of this iterative procedure was practiced within DT2, it was not within the analysis of DT1 diameters. Therefore, we performed a complete re-evaluation of the limb-darkened angular diameter fits for all the stars in DT1. We found that in response to the iterative procedure, the limb-darkening coefficient did not change for 19 of the 44 stars, even though the assumed initial temperature stayed the same for only 6 of these 19. Using the modified limb-darkening coefficients changed the diameters of only 11 of the 44 stars by $<0.1\sigma$ and the other 14 of the 44 stars by 0.1σ – 0.3σ . This change of much less than 1σ using modified coefficients is on the order of what is quoted for the errors in the limb-darkening coefficients themselves.

Table 2
New Angular Diameters

Star Name	No. of Obs.	Reduced χ^2	$\theta_{\text{UD}} \pm \sigma$ (mas)	μ_λ	$\theta_{\text{LD}} \pm \sigma$ (mas)	θ_{LD} % Err
HD 166	20	0.27	0.604 ± 0.009	0.386	0.624 ± 0.009	1.5
HD 6210	20	0.14	0.508 ± 0.006	0.307	0.520 ± 0.006	1.2
HD 10476	12	0.65	0.963 ± 0.004	0.410	1.000 ± 0.004	0.4
HD 10697	10	0.29	0.531 ± 0.012	0.362	0.547 ± 0.013	2.3
HD 11964	12	0.05	0.589 ± 0.015	0.362	0.607 ± 0.015	2.5
HD 16765	14	0.06	0.486 ± 0.007	0.307	0.497 ± 0.007	1.4
HD 21019	13	0.23	0.588 ± 0.015	0.382	0.606 ± 0.015	2.5
HD 38858	22	0.50	0.556 ± 0.009	0.349	0.572 ± 0.009	1.6
HD 69897	15	0.26	0.689 ± 0.013	0.307	0.706 ± 0.013	1.9
HD 130948	23	0.32	0.553 ± 0.011	0.347	0.569 ± 0.011	2.0
HD 136202	10	0.24	0.766 ± 0.023	0.307	0.785 ± 0.024	3.0
HD 140538	22	0.64	0.581 ± 0.015	0.347	0.597 ± 0.015	2.5
HD 157214	14	0.71	0.704 ± 0.012	0.347	0.725 ± 0.012	1.7
HD 158633	14	0.25	0.555 ± 0.010	0.386	0.573 ± 0.010	1.8
HD 168151	19	0.25	0.696 ± 0.008	0.307	0.713 ± 0.009	1.2
HD 186408	23	0.48	0.539 ± 0.011	0.347	0.554 ± 0.011	2.0
HD 186427	24	0.33	0.499 ± 0.011	0.347	0.513 ± 0.012	2.3
HD 195564	18	0.89	0.691 ± 0.030	0.362	0.712 ± 0.031	4.4
HD 206860	12	0.32	0.515 ± 0.014	0.347	0.530 ± 0.015	2.7
HD 217014	12	0.06	0.666 ± 0.011	0.342	0.685 ± 0.011	1.6
HD 217107	14	0.06	0.550 ± 0.008	0.382	0.567 ± 0.008	1.4
HD 219623	17	0.56	0.529 ± 0.016	0.312	0.542 ± 0.016	3.0
HD 222603	12	0.23	0.570 ± 0.012	0.242	0.581 ± 0.012	2.1

Note. Refer to Section 2.1 for details.

(SED) fitting, and surface brightness (SB) relations (Ramírez & Meléndez 2005; Casagrande et al. 2010; González Hernández & Bonifacio 2009; van Belle et al. 2008; Lafrasse et al. 2010). Our new measurements of the five exoplanet host star diameters are compared to the various literature values in Figure 5. Figure 5 shows that the SB technique (*squares*; Lafrasse et al. 2010) provides the best agreement with our directly measured diameters, where $\theta_{\text{this work}}/\theta_{\text{SB}} = 1.028 \pm 0.047$ is the average and standard deviation of the two methods. This is similar agreement of angular diameters measured in DT2 compared to values by other interferometers of $\theta_{\text{DT2}}/\theta_{\text{Reference}} = 1.008$.

2.2. Angular Diameters in the Literature and Stars with Multiple Measurements: The Anthology

All stars with published angular diameters are listed in Table 3, which includes 94 measurements from 24 papers. Like DT2, this collection only admits stars with diameter errors $<5\%$. Each star’s respective state of evolution is also considered, and we filter the results to stars on or near the main-sequence stars (luminosity class V or IV). There are several stars meeting these requirements that have multiple measurements, and we mark them as such in Table 3, reducing the total count from 94 down to 71 unique sources. In the bottom portion of Table 3, we list the weighted mean of these values for each of these sources with multiple measurements. These stars with measurements from multiple sources agree by $<1\%$ on average, with the exception of two cases: HD 146233 and HD 185395. The reason for the disagreement between these two measurements can only be associated with errors in calibration, and thus these data are omitted in the remainder of the analysis.

We do not include data for the rapidly rotating early-type stars observed by Monnier et al. (2007); van Belle et al. (2001) (Altair; α Aql; HR 7557; HD 187642: A7 Vn), Zhao et al. (2009); van Belle et al. (2006) (Alderamin; α Cep; HR 8162; HD 203280: A8 Vn), Zhao et al. (2009) (Rasalhague; α Oph;

HR 6556; HD 159561: A5 IVnn), Che et al. (2011) (Caph; β Cas; HR 21, HD 432: F2 III), and Che et al. (2011); McAlister et al. (2005) (Regulus; α Leo; HR 3982; HD 87901: B8 IVn) in Table 3. Due to their high rotational velocities observed at close to breakup speeds, observations of stars such as these show polar to equatorial temperature gradients on the order of several thousands of Kelvin. These characteristics make the stars unfavorable as calibrators for the relationships we derive in this paper linking color to effective temperature.

Finally, we note that we do not repeat the information in Table 3 for the low-mass K and M dwarfs studied in DT2. That selection consists of 33 stars, and their stellar properties are collected in a manner identical to the one followed here. Inclusion of the low-mass stars in DT2 leads to a total of 125 main-sequence stars studied with interferometry (33 from DT2, 69 from the literature + 23 from this work that are new).

2.3. Stellar Radii, Effective Temperatures, and Luminosities

Each measurement of the stellar angular diameter is converted to a linear radius using *Hipparcos* distances from van Leeuwen (2007). Errors in distance and interferometrically measured angular diameter are propagated into the uncertainty of the linear radius, however due to the close proximity of the targets to the Sun, the error in angular diameter is the dominant source of error, not the distance.

We present new measurements of the stellar bolometric flux F_{BOL} for all stars with interferometric measurements listed in Table 3. The technique is described in detail in van Belle et al. (2008), and is the same tool we employed in several previous works (for example, see von Braun et al. 2011a, 2011b; Boyajian et al. 2012a, 2012b). This approach involves collecting all broadband photometric measurements available in the literature and fitting an observed spectral template from the Pickles (1998) spectral atlas, essentially resulting in a model-independent bolometric flux for each star.

We have further expanded upon this technique by adding the spectrophotometric data found in the catalogs of Burnashev (1985), Kharitonov et al. (1988), Alekseeva et al. (1996, 1997), and Glushneva et al. (1998b, 1998a). Once an initial F_{BOL} fit was derived using the established technique, spectrophotometry from these catalogs was included in a second SED fit, which typically resulted in an improvement in the formal error for F_{BOL} dropping from $\sim 0.56\%$ to $\sim 0.14\%$ for 61 of our stars present in these catalogs. This iterative approach allowed us to screen for outlying spectrophotometric data that did not agree with the photometry; the multiple spectrophotometric data sets permitted a further check against each other for those stars present in multiple catalogs. *Note that only statistical uncertainties are taken into account, assuming that photometry from different sources have uncorrelated error bars.* Although our SED fitting code has the option to fit the data for reddening, we fixed $A_V = 0$ for these stars, given their distances were all $d < 40$ pc. For each star, Table 4 lists the input photometry and corresponding reference. The results and description of the iterative SED fitting routine are in Table 5.

The bolometric flux is then used to calculate the temperature of the star through the Stefan–Boltzmann equation:

$$T_{\text{eff}} = 2341(F_{\text{BOL}}/\theta^2)^{0.25}, \quad (1)$$

where the units for F_{BOL} are in 10^{-8} erg s $^{-1}$ cm $^{-2}$ and the angular diameter θ is the interferometrically measured limb-darkened angular diameter in units of milli-arcseconds. The

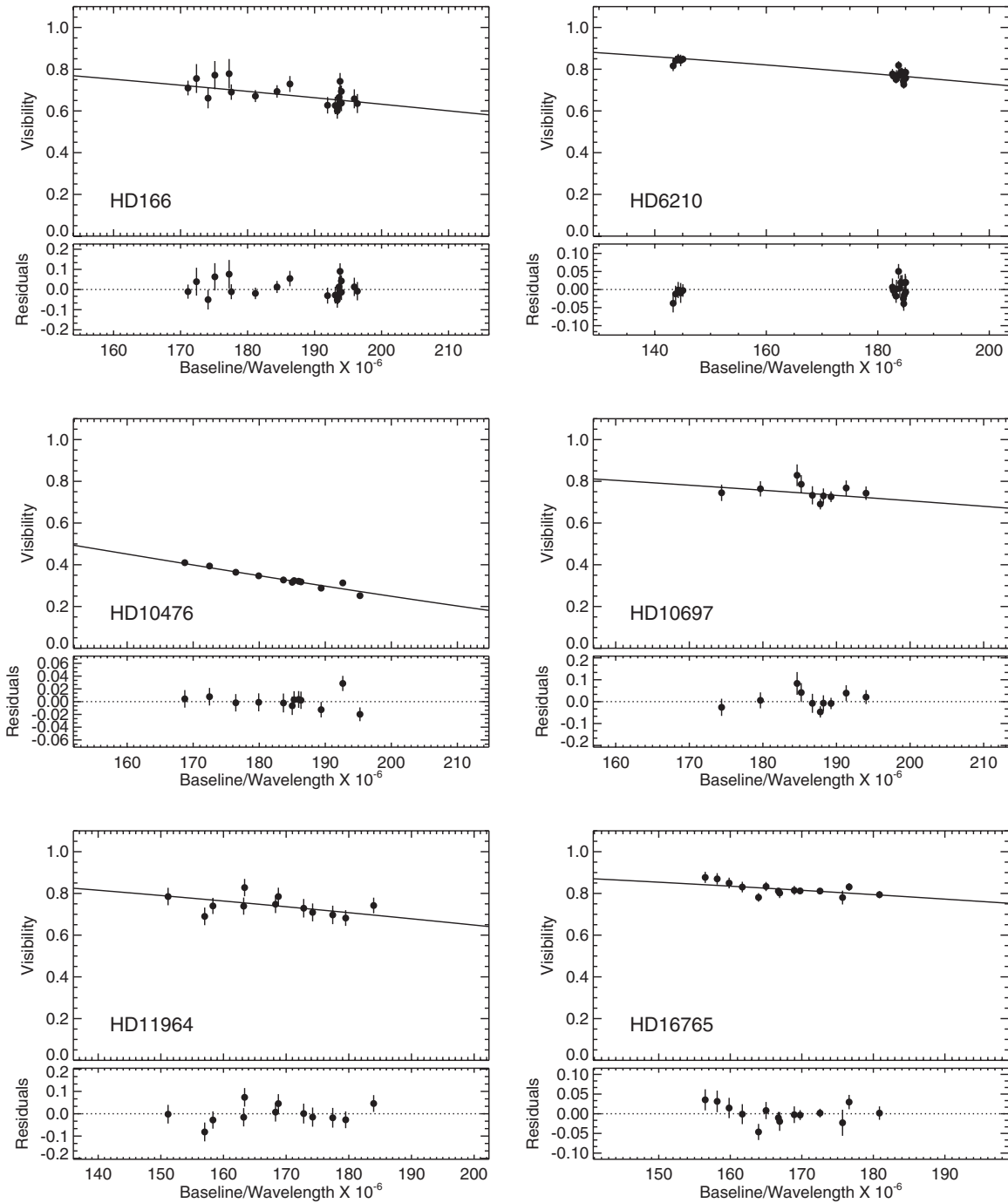


Figure 1. Calibrated observations plotted with the limb-darkened angular diameter fit for each star. See Section 2.1 for details.

stellar absolute luminosity is also calculated from the bolometric flux and *Hipparcos* distance. These values are given in Table 3, which includes properties for all new stars presented in this work (Section 2.1), as well as the collection of literature stars described in Section 2.2.

No single publication has metallicity estimates for all the stars in the sample, so instead we use metallicities gathered from the Anderson & Francis (2011) catalog, where the values they quote are averages from numerous available references. The four stars that have no metallicity data are HD 56537, HD 213558, HD 218396, and HD 222603, as noted in Table 3.¹¹ A histogram

showing the distribution of the stellar metallicities is plotted in Figure 6. Figure 6 shows that the metallicity distribution of the stars is fairly evenly distributed around $-0.5 < [\text{Fe}/\text{H}] < 0.4$, with a strong peak for stars with solar metallicity.

In Figures 7 and 8, we show H-R diagrams on the temperature–luminosity and temperature–radius planes for all the stars in Table 3 and the stars in Table 7 of DT2. In these figures, the color of the respective data point reflects the metallicity $[\text{Fe}/\text{H}]$ of the star, ranging from -1.26 to $+0.38$ dex, and the size of the respective data point reflects the linear radius R ranging from 0.1869 to $4.517 R_{\odot}$. Temperatures range from 3104 to 9711 K and luminosities range from 0.00338 to $58.457 L_{\odot}$. A representative view of main-sequence stellar properties is summarized in Table 6, showing the spectral type, number of

¹¹ Because these stars are A-type stars and are likely to have solar abundances, we assign them a $[\text{Fe}/\text{H}] = 0$ when constructing the color–temperature relations (Section 3).

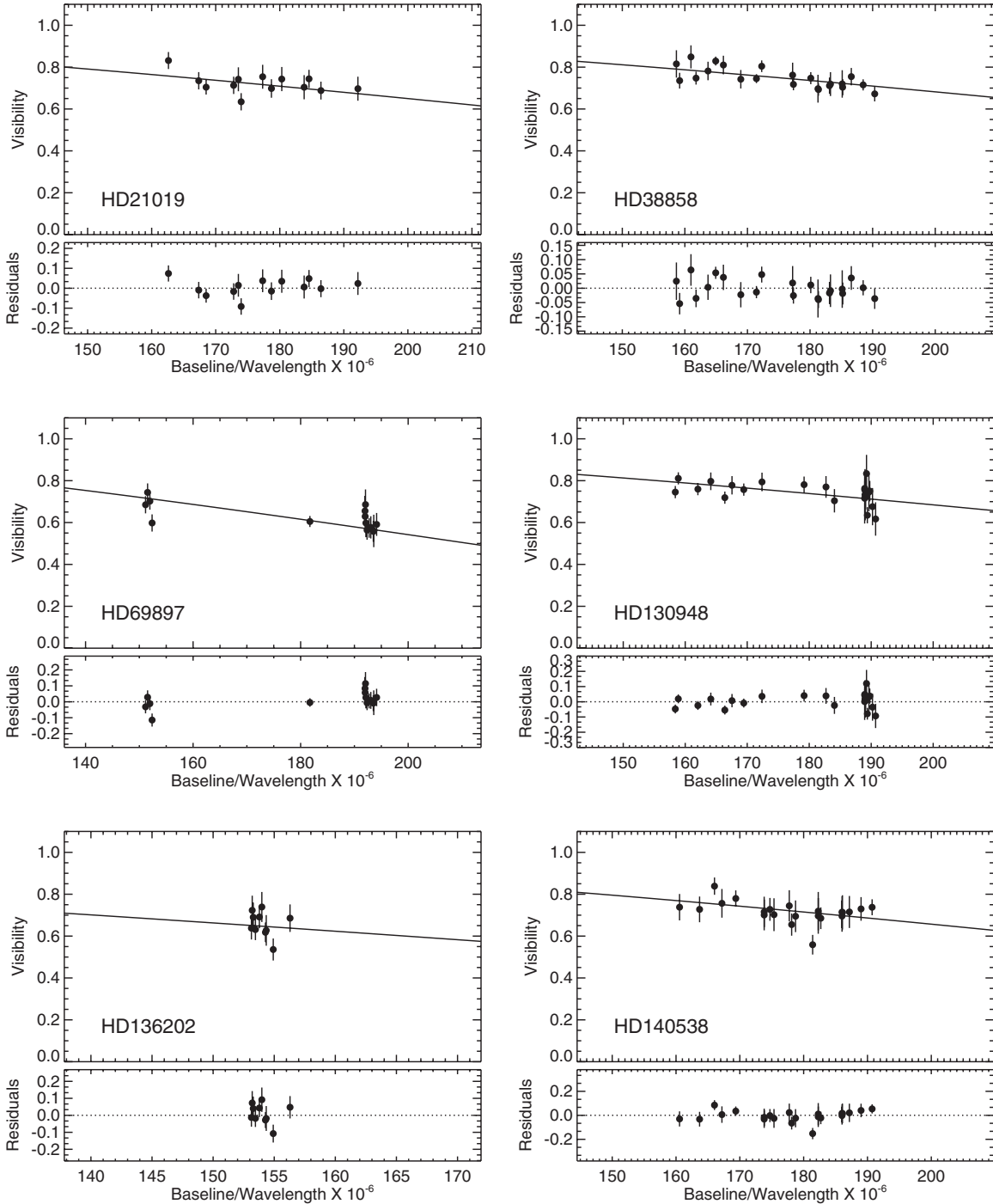


Figure 2. Calibrated observations plotted with the limb-darkened angular diameter fit for each star. See Section 2.1 for details.

stars n , mean color index, and mean effective temperature of each spectral type for the stars in Table 3.

Figure 9 marks the accomplishments of our work in supplying fundamental measurements to main-sequence stars over the past few years. Each panel in Figure 9 shows measurements plotted as black open circles, dubbed as *other*. These data are published measurements from works other than those included in DT1, DT2, and DT3 (this work). The *other* measurements also include stars in DT1, DT2, and DT3 that have multiple measurements, and thus are not unique contributions to the ensemble of data (i.e., stars marked with a \dagger in Table 3 and a \dagger or \ddagger in Table 7 of DT2). The descending panels add the contributions of DT1,

DT2, and DT3, indicated as red, green, and blue points within the plot, respectively. A breakdown of the number of stars in each category is as follows. The *other* category totals 52 stars. With the additional measurements presented in this work ($n = 23$), our contributions have more than doubled the number of existing main-sequence diameter measurements, yielding a total of 75 unique sources.

2.4. Estimated Stellar Masses and Ages

The sample of stars with interferometric measurements represents the largest (in linear size, inversely proportional to distance) and brightest (inversely proportional to the square

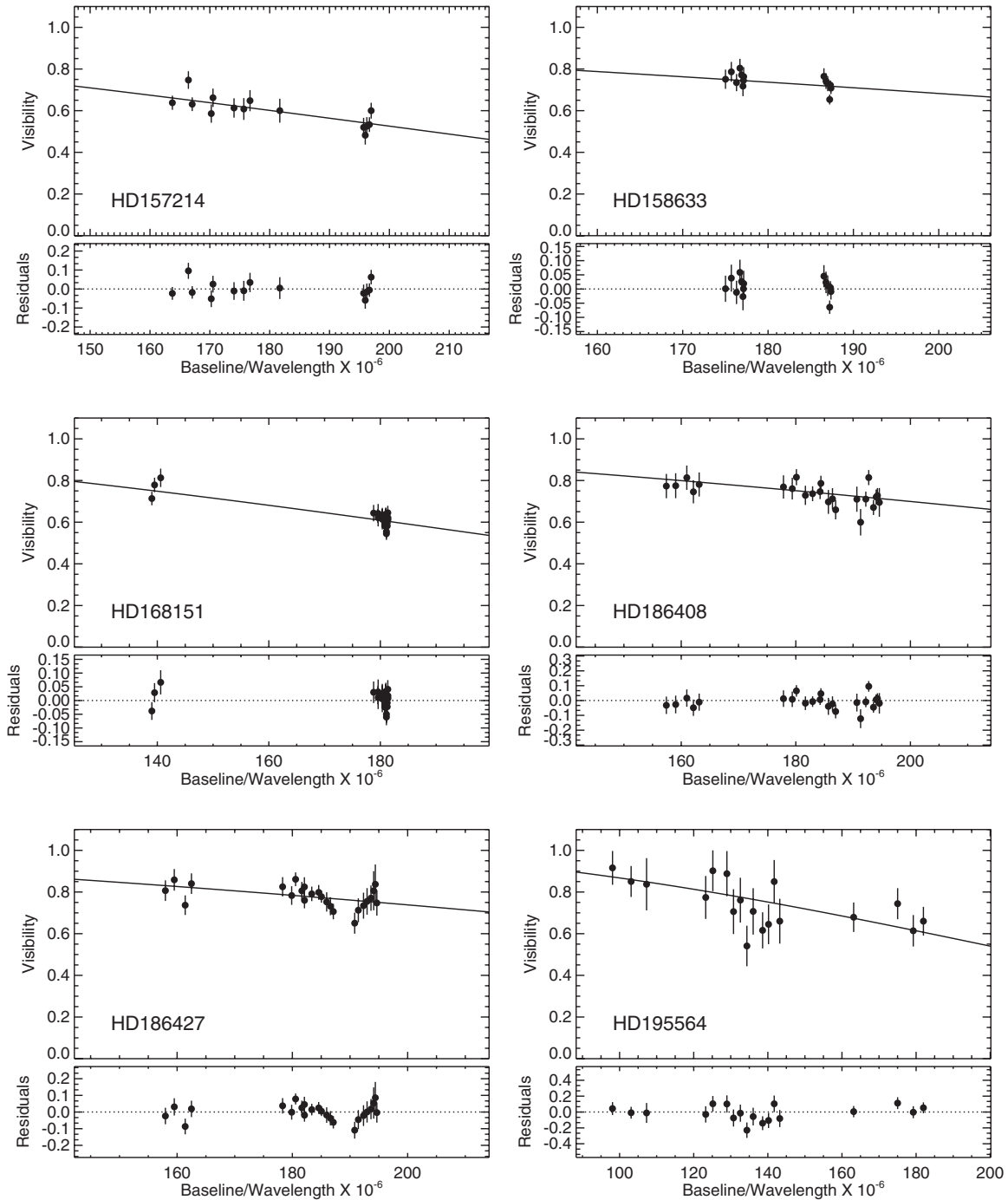


Figure 3. Calibrated observations plotted with the limb-darkened angular diameter fit for each star. See Section 2.1 for details.

of the distance) population of stars in the local neighborhood. Once we can determine to great accuracy the fundamental properties of these nearby stars, the knowledge may then be used to extend to much broader applications. For stars more massive than $\sim 0.8 M_{\odot}$, their physical properties are likely to have been affected by stellar evolution as they have lived long enough to display observable characteristics marking their journey off the zero-age main sequence (ZAMS).

We derive ages and masses for stars in Table 3 by fitting the measured radii and temperatures to the Yonsei–Yale (Y^2) stellar isochrones (Yi et al. 2001, 2003; Kim et al. 2002; Demarque et al. 2004). Isochrones are generated in increments of 0.1 Gyr steps for each star’s metallicity [Fe/H] (Table 3), assuming an alpha-

element enrichment of $[\alpha/\text{Fe}] = 0$, acceptable for stars with iron abundances close to solar. Errors in the age and mass are dependent on the measurement errors in radii and temperature but also in metallicity. However, metallicities for the stars in our sample are averages from numerous available references (Anderson & Francis 2011; see Section 2.3), and thus do not come with uncertainties. Simply assigning a characteristic error on this average metallicity is also not justified, because the stars cover a broad range in spectral type, and metallicities of solar-type stars are typically determined to greater accuracy than the stars on the hotter and cooler ends of the sample. Due to the complexity of this aspect, we refrain from quoting errors in the isochrone ages and masses. Typical uncertainty in age and mass

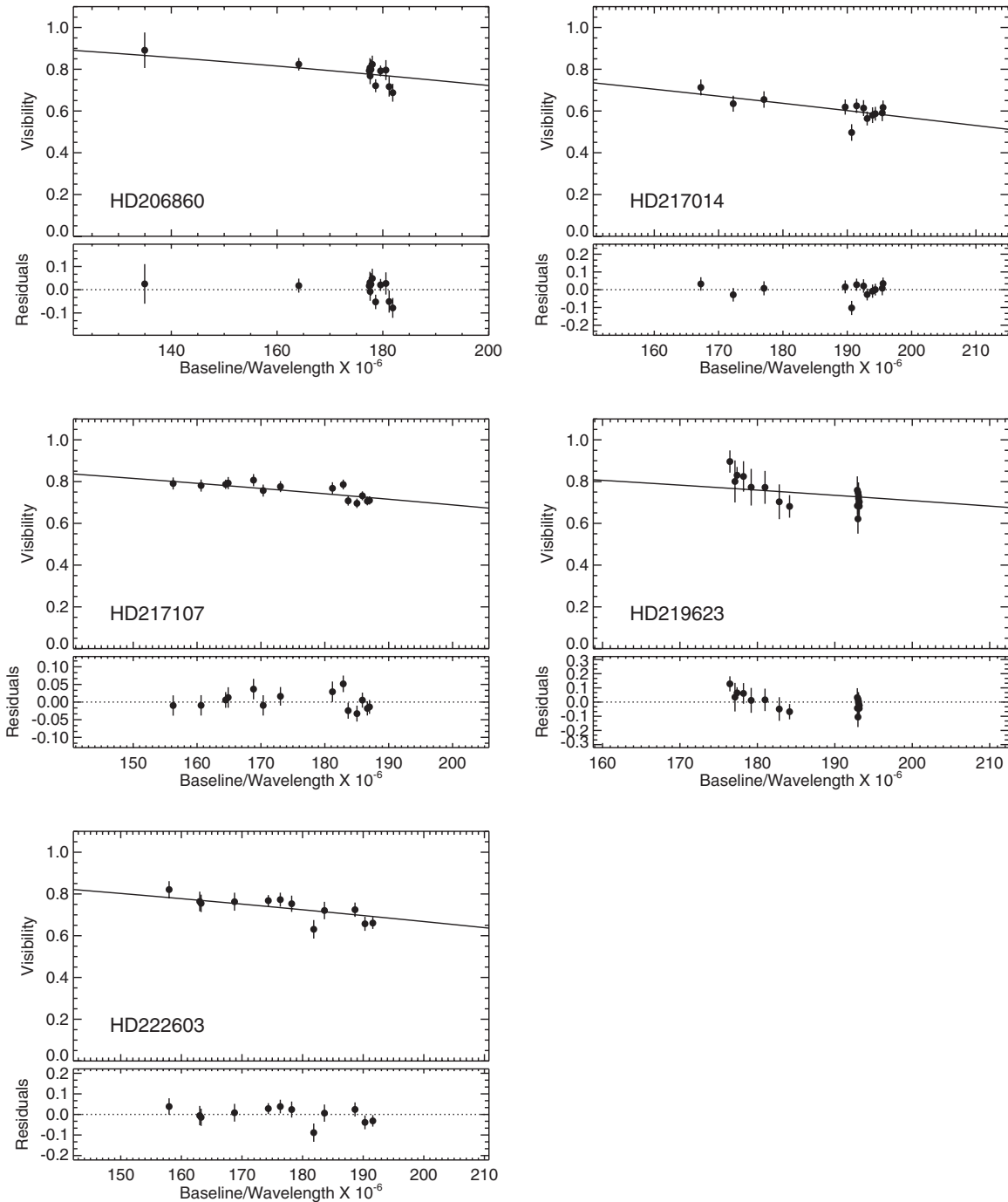


Figure 4. Calibrated observations plotted with the limb-darkened angular diameter fit for each star. See Section 2.1 for details.

can be estimated given a solar-type star ($T_{\text{eff}} = 5778$ K and $R = 1 R_{\odot}$, assuming a very conservative 2% and 4% error in T_{eff} and R , respectively), are estimated to be ± 5 Gyr, and 5% in mass. These ages become less reliable for the lowest luminosity stars, as the sensitivity to age from isochrone fitting is minimal. This ultimately leads to unrealistic ages greater than the age of the universe, and thus this region should be regarded with special caution. On the other hand, the ages and masses of the earlier-type stars will be determined to better precision (uncertainty of 20% and 1%, in age and mass, respectively).

Figures 10 and 11 show the data on the mass–radius and mass–temperature planes, where again the color of the data point reflects the metallicity of the star, and the size of the data

point reflects the linear radius.¹² Inspection of Figures 10 and 11 clearly shows that for more massive stars, stellar evolution has broadened the correlation between these parameters with stellar age.

On the mass–luminosity plane however, broadening due to evolution is not observed (e.g., see Böhm-Vitense 1989, chap. 9.6): the data in the top panel of Figure 12 show the stellar mass versus luminosity, where the size of each data point reflects the linear size of the corresponding star. The bottom panel plots the data without radius information (and thus making

¹² As opposed to isochrone fitting, masses for the low-mass stars studied in DT2 are found using the empirically based mass–luminosity relation from Henry & McCarthy (1993, see the text in DT2 for details).

Table 3
Angular Diameter Anthology

Star HD	Spectral Type	Metallicity [Fe/H]	Radius (R_{\odot})	Radius Reference	F_{BOL} ($10^{-8} \text{ erg s}^{-1} \text{ cm}^{-2}$)	L (L_{\odot})	T_{eff} (K)	Age (Gyr) ^a	Mass (M_{\odot}) ^a
166	G8V	0.08	0.9172 ± 0.0090	This work	10.4400 ± 0.0600	0.6078 ± 0.0099	5327 ± 39	9.6	0.889
3651	K0V	0.15	0.9470 ± 0.0320	1	13.4700 ± 0.0600	0.5131 ± 0.0043	5046 ± 86	14.9	0.839
4614	F9V	-0.28	1.0386 ± 0.0038	2	111.6000 ± 0.1940	1.2321 ± 0.0074	5973 ± 8	5.9	0.967
5015	F8V	0.04	1.7426 ± 0.0233	2	31.5400 ± 0.0590	3.4521 ± 0.0432	5965 ± 35	5.3	1.194
6210	F6V ^b	-0.01	4.5170 ± 0.1522	This work	12.3800 ± 0.0227	25.1634 ± 1.5861	6089 ± 35	1.3	1.953
9826 [†]	F8V	0.08	1.6310 ± 0.0140	1	60.1500 ± 0.1260	3.4089 ± 0.0189	6177 ± 25	3.3	1.304
9826 [†]	F8V	0.08	1.7000 ± 0.0200	3	60.1500 ± 0.1260	3.4089 ± 0.0189	6027 ± 26	3.8	1.297
10476	K0V	-0.02	0.8101 ± 0.0045	This work	25.1400 ± 0.1100	0.4443 ± 0.0039	5242 ± 12	5.3	0.862
10697	G3Va	0.12	1.9155 ± 0.0521	This work	8.7400 ± 0.0600	2.8888 ± 0.0833	5442 ± 65	7.4	1.138
10700	G8.5V	-0.48	0.8154 ± 0.0122	4	112.6000 ± 0.0787	0.4674 ± 0.0007	5290 ± 39	14.9	0.733
11964	G9V CN+1	0.14	2.1425 ± 0.0687	This work	7.7500 ± 0.0500	2.6056 ± 0.1041	5013 ± 62	7.8	1.133
16765	F7V	-0.15	1.2080 ± 0.0288	This work	13.4200 ± 0.1000	2.1332 ± 0.0825	6356 ± 46	2.1	1.168
16895	F7V	0.00	1.3190 ± 0.0109	2	58.0500 ± 0.0796	2.2390 ± 0.0114	6153 ± 25	3.5	1.177
19373 [‡]	G0IV-V	0.08	1.4124 ± 0.0092	2	60.0400 ± 0.0523	2.0781 ± 0.0102	5838 ± 19	6.8	1.097
19373 [‡]	G0IV-V	0.08	1.5090 ± 0.0580	5	60.0400 ± 0.0523	2.0781 ± 0.0102	5648 ± 106	9.1	1.049
19994	F8.5V	0.17	1.9300 ± 0.0670	1	25.3200 ± 0.0458	4.0229 ± 0.0514	5916 ± 98	4.8	1.275
20630	G5V	0.05	0.9193 ± 0.0247	2	31.3000 ± 0.0443	0.8146 ± 0.0042	5723 ± 76	0.2	1.037
21019	G2V m-0.25	-0.41	2.4214 ± 0.0764	This work	9.3700 ± 0.0200	4.0279 ± 0.1529	5261 ± 65	7.2	1.056
22484	F9IV-V	-0.09	1.6219 ± 0.0242	2	50.3600 ± 0.0448	3.0585 ± 0.0462	5998 ± 39	5.7	1.140
23249	K1IV	0.12	2.3267 ± 0.0286	6	115.0000 ± 0.0815	2.9282 ± 0.0118	4955 ± 30	7.4	1.149
30652 [‡]	F6IV-V	0.00	1.3233 ± 0.0042	2	133.3000 ± 0.0092	2.7033 ± 0.0074	6439 ± 8	1.8	1.262
30652 [‡]	F6IV-V	0.00	1.2170 ± 0.0430	5	133.3000 ± 0.0092	2.7033 ± 0.0074	6701 ± 114	0.3	1.326
34411	G1V	0.05	1.3314 ± 0.0211	2	35.6200 ± 0.0442	1.7704 ± 0.0127	5774 ± 44	7.8	1.049
38858	G2V	-0.22	0.9331 ± 0.0162	This work	11.0700 ± 0.0300	0.7943 ± 0.0101	5646 ± 45	8.6	0.886
39587	G0IV-V	-0.04	0.9791 ± 0.0091	2	44.5100 ± 0.0764	1.0407 ± 0.0052	5898 ± 25	1.5	1.052
48737	F5IV-V	0.14	2.7098 ± 0.0206	2	115.1000 ± 0.1540	11.6156 ± 0.0809	6478 ± 21	1.6	1.746
48915 [†]	A0mA1Va	0.36	1.7130 ± 0.0090	7	10780.0000 ± 0.2160	23.3533 ± 0.1946	9705 ± 14	0.1	2.281
48915 [†]	A0mA1Va	0.36	1.6714 ± 0.0221	8	10780.0000 ± 0.2160	23.3533 ± 0.1946	9824 ± 62	0.1	2.283
48915 [†]	A0mA1Va	0.36	1.6805 ± 0.0248	9	10780.0000 ± 0.2160	23.3533 ± 0.1946	9797 ± 69	0.1	2.283
48915 [†]	A0mA1Va	0.36	1.7120 ± 0.0089	10	10780.0000 ± 0.2160	23.3533 ± 0.1946	9707 ± 15	0.1	2.281
48915 [†]	A0mA1Va	0.36	1.6989 ± 0.0314	11	10780.0000 ± 0.2160	23.3533 ± 0.1946	9744 ± 88	0.1	2.283
49933	F2V ^b	-0.39	1.4200 ± 0.0400	12	12.7800 ± 0.0800	3.5077 ± 0.0902	6635 ± 90	3.1	1.189
56537	A3V ^b	...	2.7773 ± 0.0469	2	91.9000 ± 0.1440	27.3901 ± 0.3416	7932 ± 62	0.8	2.098
58946	F0V ^b	-0.25	1.6553 ± 0.0275	2	49.9500 ± 0.1030	5.0681 ± 0.0451	6738 ± 55	2.3	1.344
61421 [†]	F5IV-V	-0.02	2.0362 ± 0.0145	13	1832.0000 ± 2.1100	7.0480 ± 0.0629	6597 ± 18	2.1	1.510
61421 [†]	F5IV-V	-0.02	2.0513 ± 0.0280	14	1832.0000 ± 2.1100	7.0480 ± 0.0629	6573 ± 42	2.1	1.510
61421 [†]	F5IV-V	-0.02	2.0574 ± 0.0223	11	1832.0000 ± 2.1100	7.0480 ± 0.0629	6563 ± 33	2.1	1.510
61421 [†]	F5IV-V	-0.02	2.0581 ± 0.0220	15	1832.0000 ± 2.1100	7.0480 ± 0.0629	6562 ± 32	2.1	1.510
69897	F6V	-0.26	1.3870 ± 0.0276	This work	23.4400 ± 0.1800	2.4378 ± 0.0341	6130 ± 58	5.8	1.070
75732	K0IV-V	0.35	0.9434 ± 0.0101	16	12.0400 ± 0.1000	0.5712 ± 0.0116	5172 ± 18	10.2	0.904
81937	F0IV ^b	0.17	2.9018 ± 0.0262	2	83.6200 ± 0.1070	14.7743 ± 0.1142	6651 ± 27	1.3	1.862
82328	F5.5IV-V	-0.16	2.3653 ± 0.0082	2	134.3000 ± 0.1090	7.6011 ± 0.0293	6238 ± 10	3.3	1.374
82885	G8+V	0.32	1.0029 ± 0.0158	2	18.7500 ± 0.0190	0.7550 ± 0.0055	5376 ± 43	7.9	0.964
86728	G4V	0.19	1.2466 ± 0.0205	2	19.7300 ± 0.0344	1.3915 ± 0.0136	5619 ± 44	8.9	1.026
90839	F8V	-0.11	1.0912 ± 0.0200	2	31.0700 ± 0.2400	1.5807 ± 0.0166	6203 ± 56	1.4	1.128
95418	A1IV	-0.03	3.0210 ± 0.0383	2	313.9000 ± 0.5780	58.4567 ± 0.4699	9193 ± 56	0.5	2.513
97603 [‡]	A5IV(n)	-0.18	2.5569 ± 0.0203	2	226.5000 ± 0.2990	22.6453 ± 0.2050	7881 ± 27	1.0	1.924
97603 [‡]	A5IV(n)	-0.18	2.2810 ± 0.1060	5	226.5000 ± 0.2990	22.6453 ± 0.2050	8297 ± 184	0.8	1.958
101501	G8V	-0.03	0.9400 ± 0.0100	2	21.9100 ± 0.0900	0.6306 ± 0.0041	5309 ± 27	14.2	0.841
102647 [†]	A3Va	0.07	1.6570 ± 0.0600	5	351.6000 ± 0.6490	13.2530 ± 0.1536	8604 ± 152	0.1	1.926
102647 [†]	A3Va	0.07	1.7134 ± 0.0334	4	351.6000 ± 0.6490	13.2530 ± 0.1536	8421 ± 79	0.3	1.911
102870	F8.5IV-V	0.12	1.6807 ± 0.0079	2	91.5600 ± 0.1120	3.4068 ± 0.0169	6054 ± 13	3.6	1.310
103095 [†]	K1V	-1.26	0.6805 ± 0.0057	2	8.3600 ± 0.0300	0.2153 ± 0.0018	4771 ± 18	14.9	0.611
103095 [†]	K1V	-1.26	0.6640 ± 0.0150	17	8.3600 ± 0.0300	0.2153 ± 0.0018	4831 ± 25	14.9	0.611
109358 [†]	G0V	-0.19	1.1229 ± 0.0277	2	52.1600 ± 0.2100	1.1573 ± 0.0061	5654 ± 69	12.3	0.894
109358 [†]	G0V	-0.19	1.0250 ± 0.0500	5	52.1600 ± 0.2100	1.1573 ± 0.0061	5897 ± 143	5.8	0.977
114710	G0V	0.02	1.1056 ± 0.0109	2	53.2700 ± 0.0876	1.3830 ± 0.0049	5957 ± 29	3.7	1.079
117176	G5V	-0.06	1.9680 ± 0.0470	1	28.9600 ± 0.0489	2.9194 ± 0.0257	5406 ± 64	7.9	1.091
118098	A2Van	-0.26	2.0791 ± 0.0248	2	103.9000 ± 0.2000	16.6958 ± 0.1476	8097 ± 43	1.0	1.785
120136	F7IV-V	0.24	1.3310 ± 0.0270	1	39.5100 ± 0.0355	3.0021 ± 0.0189	6620 ± 67	0.3	1.403
121370 [†]	G0IV	0.25	2.7932 ± 0.0944	14	219.4000 ± 0.3670	8.8763 ± 0.2513	5967 ± 92	2.3	1.649
121370 [†]	G0IV	0.25	2.7797 ± 0.0498	11	219.4000 ± 0.3670	8.8763 ± 0.2513	5981 ± 33	2.3	1.649
121370 [†]	G0IV	0.25	2.6952 ± 0.0538	6	219.4000 ± 0.3670	8.8763 ± 0.2513	6074 ± 43	2.2	1.658
126660 [†]	F7V	-0.02	1.7330 ± 0.0113	2	60.9700 ± 0.0537	4.0103 ± 0.0167	6212 ± 20	3.4	1.314
126660 [†]	F7V	-0.02	1.7720 ± 0.0870	5	60.9700 ± 0.0537	4.0103 ± 0.0167	6154 ± 150	3.8	1.294

Table 3
(Continued)

Star HD	Spectral Type	Metallicity [Fe/H]	Radius (R_{\odot})	Radius Reference	F_{BOL} ($10^{-8} \text{ erg s}^{-1} \text{ cm}^{-2}$)	L (L_{\odot})	T_{eff} (K)	Age (Gyr) ^a	Mass (M_{\odot}) ^a
128167	F4Vkf2mF1	-0.32	1.4307 \pm 0.0228	2	40.3900 \pm 0.0496	3.1541 \pm 0.0253	6435 \pm 50	4.1	1.143
128620	G2V	0.20	1.2329 \pm 0.0037	18	2716.0000 \pm 2.6700	1.5159 \pm 0.0051	5793 \pm 7	5.2	1.106
128621 [†]	K2IV C2+I**	0.21	0.8691 \pm 0.0035	19	898.3000 \pm 1.1200	0.5014 \pm 0.0017	5232 \pm 9	4.5	0.921
128621 [†]	K2IV C2+I**	0.21	0.8630 \pm 0.0050	18	898.3000 \pm 1.1200	0.5014 \pm 0.0017	5232 \pm 15	4.5	0.921
130948	F9IV-V	-0.05	1.1119 \pm 0.0229	This work	12.0900 \pm 0.0800	1.2437 \pm 0.0174	5787 \pm 57	7.5	0.989
131156	G7V	-0.14	0.8627 \pm 0.0107	2	43.0400 \pm 0.0739	0.6041 \pm 0.0040	5483 \pm 32	6.5	0.881
136202	F8IV	-0.04	2.1427 \pm 0.0670	This work	21.0700 \pm 0.0228	4.2283 \pm 0.0624	5661 \pm 87	5.3	1.217
140538	G5V	0.05	0.9410 \pm 0.0254	This work	12.4600 \pm 0.1800	0.8340 \pm 0.0201	5692 \pm 74	2.1	1.014
141795	kA2hA5mA7V	0.38	1.7834 \pm 0.0403	2	77.5700 \pm 0.0927	11.2725 \pm 0.0935	7928 \pm 88	0.1	1.917
142860 [†]	F6V	-0.17	1.4723 \pm 0.0065	2	73.8500 \pm 0.1080	2.9136 \pm 0.0125	6221 \pm 13	4.4	1.164
142860 [†]	F6V	-0.17	1.3890 \pm 0.0650	5	73.8500 \pm 0.1080	2.9136 \pm 0.0125	6369 \pm 148	3.3	1.200
146233 ^{†,c}	G2V	0.02	1.1656 \pm 0.0264	2	17.3400 \pm 0.0900	1.0438 \pm 0.0120	5409 \pm 59	14.9	0.892
146233 ^{†,c}	G2V	0.02	1.0100 \pm 0.0090	20	17.3400 \pm 0.0900	1.0438 \pm 0.0120	5811 \pm 28	3.5	1.031
150680 [†]	G2IV	0.02	2.7267 \pm 0.0603	11	196.2000 \pm 0.1680	7.0184 \pm 0.0710	5695 \pm 61	3.3	1.438
150680 [†]	G2IV	0.02	2.8684 \pm 0.1047	14	196.2000 \pm 0.1680	7.0184 \pm 0.0710	5552 \pm 100	3.1	1.469
157214	G0V	-0.37	1.1159 \pm 0.0191	This work	18.9700 \pm 0.0971	1.2130 \pm 0.0107	5738 \pm 48	13.7	0.847
158633	K0V ^b	-0.41	0.7891 \pm 0.0144	This work	8.0100 \pm 0.0500	0.4090 \pm 0.0040	5203 \pm 46	14.9	0.729
161797	G5IV	0.23	1.7448 \pm 0.0349	11	116.4000 \pm 0.1240	2.5043 \pm 0.0072	5502 \pm 55	8.0	1.118
162003	F5IV-V	-0.03	2.3289 \pm 0.0671	2	37.0400 \pm 0.0418	6.0174 \pm 0.1239	5928 \pm 81	3.8	1.349
164259	F2V	-0.03	1.9614 \pm 0.0713	2	34.6900 \pm 0.1600	5.9942 \pm 0.0999	6454 \pm 113	2.4	1.450
168151	F5V ^b	-0.28	1.7577 \pm 0.0225	This work	25.3500 \pm 0.0231	4.1486 \pm 0.0325	6221 \pm 39	5.0	1.156
173667	F5.5IV-V	-0.03	2.0644 \pm 0.0166	2	52.3100 \pm 0.0798	6.0126 \pm 0.0585	6296 \pm 19	2.7	1.443
173701	K0V	0.24	0.9520 \pm 0.0210	21	2.8900 \pm 0.0500 ^d	0.6412 \pm 0.0112	5297 \pm 53	9.0	0.922
175726	G5V	-0.09	0.9870 \pm 0.0230	21	5.4000 \pm 0.1000 ^d	1.1817 \pm 0.0387	6067 \pm 67	0.2	1.097
177153	G0V	-0.06	1.2890 \pm 0.0370	21	3.3900 \pm 0.0700 ^d	1.8167 \pm 0.0762	5909 \pm 69	6.8	1.051
177724	A0IV-Vnn	-0.52	2.4487 \pm 0.0464	2	181.1000 \pm 0.3110	36.5649 \pm 0.3044	9078 \pm 86	0.8	2.006
181420	F2V	-0.03	1.7300 \pm 0.0840	21	6.0000 \pm 0.2000 ^d	4.2183 \pm 0.2383	6283 \pm 106	3.1	1.334
182572	G8IV ^b	0.34	1.3785 \pm 0.0418	2	24.1000 \pm 0.0409	1.7293 \pm 0.0140	5643 \pm 84	5.9	1.147
182736	G0IV	-0.06	2.7030 \pm 0.0710	21	4.7700 \pm 0.0800 ^d	4.9364 \pm 0.2476	5239 \pm 37	3.8	1.353
185395 ^{†,c}	F3+V	0.02	1.6965 \pm 0.0301	2	39.2000 \pm 0.0366	4.1053 \pm 0.0229	6313 \pm 55	2.9	1.344
185395 ^{†,c}	F3+V	0.02	1.5030 \pm 0.0070	3	39.2000 \pm 0.0366	4.1053 \pm 0.0229	6719 \pm 13	1.3	1.395
186408	G1.5V	0.05	1.2551 \pm 0.0261	This work	11.2500 \pm 0.0187	1.5572 \pm 0.0179	5760 \pm 57	7.9	1.032
186427	G3V	0.04	1.1689 \pm 0.0274	This work	9.1080 \pm 0.0145	1.2768 \pm 0.0148	5678 \pm 66	8.9	0.989
187637	F5V	-0.09	1.3060 \pm 0.0470	21	2.5500 \pm 0.0500 ^d	2.1936 \pm 0.1144	6155 \pm 85	3.9	1.144
188512	G8IV-V	-0.14	3.2103 \pm 0.1328	22	92.7100 \pm 0.0797	5.4196 \pm 0.0301	4920 \pm 102	7.3	1.114
190360	G7IV-V	0.21	1.2000 \pm 0.0330	1	14.4300 \pm 0.0800	1.1301 \pm 0.0137	5461 \pm 75	11.3	0.971
190406	G0V	0.03	1.1153 \pm 0.0211	23	12.5300 \pm 0.0159	1.2323 \pm 0.0154	5763 \pm 49	6.9	1.010
195564	G2V	0.06	1.8673 \pm 0.0833	This work	14.5800 \pm 0.0900	2.7046 \pm 0.0466	5421 \pm 118	8.2	1.097
198149	K0IV	-0.11	4.0638 \pm 0.0617	22	127.8000 \pm 0.1020	8.1018 \pm 0.0262	4835 \pm 37	8.4	1.083
206860	G0IV-V	-0.16	1.0189 \pm 0.0291	This work	11.0300 \pm 0.0700	1.0992 \pm 0.0190	5860 \pm 83	5.8	0.975
210027	F5V	-0.13	1.5260 \pm 0.0680	5	77.4600 \pm 0.0702	3.3180 \pm 0.0491	6324 \pm 139	3.4	1.238
210418	A2V ^b	-0.38	2.6225 \pm 0.0829	2	95.0200 \pm 0.2470	23.7012 \pm 1.1418	7872 \pm 82	1.1	1.848
213558	A1V ^b	...	2.1432 \pm 0.0737	2	89.7800 \pm 0.1470	27.6750 \pm 0.2138	9050 \pm 157	0.4	2.194
215648	F6V	-0.26	1.9117 \pm 0.0160	2	54.5300 \pm 0.0684	4.5118 \pm 0.0285	6090 \pm 22	5.2	1.164
216956	A4V	0.20	1.8451 \pm 0.0202	4	846.3000 \pm 1.0600	15.6458 \pm 0.1150	8459 \pm 44	0.2	2.025
217014 [†]	G3V	0.17	1.2660 \pm 0.0460	1	17.0800 \pm 0.0313	1.2954 \pm 0.0155	5503 \pm 99	11.3	0.980
217014 [†]	G3V	0.17	1.1501 \pm 0.0195	This work	17.0800 \pm 0.0313	1.2962 \pm 0.0156	5750 \pm 46	5.6	1.064
217107	G8IV-V	0.31	1.2104 \pm 0.0195	This work	9.0400 \pm 0.0800	1.0951 \pm 0.0338	5391 \pm 40	11.9	0.969
218396	F0+ (lambda Boo)	...	1.4400 \pm 0.0600	24	10.2500 \pm 0.0500	4.9571 \pm 0.2745	7163 \pm 84	0.2	1.507
219623	F8V	0.04	1.1950 \pm 0.0359	This work	15.2600 \pm 0.1200	1.9987 \pm 0.0265	6285 \pm 94	1.2	1.215
222368	F7V	-0.14	1.5949 \pm 0.0137	2	57.3100 \pm 0.0798	3.3576 \pm 0.0146	6192 \pm 26	4.6	1.184
222603	A7V	...	2.0403 \pm 0.0451	This work	40.2200 \pm 0.0933	13.3897 \pm 0.1692	7734 \pm 80	0.9	1.806
Star [†]			$\langle R \rangle \pm \sigma$ (R_{\odot})				$\langle T_{\text{eff}} \rangle \pm \sigma$ (K)	$\langle \text{Mass} \rangle$ (M_{\odot})	$\langle \text{Age} \rangle$ (Gyr)
9826			1.6537 \pm 0.0324				6104 \pm 75	3.6	1.300
19373			1.4148 \pm 0.0149				5832 \pm 33	6.9	1.094
30652			1.3223 \pm 0.0103				6441 \pm 19	1.8	1.262
48915			1.7074 \pm 0.0124				9711 \pm 23	0.1	2.281
61421			2.0468 \pm 0.0102				6582 \pm 16	2.1	1.510
97603			2.5471 \pm 0.0510				7889 \pm 60	1.0	1.924
103095			0.6784 \pm 0.0055				4791 \pm 28	14.9	0.611
109358			1.0999 \pm 0.0415				5700 \pm 95	11.3	0.906
121370			2.7475 \pm 0.0431				6012 \pm 45	2.3	1.648
126660			1.7336 \pm 0.0112				6211 \pm 19	3.4	1.314
128621			0.8671 \pm 0.0029				5232 \pm 8	4.5	0.921

Table 3
(Continued)

Star [†]	$\langle R \rangle \pm \sigma$ (R_{\odot})	$\langle T_{\text{eff}} \rangle \pm \sigma$ (K)	$\langle \text{Mass} \rangle$ (M_{\odot})	$\langle \text{Age} \rangle$ (Gyr)
142860	1.4715 ± 0.0082	6222 ± 13	4.3	1.168
150680	2.7620 ± 0.0613	5656 ± 63	3.3	1.438
217014	1.1678 ± 0.0416	5706 ± 95	6.4	1.054

Notes. All measurements of stellar radii found in the literature, with precision of better than 5%. Stars with multiple measurements are marked with a [†]. Metallicities are from Anderson & Francis (2011) and parallaxes are from van Leeuwen (2007). The bottom portion of the table lists the stars with multiple measurements, and the weighted mean for their radii and temperatures (all other parameters remain unaffected when combining the multiple sources for measured radii). All bolometric flux, luminosity, and temperature values are computed/measured in this work. See Sections 2.2–2.4 for details.

^a Stellar mass and age determined by interpolating the Y^2 isochrones to match the measured stellar radii, effective temperature, and metallicity.

^b Spectral type from SIMBAD.

^c The measurements and associated errors are incommensurate for the two stars HD 146233 and HD 185395, likely caused from calibration errors. No measurement averages are taken due to this.

^d Bolometric flux from Huber et al. (2012).

References. (1) Baines et al. 2008; (2) Boyajian et al. 2012a; (3) Ligi et al. 2012; (4) Di Folco et al. 2004; (5) van Belle & von Braun 2009; (6) Thévenin et al. 2005; (7) Davis et al. 2011; (8) Hanbury Brown et al. 1974; (9) Davis & Tango 1986; (10) Kervella et al. 2003a; (11) Mozurkewich et al. 2003; (12) Bigot et al. 2011; (13) Chiavassa et al. 2012; (14) Nordgren et al. 2001; (15) Kervella et al. 2004; (16) von Braun et al. 2011b; (17) Creevey et al. 2012; (18) Kervella et al. 2003b; (19) Bigot et al. 2006; (20) Bazot et al. 2011; (21) Huber et al. 2012; (22) Nordgren et al. 1999; (23) Crepp et al. 2012; (24) Baines et al. 2012.

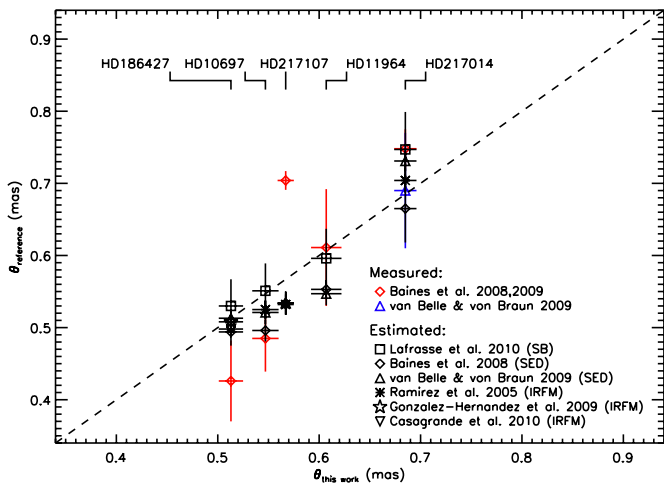


Figure 5. New angular diameter measurements of exoplanet host stars compared to previously published measurements from Baines et al. (2008), Baines et al. (2009), and van Belle & von Braun (2009). We also show the agreement with indirect diameter determinations using the surface brightness (SB) relation (Lafrasse et al. 2010), spectral energy distribution (SED) fitting (Baines et al. 2008, 2009; van Belle & von Braun 2009), and the infrared flux method (IRFM; Ramirez & Meléndez 2005; González Hernández & Bonifacio 2009; Casagrande et al. 2010). Each of the four objects is identified with a vertical marker at the top end of the plot. The dashed line indicates a 1:1 relation. See legend within plot and Section 2.1 for details.

(A color version of this figure is available in the online journal.)

the data points smaller), to illustrate more clearly that only the stellar metallicity is a contributing factor in the correlation between the stellar mass and luminosity. Note that the masses for the low-mass stars were derived using empirically based mass–luminosity relations (as described in DT2), which are currently independent of metallicity, whereas masses for the higher mass stars described here were found by isochrone fitting, with metallicity as a valid input parameter.

3. COLOR–TEMPERATURE RELATIONS

We use the full range of interferometrically characterized stars to determine relations linking color index to effective temperature. This sample consists of luminosity class V and IV

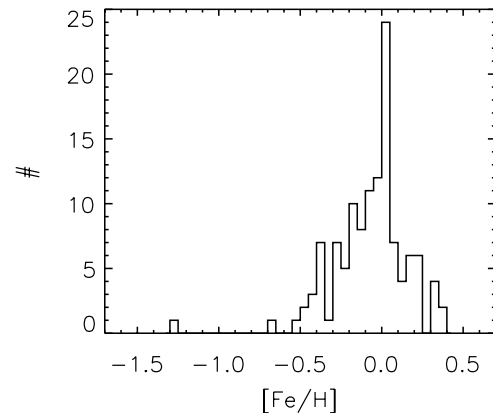


Figure 6. Histogram of metallicities for the stars with interferometrically determined radii discussed in this work and presented in Table 3. See Section 3 for details.

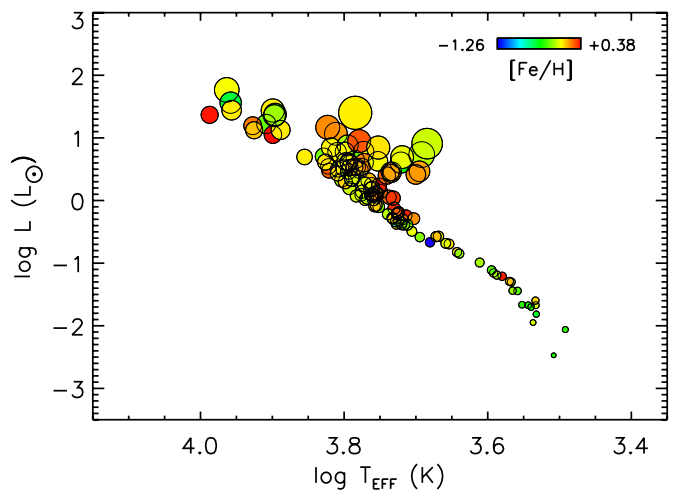


Figure 7. H-R diagram on the luminosity–temperature plane for all stars in Table 3 plus the collection of low-mass star measurements in DT2. The color and size of the data point reflect the metallicity and linear size of the star, respectively. See Section 2.3 for details.

(A color version of this figure is available in the online journal.)

Table 4
Object Photometry Used in SED Fits

Star ID	System/ Wavelength	Bandpass/ Bandwidth	Value	Error	Reference
HD166	DDO	m35	8.43	0.05	McClure (1976)
HD166	WBVR	<i>W</i>	7.00	0.05	Kornilov et al. (1991)
HD166	Johnson	<i>U</i>	7.22	0.05	Johnson & Knuckles (1957)
HD166	Johnson	<i>U</i>	7.22	0.05	Johnson et al. (1966)
HD166	Johnson	<i>U</i>	7.22	0.05	Argue (1966)
HD166	Johnson	<i>U</i>	7.15	0.05	J.-C. Mermilliod (1986, unpublished)
HD166	DDO	m38	7.54	0.05	McClure (1976)
HD166	DDO	m41	8.20	0.05	McClure (1976)
HD166	DDO	m42	8.18	0.05	McClure (1976)
HD166	WBVR	<i>B</i>	6.85	0.05	Kornilov et al. (1991)
HD166	Johnson	<i>B</i>	6.89	0.05	Johnson & Knuckles (1957)
HD166	Johnson	<i>B</i>	6.84	0.05	Niconov et al. (1957)
HD166	Johnson	<i>B</i>	6.89	0.05	Johnson et al. (1966)
HD166	Johnson	<i>B</i>	6.87	0.05	Argue (1966)
HD166	Johnson	<i>B</i>	6.85	0.05	J.-C. Mermilliod (1986, unpublished)

Notes. The collections of photometry used in the SED fitting routine for all objects. Refer to Section 2.3 for details.

(This table is available in its entirety in a machine-readable form in the online journal. A portion is shown here for guidance regarding its form and content.)

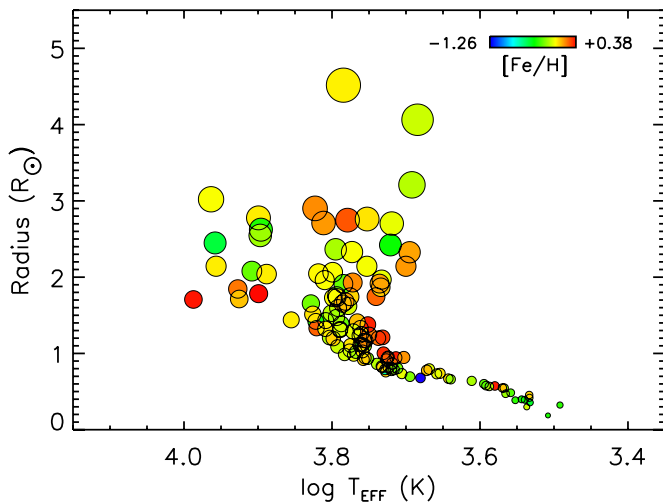


Figure 8. Stellar temperature vs. radius for all stars in Table 3 plus the collection of low-mass star measurements in DT2. The color and size of the data point reflect the metallicity and linear size of the star, respectively. See Section 2.3 for details.

(A color version of this figure is available in the online journal.)

stars, ranging from spectral types A0 to M4, having temperatures of ~ 3100 to $10,000$ K, and metallicities of $-0.5 < [\text{Fe}/\text{H}] < 0.4$. The anthology of stellar parameters for the earlier-type stars is presented in Table 3. Data for the later-type stars are taken from DT2 (Boyajian et al. 2012b).

Photometry from various sources was collected to derive the color–temperature relations. There are a total of 125 stars, however some have no measured magnitudes for some of the photometric bandpasses we use. All of the sources have Johnson *B* and *V* magnitudes. Near-infrared colors from the Two Micron All Sky Survey (2MASS) in the *J*, *H*, and *K* bands are saturated and unreliable due to the fact that these stars are quite bright. Therefore, we use alternative sources for *JHK* measurements when possible, keeping to the bandpass of the Johnson system. The cases where alternate Johnson *JHK*

magnitudes are not available, 2MASS *JHK* colors are used, and we discuss the implications of this in Section 3.1. For the stars having only 2MASS *JHK* magnitudes, we convert them to the Johnson system. This is done by combining the transformations in Carpenter (2001) for 2MASS to Bessell & Brett with the transformations in Bessell & Brett (1988) for Bessell & Brett to Johnson.¹³ Table 7 designates the magnitudes that use the transformation with footnote “c.”

Where available, we collect *R* and *I* magnitudes from the systems of Johnson *R_J*, *I_J* (e.g., Johnson et al. 1966), Cousins *R_C*, *I_C* (e.g., Cousins 1980), and Kron *R_K*, *I_K* (e.g., Kron et al. 1957). The most prevalent under sampling of photometric data is within the Cousins system and the Kron system, where of the 125 stars, only 34 and 64 stars have such measurements (for Cousins and Kron, respectively).

Magnitudes from the All-Sky Release Source Catalog from the *Wide-field Infrared Survey Explorer* (WISE) mission (Wright et al. 2010) are available for most stars with the W4 filter ($22.1 \mu\text{m}$), as it saturates on stars brighter than $W4 = -0.4$ mag. Approximately half of the stars in our sample have unsaturated WISE W3 ($11.6 \mu\text{m}$) magnitudes, where the saturation limit is for stars brighter than $W3 = 3.8$ mag. The WISE W1 and W2 systems have much fainter magnitude limits, and are completely saturated for all stars in this sample.¹⁴

Synthetic Sloan *g*, *r*, *i*, *z* magnitudes are also available for the majority of stars through the works of Ofek (2008) and Pickles & Depagne (2010). Although these synthetic magnitudes are carefully calibrated, we caution that some of the calculations rely on measurements from the 2MASS catalog that are saturated for most stars in this sample (as mentioned above). For our sample of stars, we find no statistically significant differences in the published magnitudes from the two references (the accuracies of these synthetic magnitudes are not tested here), and thus we chose to use the average of the Ofek (2008) and Pickles & Depagne (2010) values when constructing the color–temperature

¹³ We use the updated Carpenter (2001) transformations available at <http://www.astro.caltech.edu/~jmc/2mass/v3/transformations/>.

¹⁴ http://wise2.ipac.caltech.edu/docs/release/allsky/expsup/sec6_3d.html

Table 5
Spectral Types and Bolometric Fluxes

Star	Sp.Ty.	Sp.Ty.	Sp.Ty.	Sp.Ty.	Photometry				Spectrophotometry			
					DF	χ^2/DF	Best Fit Sp.Ty.	$F_{\text{BOL}} \pm \sigma$ ($1\text{e}-8 \text{ erg s}^{-1} \text{ cm}^{-2}$)	χ^2/DF	Best Fit Sp.Ty.	$F_{\text{BOL}} \pm \sigma$ ($1\text{e}-8 \text{ erg s}^{-1} \text{ cm}^{-2}$)	Spectro. Ref.
HD	First	Second	Ref.	Other								
166	G8V	...	24	...	53	0.48	G8V	10.44 ± 0.06	
3651	K0.5V	K0V	21, 24	K1V	110	2.19, 4.16, 1.91	K1V	13.47 ± 0.06	
4614	F9V	F9V	21, 23	...	80	1.19, 1.19	F9V	112.60 ± 0.59	3.66	F8V	111.60 ± 0.19	3
5015	F9V	F8V	28, 23	...	76	0.68, 0.76	F9V	31.30 ± 0.18	5.06	F9V	31.54 ± 0.06	5
6210	F6V	F7IV	9, 12	G0V	21	17.45, 13.93, 1.15	G0V	12.40 ± 0.10	5.72	G0V	12.38 ± 0.02	3
9826	F9V	F8V	28, 23	...	136	0.71, 0.64	F8V	60.07 ± 0.25	1.87	F8V	60.15 ± 0.13	3
10476	K1V	K0V	21, 24	...	110	1.36, 3.08	K1V	25.14 ± 0.11	
10697	G3Va	G4IV	21, 11	...	30	9.60, 1.28	G4IV	8.74 ± 0.06	
10700	G8V	G8.5V	21, 25	...	148	1.82, 2.26	G8V	119.00 ± 0.47	7.09	G8V	112.60 ± 0.08	1,2
11964	G9V CN+1	G8	25, 16	K0V	27	4.41, 10.87, 1.68	K0V	7.75 ± 0.05	
16765	F7V	F7IV	24, 9	...	33	0.71, 0.82	F7V	13.42 ± 0.10	
16895	F7V	F7V	23, 9	...	82	1.86, 1.86	F7V	58.19 ± 0.32	7.54	F7V	58.05 ± 0.08	1,3
19373	G0V	F9.5V	21, 24	...	33	0.49, 0.56	G0V	62.38 ± 0.63	4.79	G0V	60.04 ± 0.05	2
19994	F8.5V	G0IV	24, 9	...	54	0.74, 0.65	G0IV	25.07 ± 0.19	2.09	F9V	25.32 ± 0.05	5
20630	G5V	G5V	21, 23	...	154	0.53, 0.53	G5V	32.23 ± 0.13	2.92	G5V	31.30 ± 0.04	1
21019	G2V m-0.25	G6VgG6mG4	18, 17	G6V	61	3.35, 0.124	G6V	9.37 ± 0.02	
22484	F9IV-V	F9IV-V	21, 23	...	133	0.52, 0.52	F9IV-V	49.78 ± 0.22	4.04	F9V	50.36 ± 0.04	1
23249	K0+ IV	K1III-IV	21, 25	...	135	0.78, 1.76	K0+ IV	120.70 ± 0.49	5.57	K0IV	115.00 ± 0.08	1,2,3
30652	F6IV-V	F6V	23, 18	...	196	0.95, 1.03	F6IV-V	133.10 ± 0.46	2.52	F5IV	133.30 ± 0.09	1,3,4
34411	G1.5IV-V Fe-1	G1V	21, 24	...	136	1.83, 0.62	G1V	34.84 ± 0.14	3.64	G1V	35.62 ± 0.04	3,5
38858	G2V	...	24	...	39	1.26	G2V	11.07 ± 0.03	
39587	G0V	G0IV-V	21, 24	...	116	0.36, 0.40	G0V	45.75 ± 0.21	1.86	G0V	44.51 ± 0.08	3
48737	F5IV-V	F7IV	24, 9	...	69	2.31, 1.75	F7IV	113.60 ± 0.71	3.43	F6.5IV	115.10 ± 0.15	2
48915	A0mA1Va	kB9.5hA0mA1s	24, 22	...	59	3.08, 3.21	A0mA1Va	$10,710.00 \pm 79.72$	2.52	A0.5V	$10,780.00 \pm 21.63$	2
49933	F3V	F5V+ m-1.5	26, 18	...	48	1.19, 2.26	F3V	12.78 ± 0.08	
56537	A4IV	A3V	20, 10	...	93	1.10, 1.80	A4IV	91.88 ± 0.49	3.27	A47IV	91.90 ± 0.14	1,3
58946	F1V	F0V	24, 22	...	127	0.91, 1.01	F1V	53.91 ± 0.24	3.87	F1V	49.95 ± 0.10	3
61421	F5IV-V	F5V	24, 9	...	90	0.95, 1.40	F5IV-V	$1,815.00 \pm 9.08$	3.11	F5IV	$1,832.00 \pm 2.11$	1,3
69897	F6V	F6V	24, 9	...	55	0.23, 0.23	F6V	23.44 ± 0.18	
75732	K0IV-V	G8V	24, 2	...	45	0.92, 10.03	K0IV-V	12.04 ± 0.10	
81937	F0V	F0IV	22, 19	...	48	2.18, 1.17	F0IV	81.97 ± 0.64	4.57	F02I	83.62 ± 0.11	1,4
82328	F7V	F5.5IV-V	28, 24	...	69	0.98, 1.57	F7V	139.80 ± 0.83	2.90	F7V	134.30 ± 0.11	2,4
82885	G8Va	G8+ V	21, 24	...	142	1.61, 1.61	G8Va	19.10 ± 0.07	6.55	G8V	18.75 ± 0.02	1,5
86728	G3Va Hdel1	G4V	21, 24	...	108	0.88, 0.52	G4V	19.07 ± 0.10	2.33	G4V	19.73 ± 0.03	3
90839	F8V	F8V	24, 9	...	54	0.70, 0.70	F8V	31.07 ± 0.24	
95418	A1IVspSr	A1IV	24, 22	...	94	0.99, 0.99	A1IVspSr	313.40 ± 1.68	3.63	A1IV	313.90 ± 0.58	4,5
97603	A5IV(n)	A4Vn	24, 22	...	108	2.07, 1.89	A4Vn	234.80 ± 1.09	4.00	A4V	226.50 ± 0.30	1,3,5
101501	G8V	G8V	21, 24	...	126	1.22, 1.22	G8V	21.91 ± 0.09	
102647	A3V	A3Va	22, 20	...	134	1.75, 1.75	A3V	354.90 ± 1.53	2.72	A3V	351.60 ± 0.65	3,5
102870	F8.5IV-V	F9V	23, 6	...	185	0.73, 0.58	F9V	94.64 ± 0.34	4.05	F9V	91.56 ± 0.11	1
103095	K1V Fe-1.5	G9VgG2mG7	24, 17	G8V	201	10.28, 3.56, 3.80	G9VgG2mG7	8.36 ± 0.03	
109358	G0V	G0V	21, 24	...	145	0.68, 0.68	G0V	52.16 ± 0.21	
114710	F9.5V	G0V	21, 23	...	197	0.52, 0.56	F9.5V	52.16 ± 0.18	3.21	F9.5V	53.27 ± 0.09	3
117176	G4Va	G5V	21, 23	...	61	2.84, 1.77	G5V	27.73 ± 0.17	2.76	G5V	28.96 ± 0.05	3
118098	A2Van	A2IVn	24, 22	...	79	5.22, 2.98	A2IVn	115.20 ± 0.66	3.97	A47IV	103.90 ± 0.20	1
120136	F7IV-V	F7V	23, 9	...	117	0.81, 0.98	F7IV-V	40.56 ± 0.19	2.97	F6.5IV	39.51 ± 0.04	2
121370	G0IV	G0IV	21, 23	...	168	0.68, 0.68	G0IV	220.40 ± 0.82	1.51	G0IV	219.40 ± 0.37	5
126660	F7V	...	23	...	86	0.66	F7V	62.40 ± 0.33	2.67	F7V	60.97 ± 0.05	2
128167	F4Vkf2mF1	F5V	23, 14	...	161	1.56, 2.93	F4Vkf2mF1	41.87 ± 0.17	2.93	F4V	40.39 ± 0.05	2
128620	G2V	G2V	25, 8	G6.5V	12	12.05, 0.00, 1.39	G6.5V	$3,487.00 \pm 43.37$	4.84	G5V	2716.00 ± 2.67	1,2
128621	K2IV C2 1	K1V	25, 8	...	17	1.80, 2.45	K2IV C2 1	$1,013.00 \pm 10.80$	2.68	K1V	898.30 ± 1.12	1
130948	F9IV-V	G0V	23, 11	...	55	1.74, 1.12	G0V	12.09 ± 0.08	
131156	G7V	G8V	24, 13	...	68	2.75, 1.58	G8V	45.38 ± 0.27	5.15	G8V	43.04 ± 0.07	1
136202	F8IV	F9V	23, 9	...	17	0.74, 0.82	F8IV	24.45 ± 0.28	9.69	F8IV	21.07 ± 0.02	1,5
140538	G2.5V	G5V	21, 23	...	11	1.48, 1.32	G5V	12.46 ± 0.18	
141795	kA2hA5mA7V	kA3hA7VmA7	24, 22	...	85	1.33, 1.33	kA2hA5mA7V	80.18 ± 0.43	5.29	A5V	77.57 ± 0.09	2
142860	F6V	F6V	23, 14	...	140	0.92, 0.92	F6V	74.97 ± 0.32	1.36	F6V	73.85 ± 0.11	1
146233	G2Va	G2V	21, 24	...	88	0.66, 0.66	G2Va	17.34 ± 0.09	
150680	G0IV	G2IV	21, 23	...	106	1.84, 1.03	G2IV	203.60 ± 0.99	4.23	G2IV	196.20 ± 0.17	2
157214	G0V	77	0.98	G0V	17.98 ± 0.09	
158633	K0V	K0V	2, 3	...	45	2.82, 2.82	K0V	8.01 ± 0.05	
161797	G5IV	G5IV	21, 23	...	85	0.49, 0.49	G5IV	116.20 ± 0.63	4.32	G5IV	116.40 ± 0.12	2,4
162003	F5IV-V	F5V	23, 9	...	81	0.56, 0.67	F5IV-V	37.24 ± 0.21	3.52	F5IV	37.04 ± 0.04	1,5
164259	F2V	F2IV-V	24, 19	...	109	1.13, 1.40	F2V	34.69 ± 0.16	
168151	F5V	...	9	...	58	2.76	F5V	26.19 ± 0.18	1.79	F5V	25.35 ± 0.02	2
173667	F5.5IV-V	F5V	23, 14	...	62	0.91, 0.83	F5V	52.38 ± 0.34	1.32	F5V	52.31 ± 0.08	1
177724	A1V	A0IV-Vnn	27, 24	...	119	0.93, 1.42	A1V	181.80 ± 0.83	2.05	A1V	181.10 ± 0.31	1,3
182572	G7IV Hdel1	G8IV-V	21, 5	...	81	0.69, 0.81	G7IV Hdel1	24.77 ± 0.13	2.71	G6.5IV	24.10 ± 0.04	3
182736	K0V	...	1	...	18	1.77	K0V	4.80 ± 0.03	
185395	F3+ V	F4V	24, 15	...	105	0.32, 0.51	F3+ V	40.59 ± 0.21	2.65	F3V	39.20 ± 0.04	2
186408	G1.5Vb	G1.5V	21, 24	...	149	1.05, 1.05	G1.5Vb	10.96 ± 0.04	2.37	G1.5V	11.25 ± 0.02	3
186427	G3V	G3V	21, 25	...	122	1.69, 1.69	G3V	8.97 ± 0.03	3.13	G3V	9.108 ± 0.015	3

Table 5
(Continued)

Star	Sp.Ty.	Sp.Ty.	Sp.Ty.	Sp.Ty.	Photometry				Spectrophotometry			
					DF	χ^2/DF	Best Fit Sp.Ty.	$F_{\text{BOL}} \pm \sigma$ ($1e-8 \text{ erg s}^{-1} \text{ cm}^{-2}$)	χ^2/DF	Best Fit Sp.Ty.	$F_{\text{BOL}} \pm \sigma$ ($1e-8 \text{ erg s}^{-1} \text{ cm}^{-2}$)	Spectro. Ref.
188512	G8IV	G9.5IV	21, 25	...	202	0.94, 1.47	G8IV	94.65 ± 0.33	2.54	G8IV	92.71 ± 0.08	1,2
190360	G7IV-V	G8IV-V	25, 2	...	78	0.66, 2.52	G7IV-V	14.43 ± 0.08	
190406	G0V	G1V	25, 2	...	63	0.56, 0.41	G1V	13.00 ± 0.08	5.93	G1V	12.53 ± 0.02	2
195564	G2.5IV	...	21	...	57	0.91	G2.5IV	14.58 ± 0.09	
198149	K0IV	K0IV	21, 24	...	131	1.05, 1.05	K0IV	135.80 ± 0.56	3.32	K0IV	127.80 ± 0.10	2
206860	G0V CH-0.5	...	25	...	57	1.02	G0V CH-0.5	11.03 ± 0.07	
210027	F5V	F6Va	23, 4	...	142	0.52, 1.03	F5V	79.43 ± 0.32	4.85	F5V	77.46 ± 0.07	1,5
210418	A1Va	A2V	25, 22	...	68	3.15, 2.63	A2V	103.20 ± 0.64	2.60	A4V	95.02 ± 0.25	3
213558	A1.5V	A1V	27, 22	...	99	0.79, 0.68	A1V	88.04 ± 0.46	2.52	A1V	89.78 ± 0.15	1,3
215648	F6V	F5V	23, 9	...	122	0.69, 1.68	F6V	54.20 ± 0.24	2.79	F6V	53.55 ± 0.07	1
216956	A4V	A3V	25, 6	...	96	4.17, 1.80	A3V	879.20 ± 3.43	3.72	A3V	846.30 ± 1.06	2
217014	G2IV	G2V+	21, 25	...	190	0.74, 1.54	G2IV	17.36 ± 0.06	2.87	G2IV	17.08 ± 0.03	2
217107	G8IV-V	G8IV	24, 7	G6.5V	24	5.64, 11.12, 1.58	G6.5V	9.04 ± 0.08	
218396	F0+VkA5mA5	F0VmA5	24, 22	...	72	1.34, 1.34	F0VmA5	10.25 ± 0.05	
219623	F8V	F7V	23, 9	...	38	1.03, 1.27	F8V	15.26 ± 0.12	
222368	F7V	...	23	...	210	0.36	F7V	58.76 ± 0.20	0.95	F7V	57.31 ± 0.08	1
222603	A7V	A7IV	24, 22	...	108	0.83, 3.00	A7V	39.15 ± 0.18	1.32	A7V	40.22 ± 0.09	3

Notes. Bolometric fluxes of target stars based upon Pickles (1998) spectral templates fit to literature spectral types with photometry in the literature (in Table 4), and extended by spectrophotometry when available. References for the first and second spectral types are in the fourth column, as found from the index by Skiff (2013), with an additional spectral type if necessary for adequate SED fitting (Column 5). For the fits, degrees of freedom (DF) and χ^2 -per-DF metrics are given, along with spectral type of the template for the best fit, and its corresponding F_{BOL} value.

Spectral type references. (1) Macrae 1952; (2) Cowley et al. 1967; (3) Hagen & van den Bergh 1967; (4) Barry 1970; (5) Schmitt 1971; (6) Morgan & Keenan 1973; (7) Harlan 1974; (8) Houk & Cowley 1975; (9) Cowley 1976; (10) Levato & Abt 1978; (11) Cowley & Bidelman 1979; (12) Jensen 1981; (13) Abt 1981; (14) Bouw 1981; (15) Abt 1985; (16) Abt 1986; (17) Gray 1989; (18) Gray & Garrison 1989a; (19) Gray & Garrison 1989b; (20) Keenan & McNeil 1989; (21) Abt & Morrell 1995; (22) Gray et al. 2001; (23) Gray et al. 2003; (24) Gray et al. 2006; (25) Abt 2008; (26) Zorec et al. 2009; (27) Abt 2009.

Spectrophotometry references. (1) Burnashev 1985; (2) Alekseeva et al. 1996, 1997; (3) Kharitonov et al. 1988; (4) Glushneva et al. 1998b; (5) Glushneva et al. 1998a.

relations. All magnitudes used in the color–temperature relations are listed in Table 7 for each star.

We use MPFIT, a nonlinear, least-squares fitting routine in IDL (Markwardt 2009) to fit the observed color index to the measured temperatures of the stars in each bandpass. All stars with available photometry in said bandpass are fit to a third-order polynomial in the form of

$$T_{\text{eff}} = a_0 + a_1 X + a_2 X^2 + a_3 X^3, \quad (2)$$

where the variable X represents the color index and a_0, a_1, a_2, a_3 are each solution’s coefficients. In Table 8, we list 33 color indices and their coefficients derived in this manner. Table 8 also lists the number of points used in the fit (where the total number of points will be <125 if photometry is not available for stars in some bandpasses), the range in color index where the relation holds true, and the standard deviation about the fit expressed as a normalized percentage, calculated as $\text{Std.Dev.}((T_{i,\text{Obs}} - T_{i,\text{Calc}})/T_{i,\text{Obs}} \times 100)$. Figures 13–17 show the solutions and the data for each of the 33 color indices analyzed. In the discussions that follow, we comment on solutions using varied approaches in detail.

3.1. Slippery Solutions and Crummy Colors

3.1.1. Further Vetting of the Sample

We investigate whether a portion of the scatter about the best-fit color–temperature relations is a consequence of slight differences among the stars in the sample. Two possible differences that we consider are (1) distortion of the photosphere caused by rapid rotation and (2) early post-main-sequence evolution. Interferometrically constructed images of rapidly rotating A-stars such as Altair ($v \sin i = 240 \text{ km s}^{-1}$) show it to be distinctively oblate ($R_{\text{pole}} = 1.63 R_{\odot}$ versus $R_{\text{equator}} = 2.03 R_{\odot}$) with severe gravity darkening ($T_{\text{pole}} = 8450 \text{ K}$ versus $T_{\text{equator}} = 6860 \text{ K}$;

Monnier et al. 2007). These effects appear to be common among many early-type stars (see review by van Belle 2012). This compromises interferometrically determined temperatures because the measured radius is orientation-dependent and the strong temperature gradients lead to the apparent luminosity being inclination-dependent. For instance, Aufdenberg et al. (2006) calculate that the apparent luminosity of the pole on star Vega is 35% larger than its bolometric luminosity, because of our pole-on line of sight.

Fortunately, these complicating effects are primarily restricted to mid-F and hotter stars. These early-type stars lack a convective zone in their outer atmosphere, and thus the ability to generate a magnetic field that could couple to the stellar wind and magnetically brake the star’s rotation. In Section 2.2 we describe the early-type stars that have been omitted from the *Anthology* because of the effects of rapid rotation, as determined from interferometric imaging. The remaining early-type stars included in the *Anthology* may nevertheless have biased radii and apparent luminosities, which could introduce additional scatter into the best-fit relations. To eliminate this possible error source, and thus determine even stricter relations for cooler, Sun-like stars, we redo the analysis omitting these early-type stars. Specifically, stars hotter than $T_{\text{eff}} = 6750 \text{ K}$ are excluded, corresponding to spectral type F3, approximately. As can be seen in the H-R diagram plotted in Figure 7, there exists a natural break in the sample at this point. A total of 13 early-type stars are removed for the re-analysis.

We use the same approach of fitting the new subset of data as we did fitting the full sample, described in Section 3. The results are plotted in Figures 13–17 as a red dash-dotted line. For each color–temperature relation, Table 8 shows the number of points used in the fit, color range where the fit is applicable, coefficients to each polynomial, and the standard deviation (each row is marked with footnote “c” to indicate that the fit was made omitting the early-type stars). For each color index, we

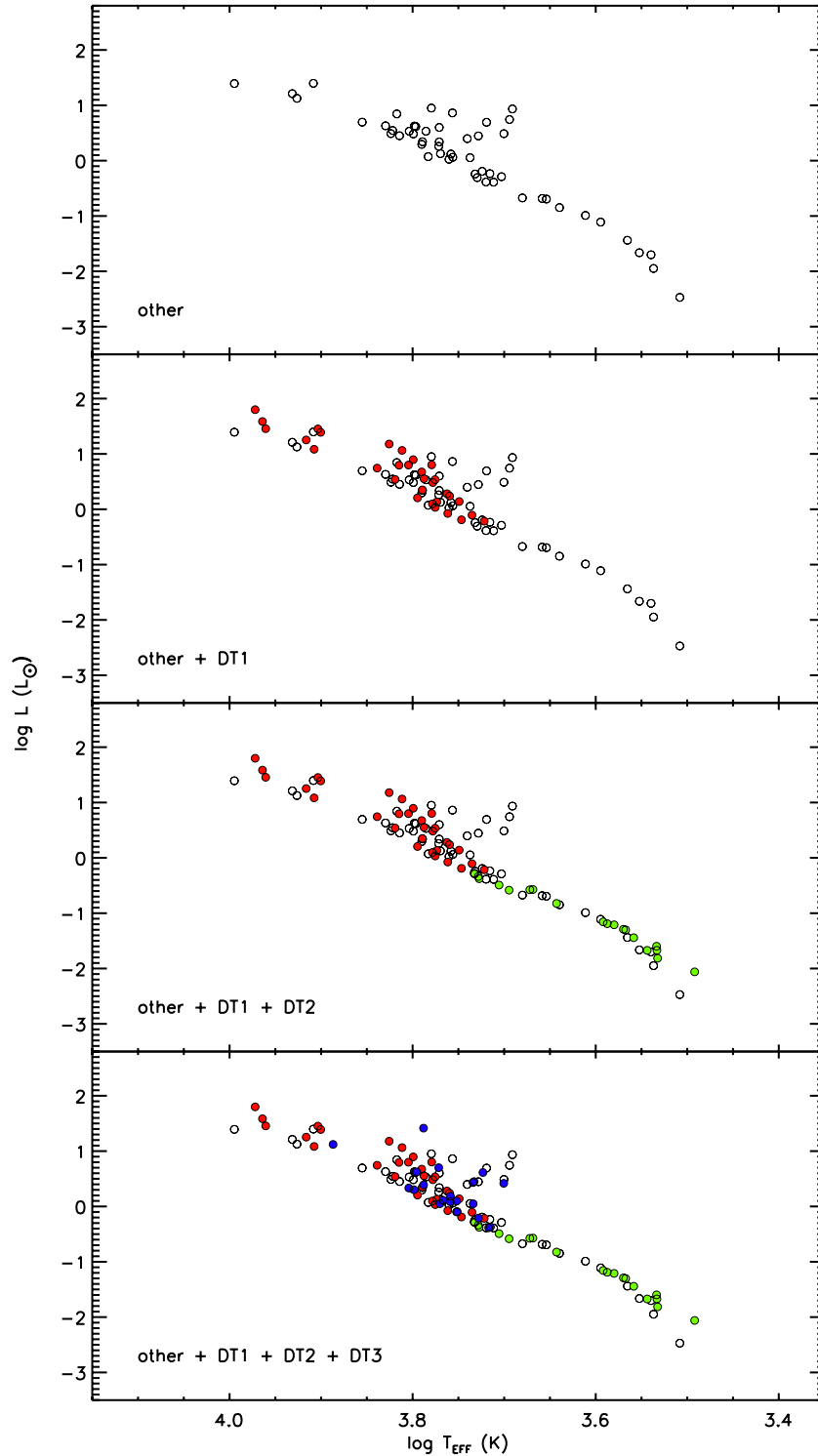


Figure 9. Each panel shows our progress in furnishing measurements to build a fundamentally determined H-R diagram on the luminosity–temperature plane. All published measurements in Table 3 plus the previously published low-mass star measurements collection in Table 7 of Boyajian et al. (2012b) (*other*; black points) are shown in all panels. The second panel adds the stars from Boyajian et al. (2012a) (DT1; red points). The third panel adds the stars from Boyajian et al. (2012b) (DT2; green points). The bottom panel adds the stars from this work (DT3; blue points). Stars with multiple measurements (i.e., marked with a [†] in Table 3 or with a ^{††} in Table 7 of Boyajian et al. 2012b) fall under the *other* category, since they are not unique contributions from our DT1, DT2, or DT3 interferometric surveys). See Section 2.3 for details.

(A color version of this figure is available in the online journal.)

document the maximum difference in temperature predicted using the fits with and without early-type stars in Table 9. Carefully inspecting the differences, we find that most of the new fits do not deviate more than a few tenths of a percent from

the full AFGKM star solution. Deviations larger than a few percent are manifested at the endpoints of the fit—where the fits omitting the early-type stars better represent the data in most cases. Exceptions are the $(R_J - J)$, $(R_J - H)$, and $(R_J - K)$ color

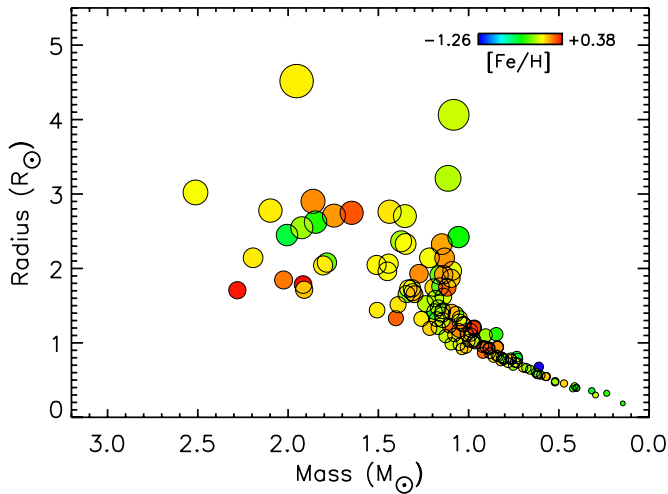


Figure 10. Stellar mass vs. radius plotted for all stars in Table 3 plus the collection of low-mass star measurements in DT2. The color and size of the data point reflect the metallicity and linear size of the star, respectively. See Section 2.4 for details.

(A color version of this figure is available in the online journal.)

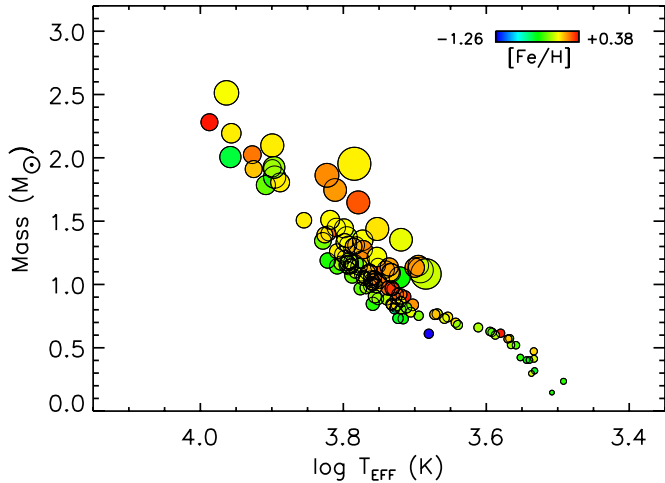


Figure 11. Stellar mass vs. radius plotted for all stars in Table 3 plus the collection of low-mass star measurements in DT2. The color and size of the data point reflect the metallicity and linear size of the star, respectively. See Section 2.4 for details.

(A color version of this figure is available in the online journal.)

relations, which are subject to poor fitting from lack of sampling on the coolest end of the fits, and use of these three relations in this region should be used with caution. Detailed discussion of the $(B - V)$ -temperature fits follow in Section 3.1.2.

Regarding the latter possible source of error in the color-temperature relations: the *Anthology* is restricted to be “stars on or near the main sequence (luminosity class V or IV).” However, inspection of the H-R diagram in Figure 7 hints that there is moderate girth in the band of the main sequence for stars greater than a few tenths of a solar luminosity. While these stars are far off from being giants—and we do not claim to re-classify them as such—their less-than-ZAMS surface gravity could lead to a distinctively different temperature scale than the truly qualified ZAMS population. We do not think that this is a source of error in our analysis for several reasons. The first clue to this not being an issue is that the sample of low-mass stars (i.e., the KM dwarfs from DT2) does not have any less-than-ZAMS surface gravity interlopers, since they are all low-mass enough

Table 6
Spectral Type Lookup Table

Spectral Type	n	$B - V$ (mag)	$V - K$ (mag)	$T_{\text{eff}} \pm \sigma$ (K)
A0	2	0.00	-0.04	9394 ± 44
A1	2	-0.01	-0.03	9121 ± 71
A2	3	0.12	0.27	7965 ± 24
A3	2	0.10	0.10	8176 ± 12
A4	1	0.09	0.19	8459 ± 44
A5	1	0.12	0.29	7889 ± 60
A7	1	0.21	0.51	7734 ± 80
F0	3	0.30	0.79	6850 ± 28
F2	3	0.41	1.04	6457 ± 11
F3	1	0.37	0.98	6435 ± 50
F5	8	0.44	1.14	6277 ± 45
F6	5	0.49	1.24	6194 ± 17
F7	5	0.50	1.18	6306 ± 19
F8	7	0.54	1.25	6026 ± 32
F9	3	0.57	1.40	5919 ± 24
G0	10	0.61	1.46	5790 ± 23
G1	2	0.63	1.43	5767 ± 9
G2	5	0.67	1.60	5555 ± 40
G3	3	0.69	1.58	5608 ± 17
G4	1	0.66	1.53	5619 ± 44
G5	5	0.68	1.57	5678 ± 8
G7	2	0.74	1.81	5472 ± 30
G8	7	0.77	1.77	5322 ± 27
G9	1	0.82	1.93	5013 ± 62
K0	5	0.79	1.87	5347 ± 20
K1	1	0.82	2.02	5147 ± 14
K2	2	0.88	2.12	5013 ± 14
K3	2	0.98	2.36	4680 ± 15
K4	1	1.10	2.63	4507 ± 58
K5	3	1.11	2.76	4436 ± 74
K7	3	1.35	3.41	3961 ± 11
M0	1	1.41	3.55	3907 ± 35
M0.5	2	1.47	3.97	3684 ± 9
M1	1	1.55	4.01	3497 ± 39
M1.5	4	1.49	4.07	3674 ± 10
M2	1	1.51	4.14	3464 ± 15
M2.5	1	1.61	4.75	3442 ± 54
M3	3	1.52	4.54	3412 ± 19
M3.5	1	1.59	4.71	3104 ± 28
M4	1	1.73	5.04	3222 ± 10
M5.5	1	1.97	6.68	3054 ± 79

Notes. The value of the parameter given is the average value of all stars within the spectral type bin, and the σ is the standard deviation of the parameter uncertainties for each spectral type bin. The spectral types with only one measurement ($n = 1$) simply lists the individual value and the measured error of that measurement. Refer to Section 2.3 for details.

to be considered un-evolved over the lifetime of the galaxy. Regarding the residuals of the color-temperature relations in this region of low-mass stars, we see that the residuals are of comparable magnitude to the higher-mass stars that are tainted with evolutionary effects.

We apply a more quantitative approach by inspecting the temperature residuals as a function of surface gravity $\log g$. For this exercise, we derive $\log g$ by the equation $g = GMR^{-2}$, where G is the gravitational constant, R is the interferometrically measured radius, and M is the mass derived from isochrone fitting. This yields surface gravities for the sample ranging from $\log g = 3.3$ to 5.0, with a mean value of 4.3 and standard deviation of 0.3 dex. By comparing the fractional residuals of the color-temperature fits with surface gravity, we find no

Table 7
Photometry Used in Color–Temperature Relations

Star	<i>B</i>	<i>V</i>	<i>R_J</i>	<i>I_J</i>	<i>J</i>	<i>H</i>	<i>K</i>	<i>R_C</i>	<i>I_C</i>	<i>R_K</i>	<i>I_K</i>	<i>g</i> ^a	<i>r</i> ^a	<i>i</i> ^a	<i>z</i> ^a	<i>W3</i> ^b	<i>W4</i> ^b
166	6.89	6.14	4.65 ^c	4.60 ^c	4.28 ^c	6.42	5.86	5.67	5.62	4.33	4.12
3651	6.71	5.86	5.21	4.82	4.48	4.03	3.97	5.52	5.25	6.27	5.66	5.44	5.35	3.93	3.91
4614	4.02	3.44	2.94	2.58	2.35	2.02	1.96	3.30	3.08
5015	5.35	4.82	4.34	4.04	3.85	3.56	3.54	3.50	3.46
6210	6.38	5.84	4.67 ^c	4.76 ^c	4.41 ^c	6.08	5.71	5.58	5.55	4.46	4.43
9826	4.64	4.10	3.64	3.35	3.17	2.99	2.85	2.88	2.84
10476	6.08	5.24	4.55	4.12	3.85	3.44	3.21	4.87	4.58	5.68	5.04	4.84	4.75	3.09	3.31
10697	6.99	6.26	4.98	4.66	4.58	6.57	6.07	5.93	5.88	4.64	4.58
10700	4.22	3.50	2.88	2.41	2.16	1.72	1.68	3.06	2.68	3.16	2.90	2.07	1.67
11964	7.24	6.42	5.02	4.64	4.49	5.96	5.56	6.83	6.23	6.01	5.94	4.53	4.48
16765	6.23	5.71	4.65 ^c	4.63 ^c	4.47 ^c	5.99	5.66	5.56	5.56	4.54	4.45
16895	4.62	4.13	3.67	3.37	3.34	3.07	2.98	3.94	3.76	2.89	2.84
19373	4.65	4.05	3.52	3.23	3.06	2.73	2.69	3.83	3.63	4.30	3.93	3.78	3.76	2.70	2.64
19994	5.63	5.06	4.17 ^c	3.77 ^c	3.75 ^c	4.72	4.41	5.33	4.98	4.86	4.85	3.66	3.64
20630	5.52	4.84	4.27	3.91	3.71	3.35	3.34	4.46	4.12	4.57	4.35	5.14	4.66	4.51	4.46	3.33	3.24
21019	6.90	6.20	4.91 ^c	4.58 ^c	4.42 ^c	6.52	6.04	5.90	5.84	4.42	4.38
22484	4.85	4.28	3.79	3.47	3.29	3.01	2.92	3.95	3.64	4.54	4.19	4.08	4.07	2.94	2.85
23249	4.46	3.54	2.82	2.32	1.96	1.52	1.40	3.02	2.59	3.15	2.83	3.98	3.32	3.12	3.05	1.46	1.38
30652	3.65	3.19	2.77	2.51	2.35	2.15	2.07	2.92	2.66	3.05	2.89	3.34	3.05	2.98	2.98	2.17	2.08
34411	5.33	4.71	4.18	3.86	3.62	3.33	3.28	4.45	4.25	3.28	3.22
38858	6.61	5.97	5.19 ^c	4.58 ^c	4.37 ^c	6.23	5.78	5.65	5.62	4.42	4.33
39587	5.00	4.41	3.90	3.59	3.34	3.04	2.97	4.16	3.96	4.66	4.29	4.15	4.13	2.91	2.87
48737	3.79	3.36	2.97	2.74	2.57	1.87	2.30	3.47	3.22	3.18	3.19	2.17	2.24
48915	−1.46	−1.46	−1.46	−1.43	−1.34	−1.33	−1.31	−1.45	−1.44	−1.25	−1.13	0.50	−1.33
49933	6.16	5.77	4.91	4.71	4.67	5.93	5.71	5.67	5.70	4.67	4.58
56537	3.70	3.58	3.46	3.41	3.49 ^c	3.49 ^c	3.49 ^c	3.64	3.69	3.58	3.69	3.85	3.98	3.32	3.31
58946	4.50	4.18	3.86	3.67	3.58	3.34	3.36	4.23	4.13	4.14	4.19	3.28	3.23
61421	0.79	0.37	−0.05	−0.28	−0.40	−0.56	−0.64	0.12	−0.12	0.26	0.12	1.15	−0.65
69897	5.61	5.14	4.17	3.94	3.91	5.32	5.07	5.03	5.04	3.89	3.89
75732	6.80	5.94	4.59	4.14	4.07	6.38	5.73	5.54	5.46	4.06	4.01
81937	4.00	3.67	3.33	3.15	3.01	3.00	2.82	2.84	2.75
82328	3.64	3.18	2.74	2.47	2.28	2.03	2.02	1.88	1.94
82885	6.18	5.41	4.79	4.42	4.14	3.77	3.70	5.06	4.80	5.78	5.22	5.04	4.99	3.63	3.60
86728	6.01	5.35	4.19 ^c	4.02 ^c	3.78 ^c	5.69	5.24	5.11	5.08	3.86	3.82
90839	5.36	4.84	4.36	4.08	3.84	3.58	3.54	4.64	4.48	5.02	4.70	4.61	4.61	3.56	3.54
95418	2.35	2.37	2.31	2.35	2.35	2.35	2.35	2.23	2.11
97603	2.68	2.56	2.43	2.40	2.33	2.27	2.27	2.46	2.31
101501	6.08	5.34	4.73	4.37	4.02	3.61	3.60	5.01	4.74	5.64	5.13	5.00	4.95
102647	2.22	2.14	2.08	2.06	2.03	1.99	1.99	2.18	2.24	2.20	2.29	2.45	2.59	1.70	1.67
102870	4.15	3.60	3.12	2.84	2.63	2.35	2.33	3.28	2.99	3.39	3.23	3.86	3.50	3.41	3.37	2.31	2.28
103095	7.20	6.45	5.79	5.34	4.95	4.44	4.40	6.05	5.76
109358	4.86	4.27	3.73	3.42	3.23	2.85	2.84	4.01	3.80	4.52	4.14	3.99	3.99	2.59	2.78
114710	4.84	4.26	3.77	3.47	3.22	2.95	2.89	4.05	3.84	4.51	4.14	3.99	3.97	2.94	2.81
117176	5.69	4.98	4.37	3.98	3.65	3.26	3.24	4.68	4.44	5.30	4.83	4.67	4.61	3.24	3.19
118098	3.50	3.38	3.31	3.25	3.18	3.05	3.06	3.32	3.26	3.03	3.07
120136	4.98	4.50	4.09	3.85	3.61	3.40	3.35	4.72	4.44	4.36	4.37	3.33	3.29
121370	3.26	2.68	2.24	1.95	1.70	1.38	1.37	2.45	2.25	1.38	1.37
126660	4.56	4.06	3.64	3.39	3.10	2.86	2.82	4.26	3.98	3.90	3.91	2.61	2.78
128167	4.84	4.47	4.13	3.94	3.65	3.50	3.49	4.59	4.43	4.43	4.49	3.49	3.44
128620	0.69	0.00	−1.15	−1.38	−1.49	−0.35	−0.68	−0.30	−0.52	−1.96	−1.84
128621	2.25	1.35	−0.01	−0.49	−0.60	0.91	0.67
130948	6.41	5.85	4.79	4.53	4.48	6.14	5.76	5.61	5.62	4.47	4.41
131156	5.31	4.54	3.91	3.48	3.01	2.59	2.57	2.89	2.83
136202	5.60	5.06	4.65	4.38	4.34 ^c	3.95 ^c	4.01 ^c	4.75	4.44	4.92	4.75	5.33	5.00	4.90	4.90	3.76	3.68
140538	6.57	5.88	4.58 ^c	4.08 ^c	4.26 ^c	5.48	5.12	6.19	5.74	5.61	5.58	4.17	4.14
141795	3.86	3.70	3.62	3.57	3.51 ^c	3.44 ^c	3.38 ^c	3.65	3.58	3.74	3.82	3.93	4.01	3.49	3.44
142860	4.34	3.86	3.37	3.13	2.93	2.64	2.65	3.67	3.53	2.71	2.63
146233	6.14	5.51	4.67 ^c	4.16 ^c	4.19 ^c	5.13	4.79	5.84	5.38	5.26	5.23	3.99	3.97
150680	3.46	2.81	2.30	1.98	1.70	1.34	1.30	2.56	2.33	1.48	1.35
157214	6.00	5.38	4.87	4.53	4.22	3.86	3.84	5.33	5.00	4.90	4.90	3.82	3.79
158633	7.19	6.43	4.91 ^c	4.63 ^c	4.48 ^c	6.79	6.19	5.97	5.90	4.52	4.48
161797	4.17	3.42	2.89	2.51	2.18	1.81	1.77	3.12	2.88	3.75	3.19	3.01	2.95	1.65	1.75
162003	5.01	4.58	4.20	3.97	3.70	3.47	3.43	4.75	4.53	4.50	4.53	3.46	3.39
164259	5.01	4.62	4.29	4.10	3.87	3.70	3.67	4.40	4.18	4.75	4.60	4.62	4.66	3.69	3.64
168151	5.49	5.09	4.11	3.88	3.85	5.17	4.94	4.90	4.93	3.86	3.82
173667	4.65	4.19	3.80	3.54	3.30	3.08	3.04	4.42	4.15	4.11	4.14	3.00	3.02

Table 7
(Continued)

Star	<i>B</i>	<i>V</i>	<i>R_J</i>	<i>I_J</i>	<i>J</i>	<i>H</i>	<i>K</i>	<i>R_C</i>	<i>I_C</i>	<i>R_K</i>	<i>I_K</i>	<i>g^a</i>	<i>r^a</i>	<i>i^a</i>	<i>z^a</i>	<i>W3^b</i>	<i>W4^b</i>
173701	8.38	7.54	6.09 ^c	5.75 ^c	5.67 ^c	7.96	7.34	7.12	7.03	5.69	5.66
175726	7.29	6.71	5.70 ^c	5.42 ^c	5.35 ^c	5.32	4.75
177153	7.77	7.20	6.15 ^c	5.92 ^c	5.83 ^c	7.49	7.11	6.97	6.95	5.85	5.80
177724	3.00	2.99	2.98	2.98	2.93	3.03	2.92	3.10	3.17	2.91	3.14	3.34	3.49	2.90	2.94
181420	7.01	6.57	5.75 ^c	5.56 ^c	5.51 ^c	6.77	6.54	6.49	6.53	5.57	5.46
182572	5.94	5.16	3.84	3.55	3.49	5.51	4.93	4.73	4.67	3.53	3.50
182736	7.82	7.01	5.52 ^c	5.14 ^c	5.03 ^c	7.50	6.86	6.65	6.55	5.05	4.98
185395	4.86	4.47	4.12	3.91	3.75	3.72	3.52	4.64	4.50	4.54	4.57	3.47	3.40
186408	6.59	5.95	5.50	5.17	4.91	4.44	4.52	6.20	5.79	5.63	5.59	4.44	4.41
186427	6.86	6.20	5.76	5.42	5.04	4.70	4.65	6.48	6.05	5.90	5.86	4.69	4.66
187637	8.04	7.53	6.54 ^c	6.35 ^c	6.28 ^c	7.75	7.46	7.37	7.38	6.32	6.36
188512	4.58	3.72	3.06	2.57	2.26	1.71	1.71	3.26	2.83	3.35	3.04	4.12	3.48	3.29	3.20	1.54	1.50
190360	6.42	5.70	4.45	4.11	4.05	6.08	5.55	5.38	5.33	4.09	4.04
190406	6.41	5.80	4.69 ^c	4.43 ^c	4.39 ^c	6.07	5.69	5.54	5.55	4.38	4.35
195564	6.33	5.65	4.31 ^c	3.91 ^c	4.00 ^c	5.28	4.92	6.00	5.50	5.36	5.31	3.97	3.95
198149	4.35	3.43	2.76	2.27	1.90	1.50	1.28	3.02	2.69	3.86	3.21	3.00	2.92	1.20	1.19
206860	6.53	5.94	4.74 ^c	4.60 ^c	4.52 ^c	6.22	5.84	5.69	5.70	4.56	4.49
210027	4.20	3.76	3.36	3.11	2.98	2.71	2.66	3.96	3.70	3.66	3.68	2.37	2.61
210418	3.62	3.55	3.50	3.46	3.38	3.38	3.33	3.49	3.44	3.32	3.29
213558	3.78	3.77	3.77	3.80	3.77 ^c	3.86 ^c	3.80 ^c	3.79	3.74
215648	4.69	4.19	3.76	3.45	3.22	3.06	2.92	4.42	4.14	4.06	4.07	2.94	2.89
216956	1.25	1.16	1.10	1.08	1.02	1.05	0.97	1.10	1.08	1.24	1.30	1.32	1.40	1.49	1.58	0.93	0.82
217014	6.17	5.50	4.96	4.62	4.36	4.03	3.99	5.77	5.32	5.19	5.16	3.93	3.91
217107	6.90	6.16	4.95 ^c	4.77 ^c	4.54 ^c	6.52	5.99	5.82	5.78	4.53	4.52
218396	6.24	5.98	5.46	5.30	5.28	6.05	5.97	5.99	6.04	5.22	4.87
219623	6.10	5.58	4.79 ^c	4.57 ^c	4.27 ^c	5.85	5.52	5.42	5.42	4.30	4.20
222368	4.64	4.13	3.69	3.38	3.24 ^c	2.99 ^c	2.91 ^c	3.84	3.55	3.94	3.75	4.35	4.07	3.99	4.00	2.87	2.88
222603	4.72	4.51	4.33	4.23	4.10	4.20	4.00	4.39	4.28	4.55	4.61	4.72	4.80

Notes. Photometry sources include: Johnson et al. (1966, 1968), Epps (1972), Glass (1974, 1975), Guetter (1977), Blackwell et al. (1979, 1990), Noguchi et al. (1981), Sandage & Kowal (1986), Arribas & Martinez Roger (1989), Aumann & Probst (1991), Alonso et al. (1994), Sylvester et al. (1996), Mermilliod (1997), Ducati (2002), Cousins (1980), Kron et al. (1957), and Wright et al. (2010). See Section 3 for details.

^a Average from Ofek (2008) and Pickles & Depagne (2010).

^b The *WISE* *W3* and *W4* magnitudes have been filtered to only allow values that have not reached saturation limits (*W3* < 3.8 mag and *W4* < −0.4 mag).

^c 2MASS magnitudes converted to the Johnson system. See Section 3 for details.

evidence that stars with lower values of $\log g$ will bias the color–temperature fits.

Although the luminosity classes IV and V do not differentiate the evolutionary state of the stars very well, as pointed out in Section 2.4, we also checked for correlation with luminosity class in the residuals of the color–temperature fits and found none.

3.1.2. Improvement on $(B - V)$ Relations

The robustness of the $(B - V)$ –temperature solution suffers from two artifacts: (1) the need for a higher order polynomial to properly model the data and (2) trends in the residuals with respect to metallicity. Pertaining to the first issue, the residuals in the $(B - V)$ –temperature relation shown in Figure 13 show that the solution using a third-order polynomial does not model the inflection point in the data ($\sim 0.2 < (B - V) < 0.5$; $\sim 6500 < T_{\text{eff}} < 7500$) well, thus yielding temperatures $\sim 5\%$ cooler than observed in this range. In fact, the $(B - V)$ –temperature fit omitting the early-type stars produces temperatures 5% different from the third-order polynomial solution (Table 9, Figure 13). Thus, in order to model the full AFGKM sample correctly, we use the approach in DT1 and apply a sixth-order polynomial in order to remove this artifact. The form of this equation is expressed as

$$T_{\text{eff}} = a_0 + a_1(B - V) + a_2(B - V)^2 + a_3(B - V)^3 + a_4(B - V)^4 + a_5(B - V)^5 + a_6(B - V)^6, \quad (3)$$

where the coefficients are

$$\begin{aligned} a_0 &= 9552 \pm 19, \\ a_1 &= -17443 \pm 350, \\ a_2 &= 44350 \pm 1762, \\ a_3 &= -68940 \pm 3658, \\ a_4 &= 57338 \pm 3692, \\ a_5 &= -24072 \pm 1793, \\ a_6 &= 4009 \pm 334. \end{aligned}$$

The standard deviation of the fit for Equation (3) is 3.1%, and data are plotted along with the solution and residuals in the top panel of Figure 19. The solution is also displayed in Figure 13 as a dashed line. Although this standard deviation is only slightly smaller than the solution using the third-order polynomial fit (3.3%), we note that it maps the region of concern containing the inflection point more accurately. This solution using this sixth-order polynomial fitting the whole sample produces temperatures identical to the solution found by eliminating the early-type stars from the fitting in Section 3.1.1.

With the exception of the $(B - V)$ –temperature relation, the residuals in each color–temperature relation, plotted in Figures 13–18, reveal no pattern with respect to the metallicity of the star. Attempts to fit functions dependent on color and metallicity, such as the one developed for the low-mass stars in DT2,

Table 8
Solutions to Temperature Relations

Color Index	No. of Points	Range (mag)	$a_0 \pm \sigma$	$a_1 \pm \sigma$	$a_2 \pm \sigma$	$a_3 \pm \sigma$	σ (%)
$(B - V)^a$	124	$[-0.02 - 1.73]$	9084 ± 15	-7736 ± 57	4781 ± 69	-1342.9 ± 25.1	3.3
$(B - V)^{a,b}$	111	$[0.32 - 1.73]$	7722 ± 38	-3144 ± 129	112 ± 136	114.2 ± 44.3	3.0
$(V - J)$	122	$[-0.12 - 4.24]$	9052 ± 13	-3972 ± 20	1039 ± 9	-101.0 ± 1.5	3.7
$(V - J)^c$	109	$[0.60 - 4.24]$	9041 ± 25	-3950 ± 39	1028 ± 17	-99.4 ± 2.3	3.7
$(V - J)^d$	95	$[-0.12 - 4.24]$	9127 ± 13	-4084 ± 21	1082 ± 10	-106.0 ± 1.5	2.6
$(V - J)^{c,d}$	85	$[0.60 - 4.24]$	9183 ± 26	-4163 ± 40	1114 ± 17	-109.9 ± 2.3	2.5
$(V - H)$	122	$[-0.13 - 4.77]$	8958 ± 13	-3023 ± 18	632 ± 7	-52.9 ± 1.1	3.3
$(V - H)^c$	109	$[0.67 - 4.77]$	8595 ± 28	-2556 ± 37	458 ± 14	-33.2 ± 1.7	3.2
$(V - H)^d$	86	$[-0.13 - 4.77]$	9084 ± 14	-3162 ± 19	675 ± 8	-56.9 ± 1.1	2.5
$(V - H)^{c,d}$	79	$[0.67 - 4.77]$	8935 ± 32	-2970 ± 41	604 ± 15	-48.8 ± 1.8	2.4
$(V - K)$	124	$[-0.15 - 5.04]$	8984 ± 13	-2914 ± 17	588 ± 7	-47.4 ± 0.9	2.9
$(V - K)^c$	111	$[0.82 - 5.04]$	8649 ± 28	-2503 ± 35	442 ± 12	-31.7 ± 1.5	2.7
$(V - K)^d$	97	$[-0.15 - 5.04]$	9030 ± 13	-2968 ± 17	606 ± 7	-49.2 ± 0.9	2.4
$(V - K)^{c,d}$	87	$[0.82 - 5.04]$	8669 ± 29	-2528 ± 35	450 ± 13	-32.5 ± 1.5	2.3
$(V - R_J)$	81	$[0.00 - 1.69]$	9335 ± 16	-9272 ± 71	5579 ± 102	-1302.5 ± 43.4	3.8
$(V - R_J)^c$	69	$[0.32 - 1.69]$	9238 ± 54	-8844 ± 213	5029 ± 254	-1094.6 ± 92.7	3.5
$(V - I_J)$	81	$[-0.03 - 3.12]$	9189 ± 15	-5372 ± 37	1884 ± 30	-245.1 ± 7.3	3.3
$(V - I_J)^c$	69	$[0.51 - 3.12]$	9072 ± 42	-5080 ± 97	1674 ± 66	-200.8 ± 14.0	3.0
$(V - R_C)$	34	$[-0.01 - 1.24]$	9317 ± 17	-13886 ± 92	12760 ± 150	-4468.7 ± 75.0	3.3
$(V - R_C)^c$	28	$[0.22 - 1.24]$	9035 ± 49	-12493 ± 242	10831 ± 337	-3663.7 ± 144.9	2.7
$(V - I_C)$	34	$[-0.02 - 2.77]$	9354 ± 17	-7178 ± 42	3226 ± 30	-518.2 ± 6.6	3.1
$(V - I_C)^c$	28	$[0.44 - 2.77]$	9440 ± 44	-7360 ± 102	3333 ± 65	-536.9 ± 12.6	2.6
$(V - R_K)$	64	$[-0.21 - 1.32]$	7371 ± 7	-7940 ± 43	6947 ± 90	-2557.8 ± 54.2	4.0
$(V - R_K)^c$	59	$[0.11 - 1.32]$	6878 ± 14	-4708 ± 91	1329 ± 166	230.5 ± 88.3	3.6
$(V - I_K)$	64	$[-0.33 - 2.42]$	7694 ± 8	-5142 ± 25	2412 ± 26	-428.4 ± 8.4	2.8
$(V - I_K)^c$	59	$[0.25 - 2.42]$	7639 ± 17	-4964 ± 56	2256 ± 51	-388.7 ± 13.9	2.7
$(R_J - J)$	81	$[-0.12 - 2.21]$	8718 ± 12	-6740 ± 44	3164 ± 54	-547.0 ± 19.2	4.6
$(R_J - J)^c$	69	$[0.28 - 2.21]$	8301 ± 32	-5334 ± 110	1784 ± 113	-144.0 ± 35.0	4.3
$(R_J - J)^d$	75	$[-0.12 - 2.21]$	8779 ± 12	-6901 ± 46	3259 ± 55	-560.8 ± 19.5	3.4
$(R_J - J)^{c,d}$	66	$[0.28 - 2.21]$	8388 ± 32	-5589 ± 111	1980 ± 114	-188.7 ± 35.1	3.3
$(R_J - H)$	81	$[-0.13 - 2.80]$	8689 ± 13	-4292 ± 35	1356 ± 31	-180.8 ± 8.2	4.3
$(R_J - H)^c$	69	$[0.33 - 2.80]$	7066 ± 39	-320 ± 98	-1531 ± 74	447.3 ± 16.7	4.2
$(R_J - H)^d$	66	$[-0.13 - 2.80]$	8856 ± 14	-4566 ± 38	1434 ± 33	-178.1 ± 8.6	2.9
$(R_J - H)^{c,d}$	60	$[0.33 - 2.80]$	7640 ± 49	-1650 ± 118	-650 ± 86	270.4 ± 19.2	3.0
$(R_J - K)$	81	$[-0.15 - 3.06]$	8787 ± 13	-4287 ± 32	1383 ± 26	-187.0 ± 6.3	3.6
$(R_J - K)^c$	69	$[0.50 - 3.06]$	7499 ± 45	-1376 ± 102	-557 ± 70	200.1 ± 14.4	3.1
$(R_J - K)^d$	75	$[-0.15 - 3.06]$	8844 ± 13	-4400 ± 33	1444 ± 27	-197.1 ± 6.4	2.8
$(R_J - K)^{c,d}$	66	$[0.50 - 3.06]$	7552 ± 45	-1484 ± 103	-495 ± 70	189.5 ± 14.4	2.6
$(R_C - J)$	34	$[-0.11 - 3.00]$	9019 ± 15	-5767 ± 34	2209 ± 23	-310.3 ± 4.8	5.0
$(R_C - J)^c$	28	$[0.41 - 3.00]$	9191 ± 43	-6123 ± 91	2410 ± 54	-344.4 ± 9.6	5.5
$(R_C - J)^d$	27	$[-0.11 - 3.00]$	9050 ± 15	-5805 ± 34	2223 ± 23	-311.6 ± 4.8	2.4
$(R_C - J)^{c,d}$	22	$[0.41 - 3.00]$	9393 ± 45	-6519 ± 95	2629 ± 55	-380.6 ± 9.9	2.1
$(R_C - H)$	34	$[-0.12 - 3.53]$	9035 ± 15	-4354 ± 29	1334 ± 17	-160.9 ± 3.1	4.1
$(R_C - H)^c$	28	$[0.68 - 3.53]$	8956 ± 48	-4211 ± 81	1262 ± 40	-149.9 ± 6.1	3.9
$(R_C - H)^d$	26	$[-0.12 - 3.53]$	9062 ± 16	-4388 ± 29	1347 ± 17	-162.1 ± 3.2	3.0
$(R_C - H)^{c,d}$	22	$[0.68 - 3.53]$	9000 ± 48	-4278 ± 82	1292 ± 40	-153.9 ± 6.2	2.4
$(R_C - K)$	34	$[-0.14 - 3.80]$	9077 ± 15	-4054 ± 27	1133 ± 14	-124.1 ± 2.5	3.7
$(R_C - K)^c$	28	$[0.73 - 3.80]$	9075 ± 49	-4046 ± 76	1128 ± 34	-123.1 ± 4.9	3.9
$(R_C - K)^d$	27	$[-0.14 - 3.80]$	9087 ± 15	-4059 ± 27	1133 ± 14	-123.8 ± 2.5	2.5
$(R_C - K)^{c,d}$	22	$[0.73 - 3.80]$	9137 ± 50	-4131 ± 78	1162 ± 35	-127.5 ± 5.0	2.3
$(R_K - J)$	62	$[0.09 - 2.58]$	10087 ± 22	-7219 ± 53	2903 ± 42	-433.7 ± 10.6	4.3
$(R_K - J)^c$	57	$[0.58 - 2.58]$	9876 ± 58	-6752 ± 128	2589 ± 87	-368.1 ± 18.9	3.9
$(R_K - J)^d$	59	$[0.09 - 2.58]$	10218 ± 23	-7478 ± 55	3060 ± 43	-463.7 ± 10.7	3.2
$(R_K - J)^{c,d}$	55	$[0.58 - 2.58]$	10004 ± 59	-7009 ± 130	2748 ± 88	-399.0 ± 19.1	3.1
$(R_K - H)$	62	$[0.07 - 3.17]$	9695 ± 21	-4791 ± 43	1432 ± 29	-175.0 ± 6.0	3.5
$(R_K - H)^c$	57	$[0.82 - 3.17]$	8678 ± 69	-2980 ± 125	435 ± 70	-4.3 ± 12.4	2.9
$(R_K - H)^d$	57	$[0.07 - 3.17]$	9823 ± 22	-5001 ± 45	1543 ± 30	-193.4 ± 6.1	2.9
$(R_K - H)^{c,d}$	54	$[0.82 - 3.17]$	8676 ± 70	-2972 ± 126	431 ± 70	-3.8 ± 12.5	2.6

Table 8
(Continued)

Color Index	No. of Points	Range (mag)	$a_0 \pm \sigma$	$a_1 \pm \sigma$	$a_2 \pm \sigma$	$a_3 \pm \sigma$	σ (%)
$(R_K - K)$	64	[0.06 – 3.43]	9683 ± 21	-4479 ± 39	1268 ± 24	-147.8 ± 4.7	3.6
$(R_K - K)^c$	59	[0.90 – 3.43]	8671 ± 69	-2793 ± 117	400 ± 61	-8.9 ± 10.1	2.9
$(R_K - K)^d$	61	[0.06 – 3.43]	9794 ± 21	-4647 ± 40	1347 ± 25	-159.5 ± 4.8	2.7
$(R_K - K)^{c,d}$	57	[0.90 – 3.43]	8726 ± 70	-2875 ± 117	439 ± 61	-14.7 ± 10.2	2.4
$(g - z)^\dagger$	79	[-0.58 – 3.44]	7089 ± 11	-2760 ± 27	804 ± 16	-95.2 ± 3.0	3.2
$(g - z)^{\dagger c}$	74	[0.04 – 3.44]	7131 ± 14	-2863 ± 36	863 ± 21	-104.8 ± 3.7	3.3
$(g - i)^\dagger$	79	[-0.43 – 2.78]	7279 ± 13	-3356 ± 37	1112 ± 27	-153.9 ± 5.9	3.2
$(g - i)^{\dagger c}$	74	[0.09 – 2.78]	7325 ± 18	-3484 ± 49	1199 ± 35	-171.0 ± 7.4	3.3
$(g - r)^\dagger$	79	[-0.23 – 1.40]	7526 ± 18	-5570 ± 88	3750 ± 136	-1332.9 ± 61.5	3.2
$(g - r)^{\dagger c}$	74	[0.09 – 1.40]	7671 ± 31	-6275 ± 155	4719 ± 222	-1723.1 ± 94.0	3.3
$(g - J)^\dagger$	79	[-0.02 – 5.06]	8576 ± 28	-2710 ± 35	548 ± 12	-44.0 ± 1.4	3.5
$(g - J)^{\dagger c}$	74	[0.64 – 5.06]	8605 ± 36	-2744 ± 45	560 ± 15	-45.2 ± 1.7	3.5
$(g - J)^{\dagger d}$	60	[-0.02 – 5.06]	8759 ± 33	-2933 ± 41	623 ± 14	-51.5 ± 1.6	2.7
$(g - J)^{\dagger c,d}$	57	[0.64 – 5.06]	8695 ± 38	-2856 ± 46	597 ± 16	-48.9 ± 1.7	2.6
$(g - H)^\dagger$	79	[-0.12 – 5.59]	8589 ± 30	-2229 ± 33	380 ± 10	-27.5 ± 1.1	2.9
$(g - H)^{\dagger c}$	74	[0.88 – 5.59]	8774 ± 44	-2419 ± 46	437 ± 14	-32.7 ± 1.4	3.0
$(g - H)^{\dagger d}$	53	[-0.12 – 5.59]	8744 ± 46	-2396 ± 48	432 ± 14	-32.3 ± 1.4	2.3
$(g - H)^{\dagger c,d}$	52	[0.88 – 5.59]	8745 ± 47	-2397 ± 49	433 ± 15	-32.4 ± 1.4	2.4
$(g - K)^\dagger$	79	[-0.01 – 5.86]	8526 ± 30	-2084 ± 31	337 ± 9	-23.3 ± 0.9	2.8
$(g - K)^{\dagger c}$	74	[0.86 – 5.86]	8519 ± 40	-2078 ± 41	335 ± 12	-23.2 ± 1.2	2.7
$(g - K)^{\dagger d}$	60	[-0.01 – 5.86]	8618 ± 35	-2178 ± 36	365 ± 11	-25.8 ± 1.1	2.5
$(g - K)^{\dagger c,d}$	57	[0.86 – 5.86]	8485 ± 41	-2046 ± 42	327 ± 12	-22.5 ± 1.2	2.3
$(V - W3)$	44	[0.76 – 5.50]	9046 ± 98	-3005 ± 103	602 ± 30	-45.3 ± 2.8	2.5
$(V - W3)^c$	43	[1.00 – 5.50]	9005 ± 109	-2962 ± 114	590 ± 33	-44.3 ± 3.0	2.5
$(V - W4)$	111	[0.03 – 5.62]	9008 ± 20	-2881 ± 23	565 ± 8	-42.3 ± 0.9	3.3
$(V - W4)^c$	100	[0.92 – 5.62]	8855 ± 29	-2714 ± 33	514 ± 11	-37.5 ± 1.1	2.8
$(R_J - W4)$	74	[0.03 – 3.56]	9055 ± 24	-4658 ± 52	1551 ± 33	-199.8 ± 6.3	3.6
$(R_J - W4)^c$	64	[0.58 – 3.56]	8694 ± 42	-3964 ± 85	1160 ± 51	-133.4 ± 9.2	2.5
$(I_J - W4)$	74	[0.04 – 2.13]	9140 ± 28	-7347 ± 93	3981 ± 92	-873.1 ± 27.7	4.7
$(I_J - W4)^c$	64	[0.40 – 2.13]	8541 ± 48	-5594 ± 151	2453 ± 141	-465.5 ± 40.4	3.1
$(R_C - W4)$	30	[0.20 – 4.38]	9015 ± 31	-3833 ± 45	1004 ± 19	-98.5 ± 2.4	3.1
$(R_C - W4)^c$	26	[0.76 – 4.38]	8853 ± 51	-3620 ± 71	924 ± 28	-89.4 ± 3.4	2.9
$(I_C - W4)$	30	[0.14 – 2.85]	8971 ± 34	-5296 ± 75	1997 ± 48	-298.1 ± 9.5	3.7
$(I_C - W4)^c$	26	[0.54 – 2.85]	8493 ± 55	-4360 ± 114	1466 ± 69	-205.6 ± 12.9	3.1
$(R_K - W4)$	52	[0.17 – 3.93]	9753 ± 42	-4530 ± 66	1271 ± 31	-137.7 ± 4.7	2.9
$(R_K - W4)^c$	48	[0.97 – 3.93]	9433 ± 64	-4071 ± 97	1072 ± 44	-110.8 ± 6.4	2.4
$(I_K - W4)$	52	[0.23 – 2.83]	10576 ± 59	-7103 ± 123	2887 ± 79	-461.5 ± 15.9	3.7
$(I_K - W4)^c$	52	[0.23 – 2.83]	10727 ± 63	-7275 ± 128	2943 ± 81	-465.8 ± 16.2	3.6

Notes. See Sections 3, 3.1, 3.1.1, and 3.1.2, and Equation (2) for details.

^a The $(B - V)$ relation expressed as a third-order polynomial is insufficient for the full range of AFGKM stars. See Section 3.1.2 for discussion and alternate solutions.

^b For a metallicity-dependent solution, see Equation (4) in Section 3.1.2.

^c Solutions derived omitting hot stars ($T_{\text{eff}} > 6750$ K). See Section 3.1.1.

^d Solutions derived omitting all stars that only have 2MASS magnitudes. See Section 3.1.

were shown not to improve the fits. We note that even within the results of DT2, only mild dependence on metallicity was detected in the multi-variable, color–metallicity–temperature fits, prevalent only for the latest-type stars ($T_{\text{eff}} < 4000$ K, see Section 4.1 in DT2). The likely causes for this lack of apparent connection in the data on the color–metallicity–temperature plane are that (1) large photometric errors are prominent throughout the data set and (2) significant errors in the metallicity (especially systematics) may exist. This attribute is complicated further when combined with the fact that the range of metallicity in the sample (roughly $-0.5 < [\text{Fe}/\text{H}] < 0.4$, with two low-metallicity outliers) might not be broad enough to detect such an effect observationally.

The metallicity dependence on the $(B - V)$ colors is strongest of all color indices analyzed. For instance, both the third- and sixth-order $(B - V)$ –temperature solutions show residuals correlated with the stellar metallicity (Figures 13 and 19), where stars with higher than solar metallicity have higher temperatures than those with lower metallicities at the same $(B - V)$ color. For this reason, we construct a second-order multi-variable function dependent on both the $(B - V)$ color index and metallicity $[\text{Fe}/\text{H}]$ expressed as

$$T_{\text{eff}} = a_0 + a_1(B - V) + a_2(B - V)^2 + a_3[\text{Fe}/\text{H}] + a_4[\text{Fe}/\text{H}]^2 + a_5(B - V)[\text{Fe}/\text{H}]. \quad (4)$$

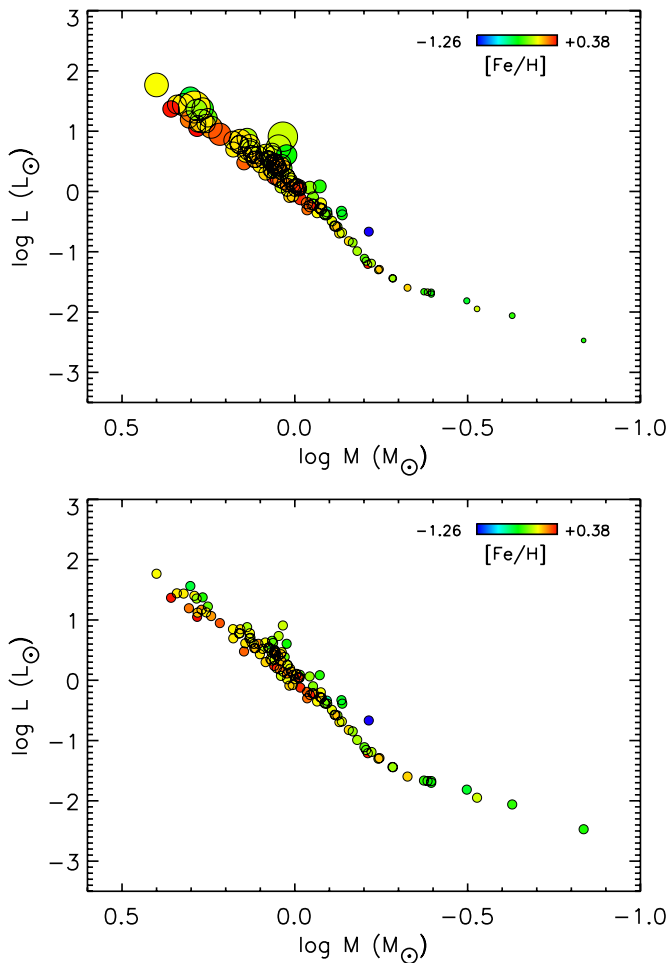


Figure 12. Stellar mass vs. luminosity plotted for all stars in Table 3 plus the collection of low-mass star measurements in DT2. The color of the data point reflects the metallicity of the star. The size of the points in the top panel is proportional to the linear size of the star. The data points in the bottom panel are all of equal size in order to more clearly visualize the splitting in the mass–luminosity plane for stars of different metallicities. See Section 2.4 for details.

(A color version of this figure is available in the online journal.)

We use the sample that omits early-type stars (easily modeled by a lower order polynomial) in order to remove effects due to metallicity. The fit produces the coefficients

$$\begin{aligned} a_0 &= 7978 \pm 16, \\ a_1 &= -3811 \pm 36, \\ a_2 &= 636 \pm 17, \\ a_3 &= 479 \pm 26, \\ a_4 &= -126 \pm 19, \\ a_5 &= -150 \pm 22. \end{aligned}$$

The fit uses a total of $n = 111$ points, is valid for $0.32 < (B - V) < 1.73$, and gives a standard deviation about the fit of $\sigma = 2.6\%$, a value now comparable to the best solutions of the other color indices analyzed. We show the data and solution in Figure 19 plotted for three metallicities $[\text{Fe}/\text{H}] = -0.25, 0.0$, and $+0.25$ (green, black, and red lines, respectively).

The addition of metallicity as a variable to model the $(B - V)$ color–metallicity–temperature connection eliminates the pattern of residuals with respect to metallicity (see bottom panels in Figure 19). Due to the metallicity range of the data, the

Table 9
Maximum Difference in Temperature Solution
when Omitting Hot Stars

Color Index	Max. % Diff.
$(B - V)$	−4.3
$(V - J)$	−0.1
$(V - H)$	−1.1
$(V - K)$	−1.0
$(V - R_I)$	−1.7
$(V - I_J)$	−2.6
$(V - R_C)$	−0.7
$(V - I_C)$	−0.4
$(V - R_K)$	−11.5
$(V - I_K)$	−0.7
$(R_I - J)$	−7.5
$(R_J - H)$	−11.8
$(R_I - K)$	−14.8
$(R_C - J)$	−1.7
$(R_C - H)$	−0.2
$(R_C - K)$	−0.2
$(R_K - J)$	−0.8
$(R_K - H)$	−4.2
$(R_K - K)$	−4.6
$(g - z)$	−0.5
$(g - i)$	−0.5
$(g - r)$	−1.2
$(g - J)$	−0.2
$(g - H)$	0.0
$(g - K)$	−0.3
$(V - W3)$	−0.1
$(V - W4)$	−0.4
$(R_I - W4)$	−4.5
$(I_J - W4)$	−4.2
$(R_C - W4)$	−0.4
$(I_C - W4)$	−1.0
$(R_K - W4)$	−1.1
$(I_K - W4)$	−2.0

Notes. For each color index, we show the maximum difference in predicted temperature using the full AFGKM sample to the sample that omits the early-type stars. Refer to Section 3.1.1 for details.

relation only holds for $-0.25 < [\text{Fe}/\text{H}] < +0.25$, where the data are heavily sampled (Figure 6). For stars with $(B - V) = 0.6$, the calculated temperatures at the high- and low-metallicity boundaries show a difference of ~ 350 K (or $\sim 5\%$), so therefore a necessary correction is needed for accurate conversions of the stellar temperature from $(B - V)$ colors.

3.1.3. Infrared Colors

As previously mentioned, transformed 2MASS JHK magnitudes are used for stars that do not have JHK magnitudes from an alternate source, and these 2MASS magnitudes are sketchy due to saturation and have large errors associated with them (e.g., magnitude errors of saturated stars are ~ 0.2 mag). In each color–temperature relation that uses JHK magnitudes, we perform an additional fit that includes only stars with alternate JHK magnitudes, omitting all stars with saturated 2MASS colors. Filtering the data in this way decreases the available number of points used in each fit in all cases (up to a 20% drop in sample size).

These solutions are plotted in Figures 13–18 as dotted lines along with the relation using the full data set that includes the

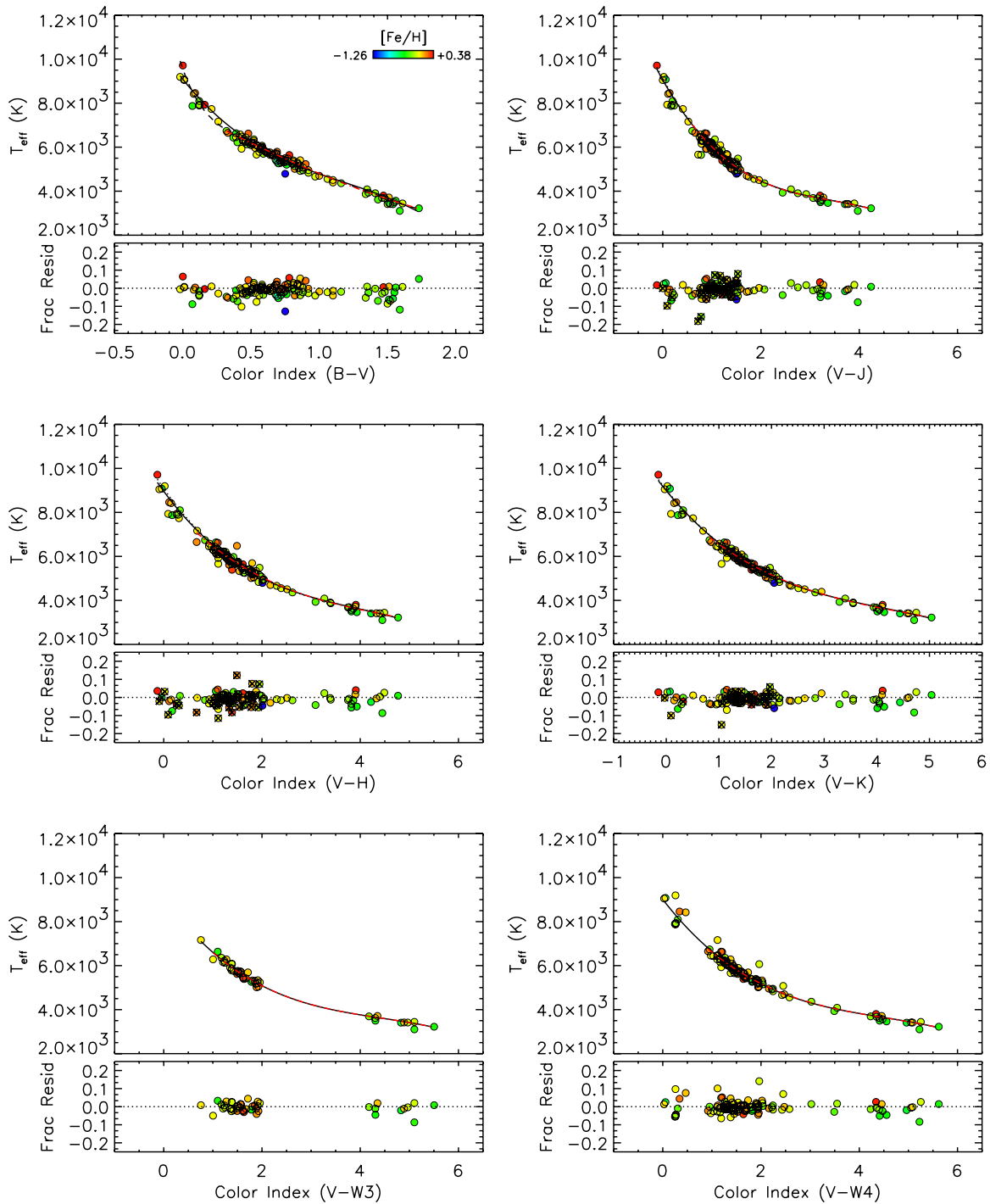


Figure 13. Solid black line represents the solution to the color–temperature relation (expressed as Equation (2) and reported in Table 8). The red dash-dotted line represents the solution omitting the early-type stars (Section 3.1.1, Equation (2), Table 8). The color of the data point reflects the metallicity of the star, and temperature errors are not shown but typically are smaller than the data point. Those panels that involve infrared *JHK* colors have a second solution plotted as a dotted line (mostly eclipsed by the solid line solution). The dashed line in the panel showing the $(B - V)$ relation is the solution using a sixth-order polynomial (Section 3.1.2, Equation (3), Figure 19). The bottom panel shows the fractional residual $(T_{\text{Obs.}} - T_{\text{Fit}})/T_{\text{Obs.}}$ to the third-order polynomial fit, where the dotted line indicates zero deviation. Points with saturated 2MASS photometry are marked with a \times in the bottom panel (see Section 3.1.3 for details). See Sections 3, 3.1, and 3.1.1 for details. (A color version of this figure is available in the online journal.)

transformed but saturated 2MASS photometry (solid line). The solutions are shown to be almost identical, deviating to hotter temperatures by only few tens of Kelvin for the earliest type stars. The fractional residuals shown in the bottom panel of each relation mark the stars having transformed 2MASS colors with a \times . These data points comprise the majority of stars with fractional deviations greater than 5% from the solution, especially

apparent for stars with temperatures >6500 K (early F- and A-type stars).¹⁵ The coefficients to the solutions derived omitting any 2MASS photometry are marked with footnote “d” in Table 8.

The removal of outliers due to suspected bad photometry improves the standard deviation of the fit by 0.3%–2.6% (see

¹⁵ These stars are also among the brightest in the sample.

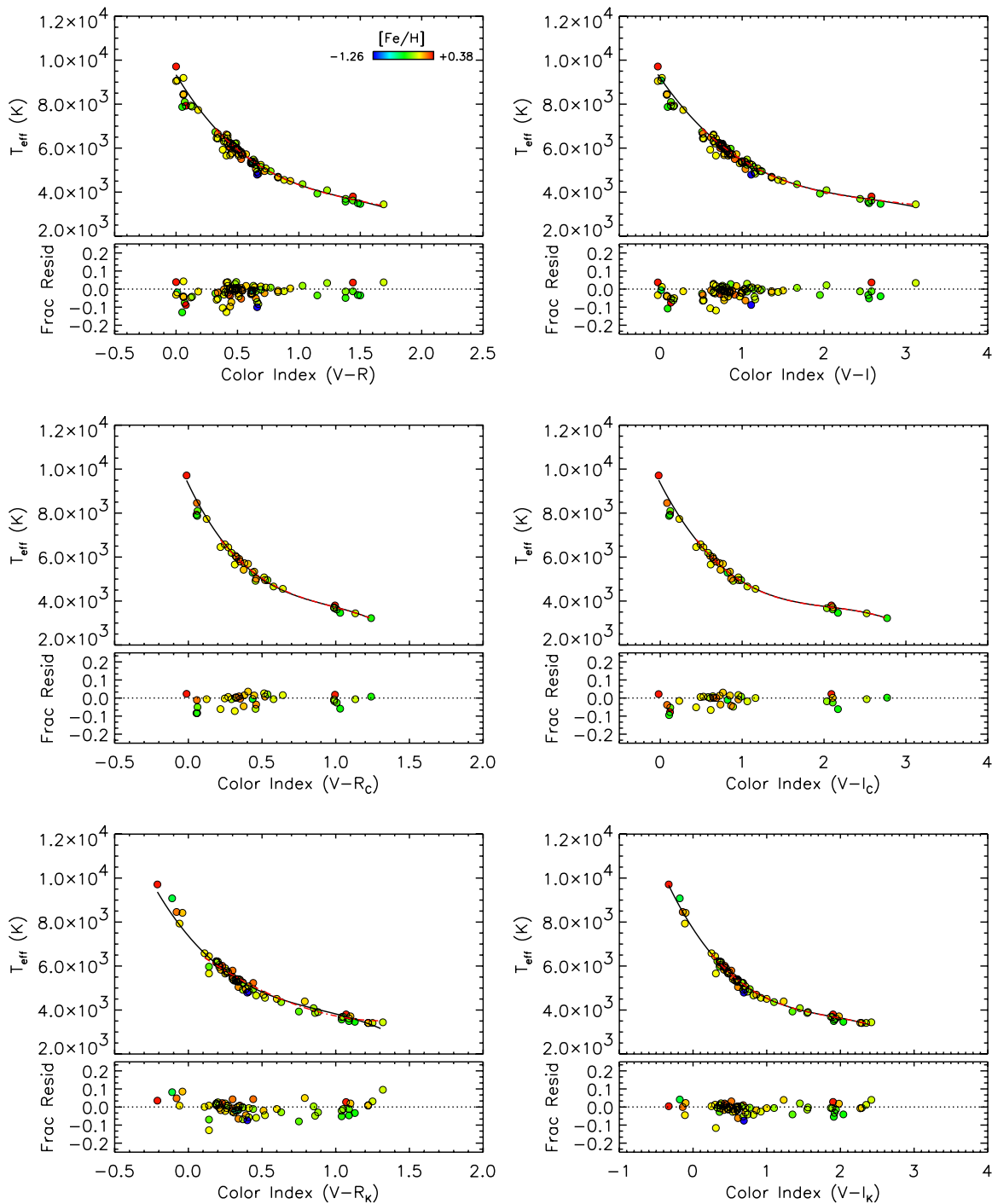


Figure 14. Solid black line represents the solution to the color–temperature relation (expressed as Equation (2) and reported in Table 8). The red dash-dotted line represents the solution omitting the early-type stars (Section 3.1.1, Equation (2), Table 8). The color of the data point reflects the metallicity of the star, and temperature errors are not shown but typically are smaller than the data point. The bottom panel shows the fractional residual $(T_{\text{Obs.}} - T_{\text{Fit}})/T_{\text{Obs.}}$ to the third-order polynomial fit, where the dotted line indicates zero deviation. See Sections 3 and 3.1.1 for details.

(A color version of this figure is available in the online journal.)

Table 8). Since the solutions remain almost identical, we estimate that the standard deviations using the modified data sets reflect the true errors of the relations.

3.1.4. Comparison to Other Works

The IRFM (Blackwell et al. 1979) is a semi-empirical method of determining stellar effective temperature, for which the results are always tested and/or calibrated with interferometric data. Here we view from the alternate perspective, and com-

pare our interferometrically derived temperatures to temperatures derived from solutions via the IRFM in the two recent works of Casagrande et al. (2010) and González Hernández & Bonifacio (2009).¹⁶ Figure 20 shows the results of this comparison, displaying side-by-side the effective temperatures using the Casagrande et al. (2010) and González Hernández &

¹⁶ Note that the transformations in Casagrande et al. (2010) and González Hernández & Bonifacio (2009) are two-dimensional, second-order polynomials, dependent on both the stellar color index and metallicity $[\text{Fe}/\text{H}]$.

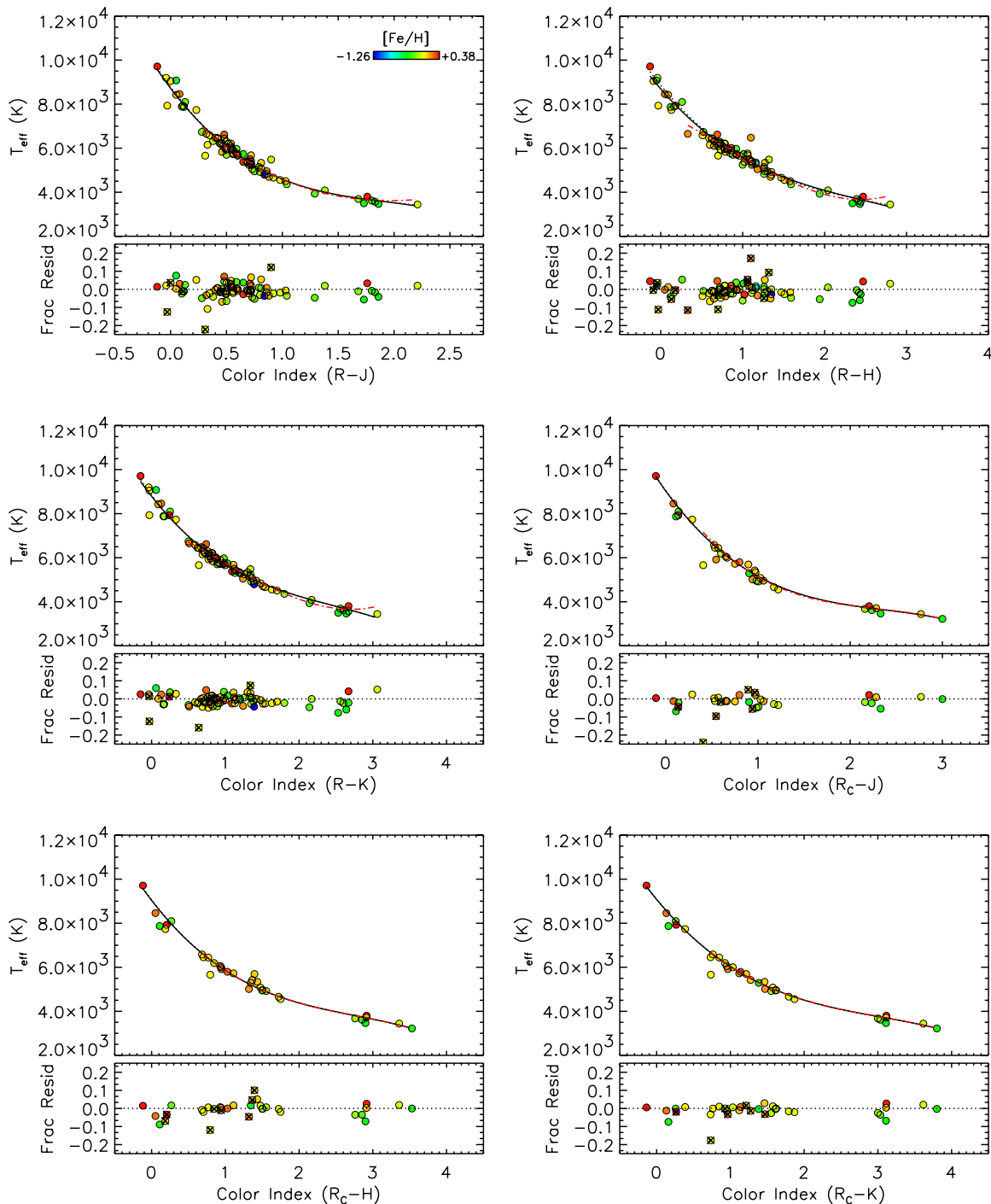


Figure 15. Solid black line represents the solution to the color–temperature relation (expressed as Equation (2) and reported in Table 8). The red dash-dotted line represents the solution omitting the early-type stars (Section 3.1.1, Equation (2), Table 8). The color of the data point reflects the metallicity of the star, and temperature errors are not shown but typically are smaller than the data point. Those panels that involve infrared *JHK* colors have a second solution plotted as a dotted line (mostly eclipsed by the solid line solution). The bottom panel shows the fractional residual $(T_{\text{Obs}} - T_{\text{Fit}})/T_{\text{Obs}}$ to the third-order polynomial fit, where the dotted line indicates zero deviation. Points with saturated 2MASS photometry are marked with a \times in the bottom panel (see Section 3.1.3 for details). See Sections 3, 3.1.1, and 3.1.3 for details.

(A color version of this figure is available in the online journal.)

Bonifacio (2009) relations (left and right, respectively). For each color index, each panel displays the fractional deviation in temperature for the stars with available photometry, allowing only the effective color ranges for each IRFM reference. Each plot also displays the average offset in the deviation of temperature (expressed in percent) as well as the standard deviation of the data, also expressed in percent. Note that the IRFM tempera-

ture scales in both González Hernández & Bonifacio (2009) and Casagrande et al. (2010) are based on the 2MASS bandpasses. As such, to make the comparison of the visual to infrared colors ($V - J$, $V - H$, $V - K$; bottom six panels in Figure 20), the infrared magnitudes of the *Anthology* stars were transformed to the 2MASS system by the expressions in Bessell & Brett (1988) and Carpenter (2001).

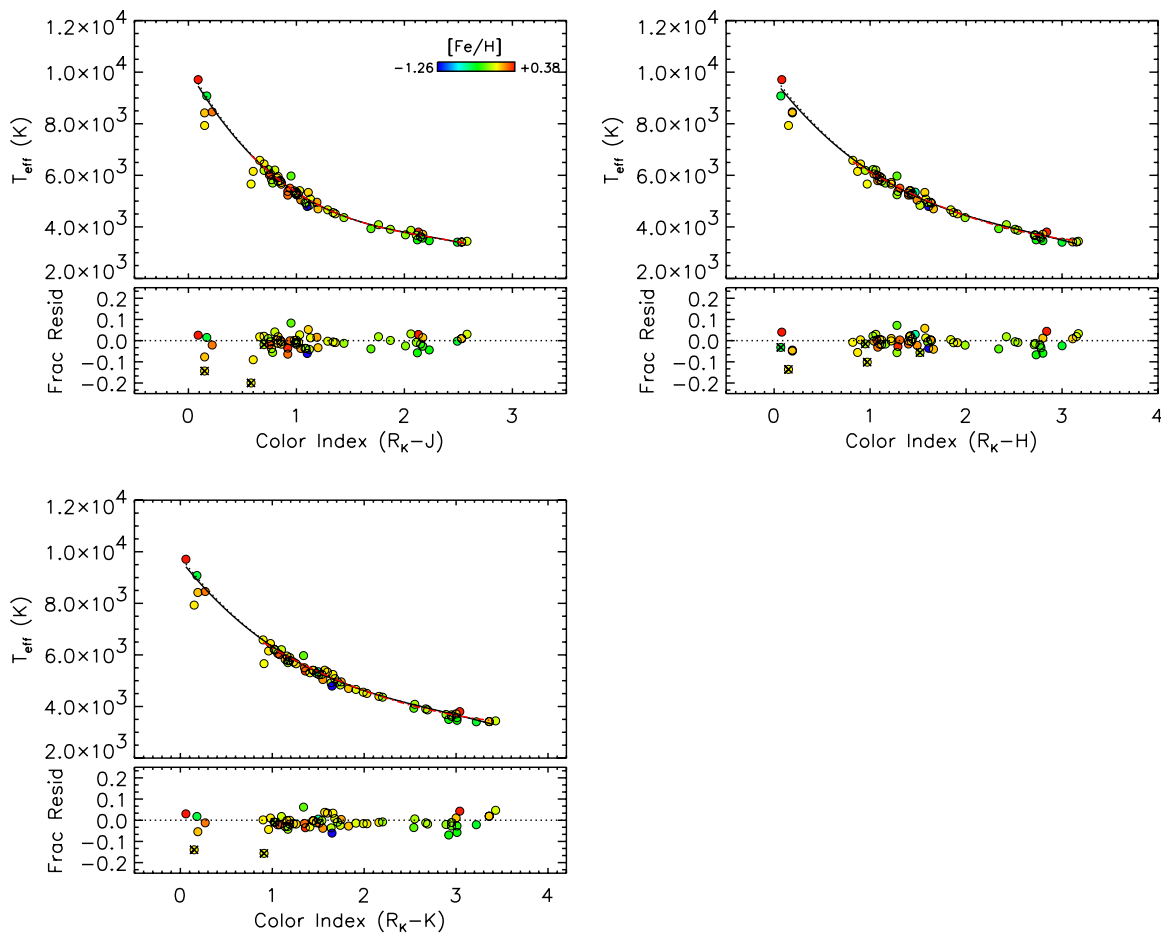


Figure 16. Solid black line represents the solution to the color–temperature relation (expressed as Equation (2) and reported in Table 8). The red dash-dotted line represents the solution omitting the early-type stars (Section 3.1.1, Equation (2), Table 8). The color of the data point reflects the metallicity of the star, and temperature errors are not shown but typically are smaller than the data point. Those panels that involve infrared *JHK* colors have a second solution plotted as a dotted line (mostly eclipsed by the solid line solution). The bottom panel shows the fractional residual $(T_{\text{Obs.}} - T_{\text{Fit}})/T_{\text{Obs.}}$ to the third-order polynomial fit, where the dotted line indicates zero deviation. Points with saturated 2MASS photometry are marked with a \times in the bottom panel (see Section 3.1.3 for details). See Sections 3, 3.1.1, and 3.1.3 for details.

(A color version of this figure is available in the online journal.)

Agreement is within a couple of percent for both references, where the offsets in the González Hernández & Bonifacio (2009) temperature scale are nearly half those from the Casagrande et al. (2010) scale. We find that in all cases, the temperatures derived via the IRFM are higher than those presented here (see the $\langle \Delta T/T \rangle$ value in Figure 20).

An effective temperature scale based on the Sloan photometric system was recently evaluated and revised in Pinsonneault et al. (2012). They use YREC isochrones in addition to MARCS stellar atmosphere models to derive their temperature relations, adopting a $[\text{Fe}/\text{H}] = -0.2$, and an isochrone age of 1 Gyr. We compare the temperatures derived in Pinsonneault et al. (2012) to ours in Figure 21 for the $(g - r)$, $(g - i)$, and $(g - z)$ color indices.¹⁷ Similar to the temperature comparisons above of the IRFM, we truncate each panel in color and temperature range to only contain data where the Pinsonneault et al. (2012) relations hold (refer to table caption in their Table 2). Within each panel is printed the average offset in the deviation of temperature and the standard deviation of the data. We find agreement of the two temperature scales $<2\%$, where

¹⁷ The temperatures are based on the Sloan *griz* filters, and do not apply the zero-point shifts described in Pinsonneault et al. (2012) to transcribing the magnitudes to the Kepler Input Catalog *griz* system.

Pinsonneault et al. (2012) temperatures are systematically higher than interferometric temperatures. This agreement improves to much less than a percent offset in all color–temperature relations if stars with temperatures >5100 K are compared. On the other hand, if we consider adjusting the temperatures to bring the Pinsonneault et al. (2012) scale (assumed $[\text{Fe}/\text{H}] = -0.2$ dex) to the characteristic metallicity of our sample of close to solar (mean $[\text{Fe}/\text{H}] = -0.02$ dex, median $[\text{Fe}/\text{H}] = -0.01$ dex; in the range that overlaps), the Pinsonneault et al. (2012) model temperatures produce even higher temperature values at a given color index (see their Table 3) typically on the order of a few tens of Kelvin. This correction for metallicity would produce a larger offset in temperature, and thus is not a source of the disagreement.

Both the polynomial relations in Casagrande et al. (2010) and González Hernández & Bonifacio (2009) are metallicity-dependent, while the Pinsonneault et al. (2012) polynomials take the same form as our own without defining a dependence on metallicity. In each subpanel for each reference/color index in Figures 20 and 21, we display the residual scatter in comparing our interferometrically determined temperatures to those derived using each polynomial relation. We find that for every instance, this scatter is equivalent to within a couple tenths

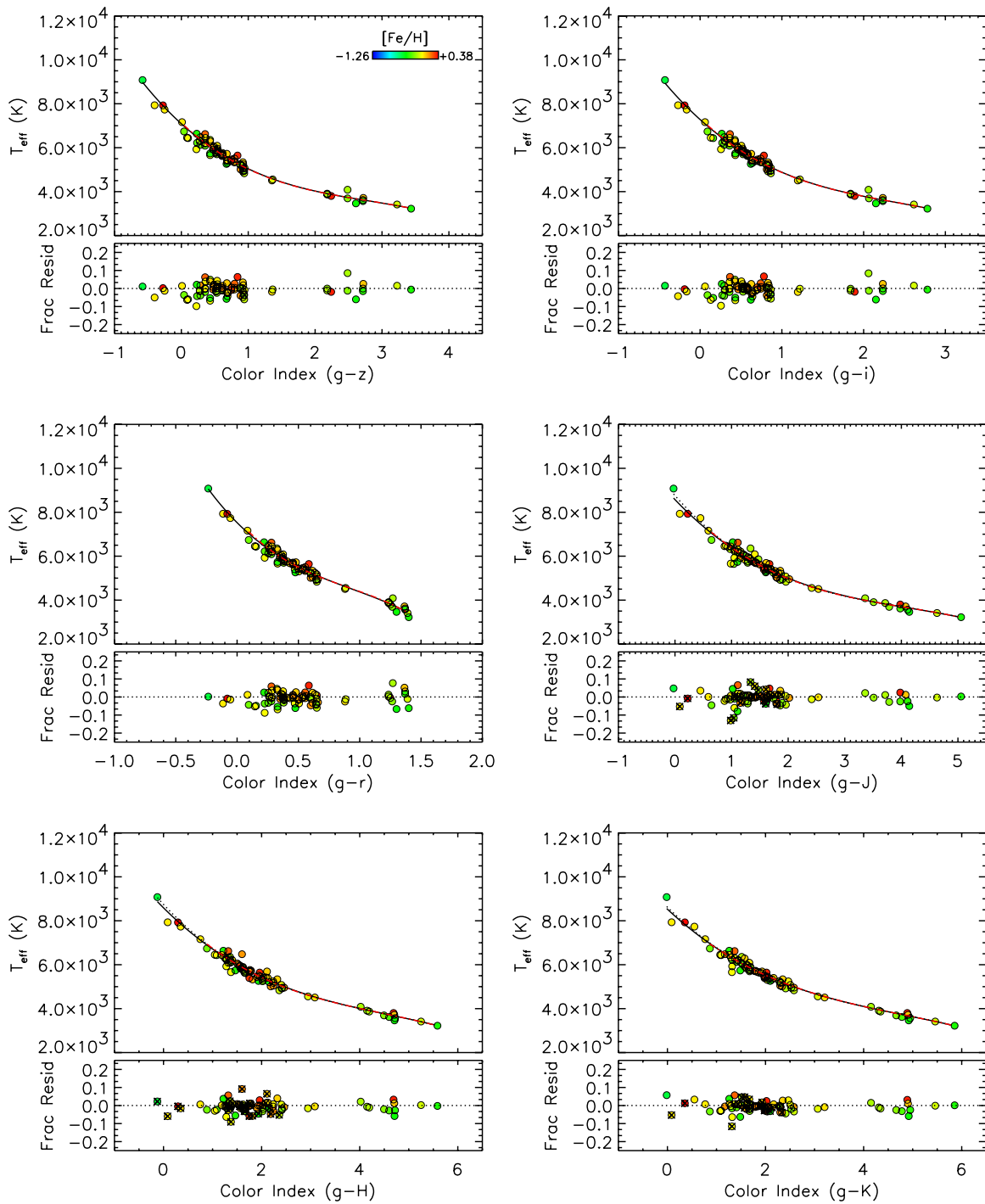


Figure 17. Solid black line represents the solution to the color–temperature relation (expressed as Equation (2) and reported in Table 8). The red dash-dotted line represents the solution omitting the early-type stars (Section 3.1.1, Equation (2), Table 8). The color of the data point reflects the metallicity of the star, and temperature errors are not shown but typically are smaller than the data point. Those panels that involve infrared *JHK* colors have a second solution plotted as a dotted line (mostly eclipsed by the solid line solution). The bottom panel shows the fractional residual $(T_{\text{Obs.}} - T_{\text{Fit}})/T_{\text{Obs.}}$ to the third-order polynomial fit, where the dotted line indicates zero deviation. Points with saturated 2MASS photometry are marked with a \times in the bottom panel (see Section 3.1.3 for details). See Sections 3, 3.1.1, and 3.1.3 for details.

(A color version of this figure is available in the online journal.)

of a percent to the scatter of our derived relations (Table 8). This supports our approach that the inclusion of metallicity as an additional variable in color–temperature relations is not a necessary factor, with the exception of the $(B - V)$ –temperature relation. While this is true based on the sample employed, it must also be pointed out that the metallicity range encompassed by the interferometric sample is relatively limited. Therefore,

any metallicity dependence could still show up in other bands, should the metallicity range be larger.

The Spectroscopic Properties of Cool Stars (SPOCS) catalog (Valenti & Fischer 2005) presents spectroscopic temperature measurements of 68 stars in common with the interferometric sample collected here. In the top panel of Figure 22, we compare the data sets in the same manner as in Figure 20, showing

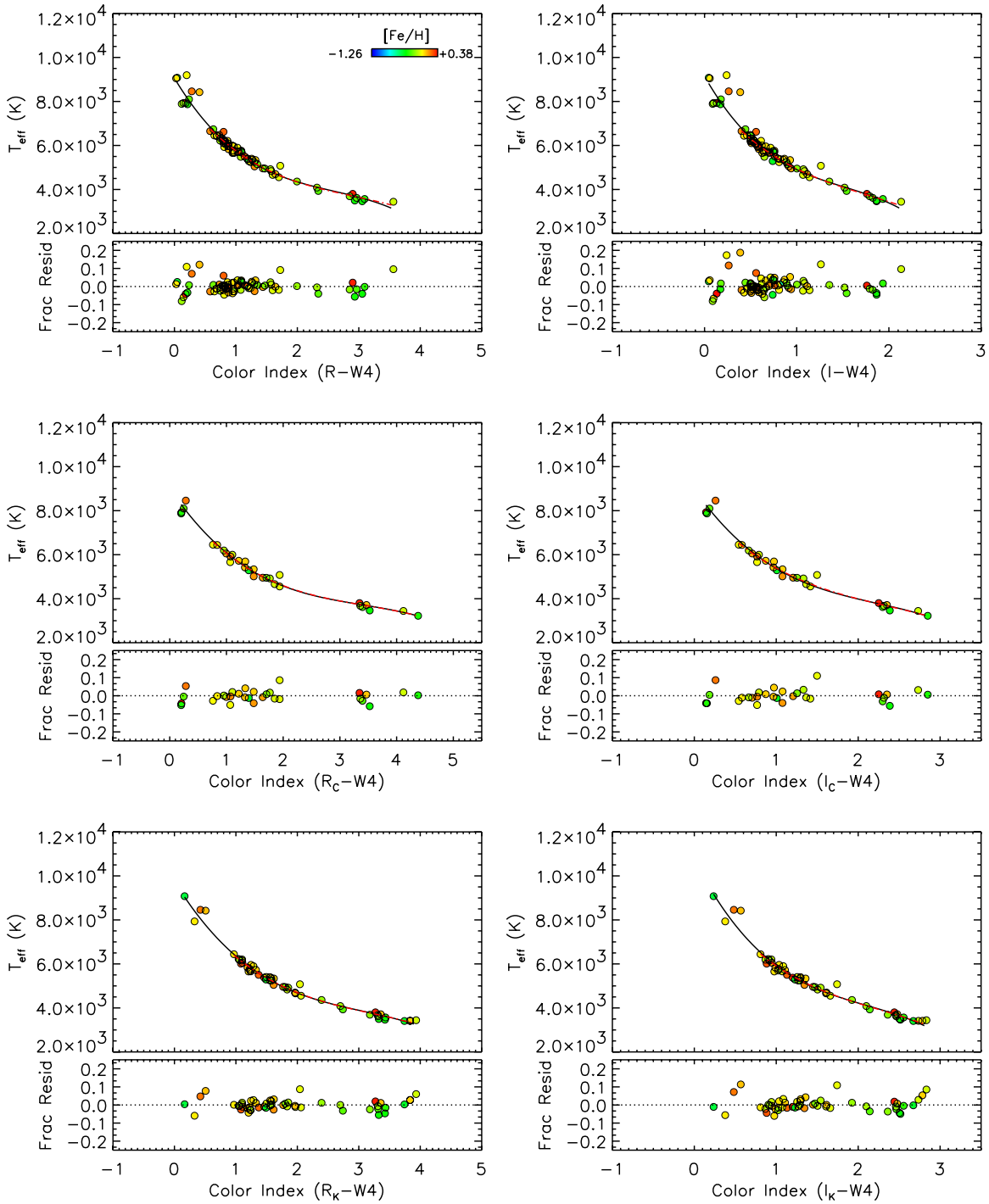


Figure 18. Solid black line represents the solution to the color–temperature relation (expressed as Equation (2) and reported in Table 8). The red dash-dotted line represents the solution omitting the early-type stars (Section 3.1.1, Equation (2), Table 8). The color of the data point reflects the metallicity of the star, and temperature errors are not shown but typically are smaller than the data point. The bottom panel shows the fractional residual $(T_{\text{Obs.}} - T_{\text{Fit}})/T_{\text{Obs.}}$ to the third-order polynomial fit, where the dotted line indicates zero deviation. See Sections 3 and 3.1.1 for details.

(A color version of this figure is available in the online journal.)

excellent agreement with spectroscopic temperatures as well, with only a 1.7% offset to spectroscopic temperatures preferring higher temperatures compared to interferometric values. The stars at the hot and cool ends of the plot hint that a linear trend could arise with an upward slope toward hotter temperatures.

Figure 22 also shows the radii published in the SPOCS catalog versus those with direct interferometric measurements

presented here. The radius values for stars in the SPOCS catalog are computed with the Stefan–Boltzmann law: $R \sim L^{0.5} T^{-2}$. The calculation uses the spectroscopically derived temperature T and the luminosity L , a function of the stellar distance, V -band magnitude, and bolometric correction from Vandenberg & Clem (2003). This comparison is shown in the middle panel of Figure 22, where the average deviation in radii is 3.4%, about

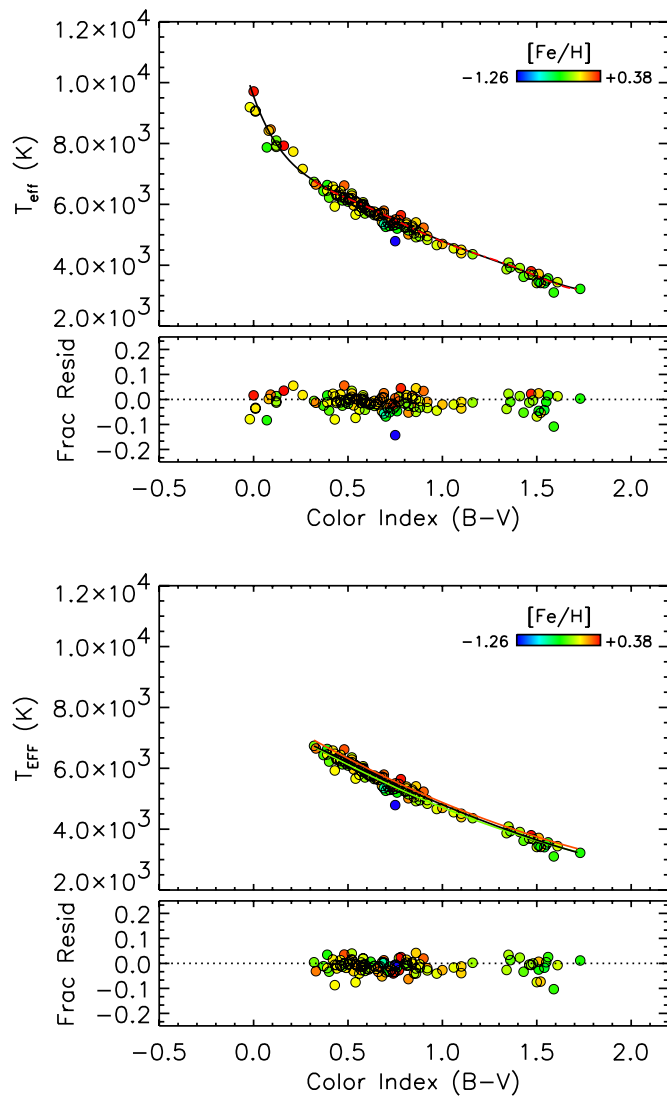


Figure 19. Alternate solutions for $(B - V)$ -temperature relations. The top plot shows the data, fit (solid black line), and fractional residuals to the sixth-order polynomial function (Section 3.1.2, Equation (3)), as well as the fit for the third-order function omitting the early-type stars (red dash-dotted line). Note the difference in the residuals between $0.3 < (B - V) < 0.5$ for this solution and the ones for the third-order polynomial fit to the full AFGKM star sample shown in Figure 13. The bottom plot shows the solution for $(B - V)$ -metallicity-temperature relation (Equation (4)) omitting early-type stars discussed in Section 3.1.2. Iso-metallicity lines of $[\text{Fe}/\text{H}] = -0.25, 0.0$, and $+0.25$ are plotted in green, black, and red, respectively. Note that there are no artifacts in the residuals with respect to metallicity or specific ranges in color index with the solution displayed in the bottom plot.

(A color version of this figure is available in the online journal.)

double that of the offset in temperature. We find that for stars with radii $< 1.3 R_{\odot}$, the offset averages $\sim 2\%$, whereas most stars larger than this radius are offset in the positive direction, with an average offset of $\sim 5\%$.

The bottom panel of Figure 22 compares the masses we derive M_{Iso} to those in the isochrone masses in the SPOCS catalog $M_{\text{Iso,SPOCS}}$, which are also derived using the same set of Y^2 isochrones. The SPOCS values are derived by fitting their spectroscopically determined effective temperature, metallicity, alpha-element enhancement, and the bolometric correction-based luminosity. We find an average offset of -3.9% , where the majority of the low-offset outliers lie between $0.9 M_{\odot}$ and $1.3 M_{\odot}$.

4. CONCLUSION AND SUMMARY OF FUTURE PROSPECTS

Using the CHARA Array, we measure the angular diameters of 23 nearby, main-sequence stars, with an average precision of a couple of percent. Five of these stars were previously measured with LBOI, and our new values show an average of 4.3 times improvement in measurement errors, as well as showing consistency through less direct methods of estimating the stellar angular size. These measurements are added to a collection dubbed as the *Angular Diameter Anthology*, which reports a collection of diameter measurements published in the literature until present time (Table 3). According to our research, the current census totals 125 main-sequence or near main-sequence stars with diameters measured to better than 5%.

We use the interferometrically measured angular diameter in combination with the star's measured bolometric flux and distance to derive the stellar radius (linear), effective temperature, and absolute luminosity. These absolute quantities are used to derive ages and masses from model isochrones. Using the observed photometric properties of the sample, we are able to build transformations to the stellar effective temperature that are precise to a few percent. The empirical temperatures compared to those derived via models, the IRFM and spectroscopy typically agree within a couple of percent, where the temperatures derived via indirect methods have a tendency to predict higher temperatures compared to those with interferometric observations.

Currently our group is using this interferometric data set to develop formula to robustly predict stellar angular sizes using broadband photometry (e.g., see Kervella & Fouqué 2008; van Belle 1999; Barnes & Evans 1976). Such methods of determining stellar sizes are applicable to the interferometry community in search of the perfect calibrator to observe (Bonneau et al. 2006, 2011). The broader impacts on the astronomical community point to such empirically based calibrations enabling the use of eclipsing binaries as standard candles (Southworth et al. 2005).

Measurements of stellar luminosities and radii are historically among the most difficult fundamental measurements in astronomy. Access to astrometric surveys from space, and availability of optical/infrared facilities on the ground, have provided a breakthrough in these measurements. The status of such studies for bright, nearby main-sequence stars is well represented graphically in Figures 7, 8, 10, 11, and 12. During the last few years, the number of direct measurements of the class as a whole has grown substantially in size and with increased precision. This improvement can be extended to fainter and more distant stars by using these results to improve the calibration of the IRFM or similar methods. We also see that the scatter (presumably astrophysical noise) is now greater than our best estimate of the measurement errors. As shown in Section 3.1, some of this scatter is likely due to metallicity and large photometric errors of such bright and saturated sources. Independent and uniform measures of metallicity will prove to be most informative on the improvement of existing calibrations presented here. Other sources of scatter must exist, but are difficult to allow for in the study of the full ensemble of targets.

The future of interferometric measurements is promising, where appropriate technical improvements (at CHARA this would involve the use of adaptive optics, at VLTI perhaps a new beam combiner) will lead to single target precision of order 1%, extending the observable number of targets with interferometry many fold. While the improvement of diameter

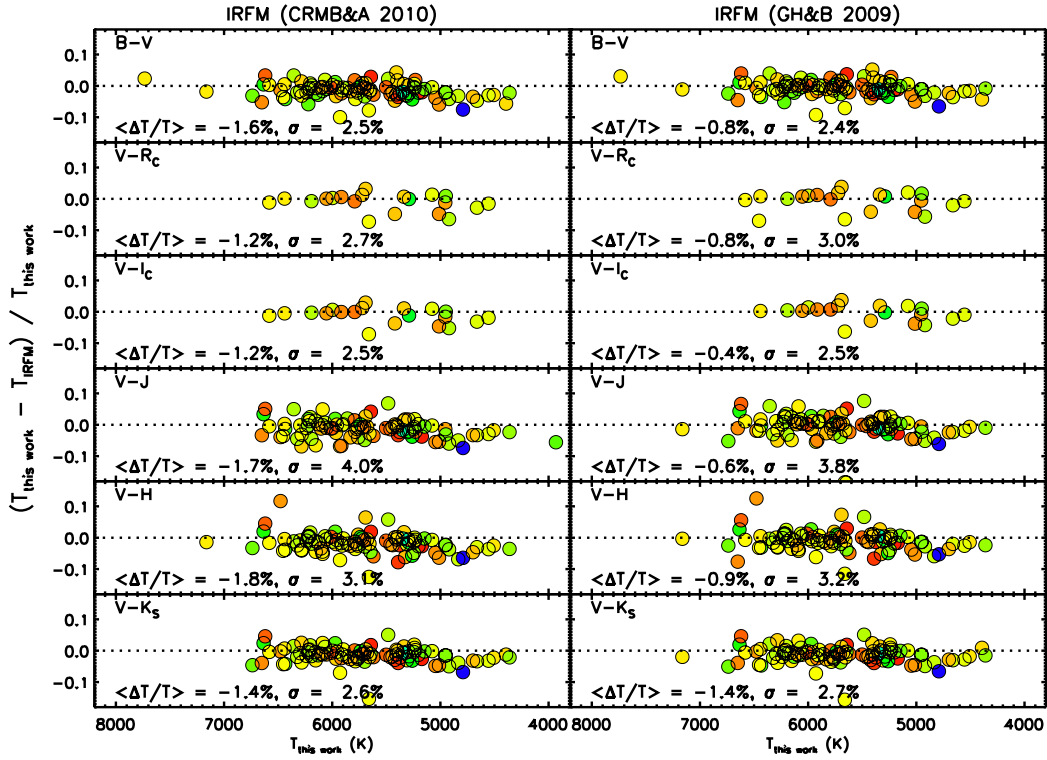


Figure 20. Fractional deviation in effective temperature for interferometrically determined temperatures ($T_{\text{this work}}$) compared to the effective temperatures derived using the polynomial relations in Casagrande et al. (2010) (left; CRMB&A 2010) and González Hernández & Bonifacio (2009) (right; GH&B 2009), established via the IRFM (T_{IRFM}). The top left of each panel lists the color index used in the IRFM relation and bottom portion displays the average percentage deviation in temperature (calculated as $(T_{\text{this work}} - T_{\text{IRFM}})/T_{\text{this work}}$), and scatter of the data σ in percent. The dotted line indicates zero deviation, and the color of the data point reflects the metallicity of the star ranging from $[\text{Fe}/\text{H}] = -1.26$ to 0.38 (see previous figures for legend). See Section 3.1.4 for details.

(A color version of this figure is available in the online journal.)

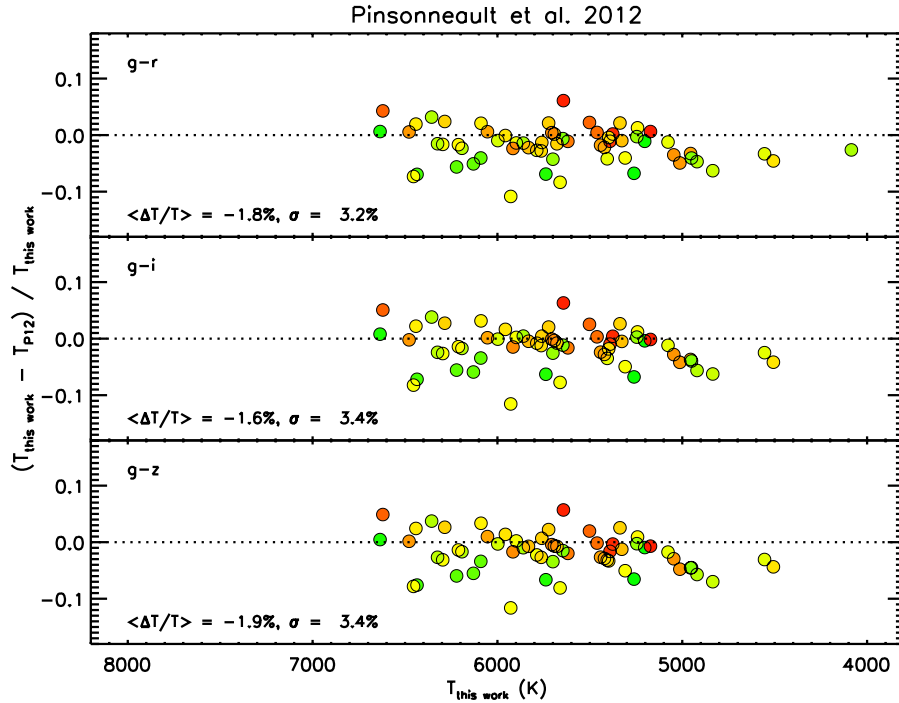


Figure 21. Fractional deviation in effective temperature for interferometrically determined temperatures ($T_{\text{this work}}$) compared to the effective temperatures derived using the polynomial relations in Pinsonneault et al. (2012, P12). The top left of each panel lists the color index used in the relation and bottom portion displays the average percentage deviation in temperature (calculated as $(T_{\text{this work}} - T_{\text{P12}})/T_{\text{this work}}$), and scatter of the data σ in percent. The dotted line indicates zero deviation, and the color of the data point reflects the metallicity of the star ranging from $[\text{Fe}/\text{H}] = -1.26$ to 0.38 (see previous figures for legend). See Section 3.1.4 for details.

(A color version of this figure is available in the online journal.)

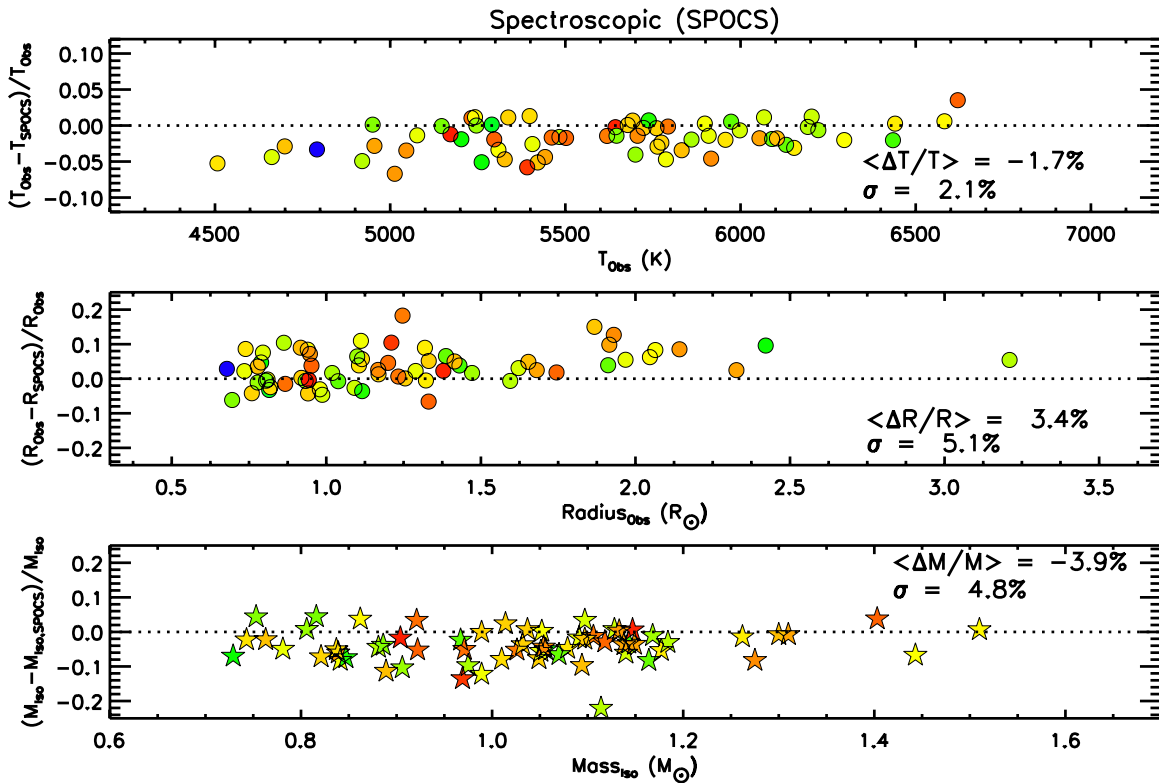


Figure 22. Top and middle panels show the fractional deviation in interferometrically determined effective temperatures and radii compared to the spectroscopic values in the SPOCS catalog (Valenti & Fischer 2005). The bottom panel shows the fractional deviation of stellar masses derived in this work vs. those derived in the SPOCS catalog by interpolation within the Y^2 isochrones. We use different symbols for the points in the bottom panel to accentuate the fact that the original masses for each are derived from model isochrones. Printed in the left-hand side of each window are the average percentage deviation for each variable, and the scatter of the data σ in percent. The dotted line indicates zero deviation, and the color of the data point reflects the metallicity of the star ranging from $[\text{Fe}/\text{H}] = -1.26$ to 0.38 (see previous figures for legend). See Section 3.1.4 for details.

(A color version of this figure is available in the online journal.)

precision from 2%–3% to $\sim 1\%$ will have great value, it will soon approach the point where the sample is limited by targets that have distance measurements, absolute photometric calibrations, and measurements of metallicities at this level. The ability to learn such absolute properties of stars can open the door to the study of essential parameters and phenomena such as age, rotation, and magnetic fields, whose impact on evolution may be important but difficult to detect.

T.S.B. acknowledges support provided through NASA grant ADAP12-0172. S.T.R. acknowledges partial support from NASA grant NNN09AK731. We thank the referee for many helpful comments to improve the paper. We thank Mike Bessell for his helpful advice on photometric transformations. We thank Mike Ireland, Tim White, Vincente Maestro, and Daniel Huber for enlightening discussions on precision bolometric flux measurements. The CHARA Array is funded by the National Science Foundation through NSF grants AST-0908253 and AST 1211129, and by Georgia State University through the College of Arts and Sciences. This research has made use of the SIMBAD literature database, operated at CDS, Strasbourg, France, and of NASA’s Astrophysics Data System. This research has made use of the VizieR catalog access tool, CDS, Strasbourg, France. This publication makes use of data products from the Two Micron All Sky Survey, which is a joint project of the University of Massachusetts and the Infrared Processing and Analysis Center/California Institute of Technology, funded

by the National Aeronautics and Space Administration and the National Science Foundation. This publication makes use of data products from the *Wide-field Infrared Survey Explorer*, which is a joint project of the University of California, Los Angeles, and the Jet Propulsion Laboratory/California Institute of Technology, funded by the National Aeronautics and Space Administration. This research has made use of the JSDC Jean-Marie Mariotti Center database, available at <http://www.jmmc.fr/jsdc>.

REFERENCES

- Abt, H. A. 1981, *ApJS*, **45**, 437
- Abt, H. A. 1985, *ApJS*, **59**, 95
- Abt, H. A. 1986, *ApJ*, **309**, 260
- Abt, H. A. 2008, *ApJS*, **176**, 216
- Abt, H. A. 2009, *ApJS*, **180**, 117
- Abt, H. A., & Morrell, N. I. 1995, *ApJS*, **99**, 135
- Alekseeva, G. A., Arkharov, A. A., Galkin, V. D., et al. 1996, *BaltA*, **5**, 603
- Alekseeva, G. A., Arkharov, A. A., Galkin, V. D., et al. 1997, *BaltA*, **6**, 481
- Alonso, A., Arribas, S., & Martínez-Roger, C. 1994, *A&AS*, **107**, 365
- Andersen, J. 1991, *A&ARv*, **3**, 91
- Anderson, E., & Francis, C. 2011, *yCat*, **5137**, 0
- Argue, A. N. 1966, *MNRAS*, **133**, 475
- Arribas, S., & Martínez Roger, C. 1989, *A&A*, **215**, 305
- Aufdenberg, J. P., Mérand, A., Coudé du Foresto, V., et al. 2006, *ApJ*, **645**, 664
- Aumann, H. H., & Probst, R. G. 1991, *ApJ*, **368**, 264
- Baines, E. K., McAlister, H. A., ten Brummelaar, T. A., et al. 2008, *ApJ*, **680**, 728
- Baines, E. K., McAlister, H. A., ten Brummelaar, T. A., et al. 2009, *ApJ*, **701**, 154
- Baines, E. K., White, R. J., Huber, D., et al. 2012, *ApJ*, **761**, 57

- Barnes, T. G., & Evans, D. S. 1976, *MNRAS*, **174**, 489
- Barry, D. C. 1970, *ApJS*, **19**, 281
- Bazot, M., Ireland, M. J., Huber, D., et al. 2011, *A&A*, **526**, L4
- Bessell, M. S., & Brett, J. M. 1988, *PASP*, **100**, 1134
- Bigot, L., Kervella, P., Thévenin, F., & Ségransan, D. 2006, *A&A*, **446**, 635
- Bigot, L., Mourard, D., Berio, P., et al. 2011, *A&A*, **534**, L3
- Blackwell, D. E., Petford, A. D., Arribas, S., Haddock, D. J., & Selby, M. J. 1990, *A&A*, **232**, 396
- Blackwell, D. E., & Shallis, M. J. 1977, *MNRAS*, **180**, 177
- Blackwell, D. E., Shallis, M. J., & Selby, M. J. 1979, *MNRAS*, **188**, 847
- Böhm-Vitense, E. 1989, *Introduction to Stellar Astrophysics* (Cambridge: Cambridge Univ. Press)
- Bonneau, D., Clausse, J.-M., Delfosse, X., et al. 2006, *A&A*, **456**, 789
- Bonneau, D., Delfosse, X., Mourard, D., et al. 2011, *A&A*, **535**, A53
- Bouw, G. D. 1981, *PASP*, **93**, 45
- Boyajian, T. S., McAlister, H. A., van Belle, G., et al. 2012a, *ApJ*, **746**, 101
- Boyajian, T. S., von Braun, K., van Belle, G., et al. 2012b, *ApJ*, **757**, 112
- Burnashev, B. I. 1985, *BCrAO*, **66**, 152
- Carpenter, J. M. 2001, *AJ*, **121**, 2851
- Casagrande, L., Ramírez, I., Meléndez, J., Bessell, M., & Asplund, M. 2010, *A&A*, **512**, A54
- Che, X., Monnier, J. D., Zhao, M., et al. 2011, *ApJ*, **732**, 68
- Chiavassa, A., Bigot, L., Kervella, P., et al. 2012, *A&A*, **540**, A5
- Claret, A. 2000, *A&A*, **363**, 1081
- Cousins, A. W. J. 1980, *SAOOC*, **1**, 166
- Cowley, A. P. 1976, *PASP*, **88**, 95
- Cowley, A. P., & Bidelman, W. P. 1979, *PASP*, **91**, 83
- Cowley, A. P., Hiltner, W. A., & Witt, A. N. 1967, *AJ*, **72**, 1334
- Creevey, O. L., Thévenin, F., Boyajian, T. S., et al. 2012, *A&A*, **545**, A17
- Crepp, J. R., Johnson, J. A., Fischer, D. A., et al. 2012, *ApJ*, **751**, 97
- Davis, J., Ireland, M. J., North, J. R., et al. 2011, *PASA*, **28**, 58
- Davis, J., & Tango, W. J. 1986, *Natur*, **323**, 234
- Demarque, P., Woo, J.-H., Kim, Y.-C., & Yi, S. K. 2004, *ApJS*, **155**, 667
- Di Folco, E., Thévenin, F., Kervella, P., et al. 2004, *A&A*, **426**, 601
- Ducati, J. R. 2002, *yCat*, **2237**, 0
- Epps, E. A. 1972, *RGOB*, **176**, 127
- Glass, I. S. 1974, *MNSSA*, **33**, 53
- Glass, I. S. 1975, *MNRAS*, **171**, 19P
- Glushneva, I. N., Doroshenko, V. T., Fetisova, T. S., et al. 1998a, *yCat*, **3208**, 0
- Glushneva, I. N., Doroshenko, V. T., Fetisova, T. S., et al. 1998b, *yCat*, **3207**, 0
- González Hernández, J. I., & Bonifacio, P. 2009, *A&A*, **497**, 497
- Gray, R. O. 1989, *AJ*, **98**, 1049
- Gray, R. O., Corbally, C. J., Garrison, R. F., McFadden, M. T., & Robinson, P. E. 2003, *AJ*, **126**, 2048
- Gray, R. O., Corbally, C. J., Garrison, R. F., et al. 2006, *AJ*, **132**, 161
- Gray, R. O., & Garrison, R. F. 1989a, *ApJS*, **69**, 301
- Gray, R. O., & Garrison, R. F. 1989b, *ApJS*, **70**, 623
- Gray, R. O., Napier, M. G., & Winkler, L. I. 2001, *AJ*, **121**, 2148
- Guetter, H. H. 1977, *AJ*, **82**, 598
- Hagen, G. L., & van den Bergh, S. 1967, *PDDO*, **2**, 479
- Hanbury Brown, R. H., Davis, J., Lake, R. J. W., & Thompson, R. J. 1974, *MNRAS*, **167**, 475
- Harlan, E. A. 1974, *AJ*, **79**, 682
- Henry, T. J., & McCarthy, D. W., Jr. 1993, *AJ*, **106**, 773
- Houk, N., & Cowley, A. P. 1975, *University of Michigan Catalogue of Two-dimensional Spectral Types for the HD Stars*, Vol. I (Ann Arbor, MI: Univ. Michigan)
- Huber, D., Ireland, M. J., Bedding, T. R., et al. 2012, *ApJ*, **760**, 32
- Jensen, K. S. 1981, *A&AS*, **45**, 455
- Johnson, H. L., & Knuckles, C. F. 1957, *ApJ*, **126**, 113
- Johnson, H. L., MacArthur, J. W., & Mitchell, R. I. 1968, *ApJ*, **152**, 465
- Johnson, H. L., Mitchell, R. I., Iriarte, B., & Wisniewski, W. Z. 1966, *CoLPL*, **4**, 99
- Keenan, P. C., & McNeil, R. C. 1989, *ApJS*, **71**, 245
- Kervella, P., & Fouqué, P. 2008, *A&A*, **491**, 855
- Kervella, P., Thévenin, F., Morel, P., Bordé, P., & Di Folco, E. 2003a, *A&A*, **408**, 681
- Kervella, P., Thévenin, F., Morel, P., et al. 2004, *A&A*, **413**, 251
- Kervella, P., Thévenin, F., Ségransan, D., et al. 2003b, *A&A*, **404**, 1087
- Kharitonov, A. V., Tereshchenko, V. M., & Knyazeva, L. N. 1988, *The Spectrophotometric Catalogue of Stars: Book of Reference* (Nauka: Alma-Ata)
- Kim, Y.-C., Demarque, P., Yi, S. K., & Alexander, D. R. 2002, *ApJS*, **143**, 499
- Kornilov, V. G., Volkov, I. M., Zakharov, A. I., et al. 1991, *TrSht*, **63**, 4
- Kron, G. E., Gascoigne, S. C. B., & White, H. S. 1957, *AJ*, **62**, 205
- Lafrasse, S., Mella, G., Bonneau, D., et al. 2010, *Proc. SPIE*, **7734**, 77344E
- Levato, H., & Abt, H. A. 1978, *PASP*, **90**, 429
- Ligi, R., Mourard, D., Lagrange, A. M., et al. 2012, *A&A*, **545**, A5
- Macrae, D. A. 1952, *ApJ*, **116**, 592
- Markwardt, C. B. 2009, in *ASP Conf. Ser. 411, Astronomical Data Analysis Software and Systems XVIII*, ed. D. A. Bohlender, D. Durand, & P. Dowler (San Francisco, CA: ASP), **251**
- McAlister, H. A., ten Brummelaar, T. A., Gies, D. R., et al. 2005, *ApJ*, **628**, 439
- McClure, R. D. 1976, *AJ*, **81**, 182
- Mermilliod, J. C. 1997, *yCat*, **2168**, 0
- Monnier, J. D., Zhao, M., Pedretti, E., et al. 2007, *Sci*, **317**, 342
- Morgan, W. W., & Keenan, P. C. 1973, *ARA&A*, **11**, 29
- Mozurkewich, D., Armstrong, J. T., Hindsley, R. B., et al. 2003, *AJ*, **126**, 2502
- Niconov, V. B., Nekrasova, S. V., Polosuina, N. S., Rachkovsky, N. D., & Chuvajev, W. K. 1957, *IzKry*, **17**, 42
- Noguchi, K., Kawara, K., Kobayashi, Y., et al. 1981, *PASJ*, **33**, 373
- Nordgren, T. E., Germain, M. E., Benson, J. A., et al. 1999, *AJ*, **118**, 3032
- Nordgren, T. E., Sudol, J. J., & Mozurkewich, D. 2001, *AJ*, **122**, 2707
- Ofek, E. O. 2008, *PASP*, **120**, 1128
- Pickles, A., & Depagne, É. 2010, *PASP*, **122**, 1437
- Pickles, A. J. 1998, *PASP*, **110**, 863
- Pinsonneault, M. H., An, D., Molenda-Zakowicz, J., et al. 2012, *ApJS*, **199**, 30
- Ramírez, I., & Meléndez, J. 2005, *ApJ*, **626**, 465
- Sandage, A., & Kowal, C. 1986, *AJ*, **91**, 1140
- Schmitt, J. L. 1971, *ApJ*, **163**, 75
- Skiff, B. A. 2013, *yCat*, **1**, 2023
- Southworth, J., Maxted, P. F. L., & Smalley, B. 2005, *A&A*, **429**, 645
- Sylvester, R. J., Skinner, C. J., Barlow, M. J., & Mannings, V. 1996, *MNRAS*, **279**, 915
- Takeda, Y. 2007, *PASJ*, **59**, 335
- ten Brummelaar, T. A., McAlister, H. A., Ridgway, S. T., et al. 2005, *ApJ*, **628**, 453
- Thévenin, F., Kervella, P., Pichon, B., et al. 2005, *A&A*, **436**, 253
- Torres, G., Andersen, J., & Giménez, A. 2010, *A&ARv*, **18**, 67
- Valenti, J. A., & Fischer, D. A. 2005, *ApJS*, **159**, 141
- van Belle, G. T. 1999, *PASP*, **111**, 1515
- van Belle, G. T. 2012, *A&ARv*, **20**, 51
- van Belle, G. T., Ciardi, D. R., ten Brummelaar, T., et al. 2006, *ApJ*, **637**, 494
- van Belle, G. T., Ciardi, D. R., Thompson, R. R., Akeson, R. L., & Lada, E. A. 2001, *ApJ*, **559**, 1155
- van Belle, G. T., & van Belle, G. 2005, *PASP*, **117**, 1263
- van Belle, G. T., van Belle, G., Creech-Eakman, M. J., et al. 2008, *ApJS*, **176**, 276
- van Belle, G. T., & von Braun, K. 2009, *ApJ*, **694**, 1085
- VandenBerg, D. A., & Clem, J. L. 2003, *AJ*, **126**, 778
- van Leeuwen, F. 2007, *A&A*, **474**, 653
- von Braun, K., Boyajian, T. S., Kane, S. R., et al. 2011a, *ApJL*, **729**, L26
- von Braun, K., Boyajian, T. S., ten Brummelaar, T. A., et al. 2011b, *ApJ*, **740**, 49
- Wright, E. L., Eisenhardt, P. R. M., Mainzer, A. K., et al. 2010, *AJ*, **140**, 1868
- Yi, S., Demarque, P., Kim, Y.-C., et al. 2001, *ApJS*, **136**, 417
- Yi, S. K., Kim, Y.-C., & Demarque, P. 2003, *ApJS*, **144**, 259
- Zhao, M., Monnier, J. D., Pedretti, E., et al. 2009, *ApJ*, **701**, 209
- Zorec, J., Cidale, L., Arias, M. L., et al. 2009, *A&A*, **501**, 297